



HAL
open science

An interpretative view of open-vent volcanoes

Sylvie Vergnolle, Nicole Métrich

► **To cite this version:**

Sylvie Vergnolle, Nicole Métrich. An interpretative view of open-vent volcanoes. *Bulletin of Volcanology*, 2022, 84 (9), pp.83. 10.1007/s00445-022-01581-5 . hal-03792044

HAL Id: hal-03792044

<https://hal.science/hal-03792044>

Submitted on 29 Sep 2022

HAL is a multi-disciplinary open access archive for the deposit and dissemination of scientific research documents, whether they are published or not. The documents may come from teaching and research institutions in France or abroad, or from public or private research centers.

L'archive ouverte pluridisciplinaire **HAL**, est destinée au dépôt et à la diffusion de documents scientifiques de niveau recherche, publiés ou non, émanant des établissements d'enseignement et de recherche français ou étrangers, des laboratoires publics ou privés.

An interpretative view of open-vent volcanoes

Vergnolle S. and Métrich N.

Université de Paris Cité, Institut de Physique du Globe de Paris, CNRS, F-75005 Paris, France

Abstract

Open-vent volcanoes are special systems where the dynamics of sustained magmatic processes can be thoroughly investigated and where new monitoring tools can be tested and applied. However, various aspects remain puzzling at open-vent volcanoes for which forecasting their behaviour can be an important challenge. Recent papers highlight the very rapid improvements in spaceborn instruments, data acquisition techniques, data treatment and modelling over the last decade, and illustrate the fundamental contribution of long time-series data, either discontinuous or continuous, and the development of multi-parameter studies.

Here we provide an interpretative overview of the main characteristics of open-vent volcanoes on the basis of selected examples chosen to be representative of the diversity of their magma composition, their eruptive activity and their geodynamic context. We choose typical open-vent volcanoes (Stromboli, Yasur and Erebus), some of them hosting a lava lake (Erta 'Ale, Nyiragongo, Villarrica, Ambrym and Masaya), to those with vigorous activity, which are associated to a long-lasting eruption (Arenal, Fuego, Popocatepetl, Santiaguito). We briefly review their surface activity and report the values of SO₂ flux and the derived magma supply rate with emphasis on the key results found on their behaviour. We show the key role of the magma viscosity and its implication on the degassing. We present the current models used to explain how an open-vent volcano could be maintained, such as by the simultaneous rise and fall of a degassing and degassed magma (bi-directional flow models) and the few thermal models at lava lakes and in the conduit. Finally we discuss the sulphur evolution for three nearby volcanoes at the triple junction in Central America (Pacaya, Fuego, Santiaguito).

The diversity of geodynamic environments, geochemical compositions and physical properties of magmas

Open-vent volcanoes are built up in various geodynamic contexts (Tables 1a and 1b). Their erupted magmas span wide ranges of chemical composition from basalts to nephelinite or trachyandesite and phonolite (Fig. 1), temperature and viscosity (see reviews of Rose et al. 2013 and Edmonds et al. 2022). Low to moderate viscosity systems are characterized by permanent plumes and gas

34 emissions, eventually explosive activity at the craters and/or emissions of lava flows, whereas high
35 viscosity, silica-rich magmas able to retain gas bubbles promote lava dome growth and possibly
36 vulcanian eruptions.

37 These systems may remain continuously active over time periods spanning decades to millennia,
38 whereas changes in activity style and intensity occurs over the short (hours-days), medium (weeks-
39 months) and long (years-decades) time scales. As an example Piton de la Fournaise (Réunion
40 Island) experienced an activity of basaltic lava lake, high lava fountaining and lava flowing, during
41 almost three centuries (1640-1848 CE; Michon et al. 2013). Arenal volcano in Costa Rica is not
42 presently active but erupted during nearly 42 years between July 1968 and 2010 (Parat et al. 2014),
43 with subplinian eruptions, pyroclastic flows and lava emissions (Cigolini et al. 1984; Wadge et al.
44 2006) and vulcanian and strombolian activity (Hagerty et al. 2000; Mora et al. 2022).

45 Short-lasting explosive and paroxysmal eruptions and hazardous fissure-type eruptions draining
46 the persistent lava lake at the craters represent ones of the major hazards at open-vent volcanoes.
47 Destructive fissure eruptions are known at Erta 'Ale (Barnie et al. 2016), Kilauea (Halema'uma'u
48 crater; Patrick et al. 2019; Fig. 2a), Nyiragongo (Komorowski et al. 2004; Morrison et al. 2020; see
49 Pouclet and Bram 2021 for a review; Fig. 2b), and Ambrym volcanoes (Németh and Cronin 2011;
50 Shreve et al. 2019). Short-term explosive eruptions, interrupting the persistent activity of the crater
51 (mild-strombolian activity, passive degassing, lava lake) occur repeatedly at Villarrica in Chile in
52 2015 CE (Aiuppa et al. 2017; Johnson and Palma 2015; Johnson et al. 2018), at Stromboli in
53 Aeolian Islands in Italy (historic and present-day eruptions, Bertagnini et al. 2011; Rosi et al. 2013;
54 Métrich et al. 2021; Aiuppa et al. 2021; Pichavant et al. 2022; Fig. 2c and 2d) or as recently
55 observed at Fuego (Naismith et al. 2019; Liu et al. 2020) and Santiaguito (Wallace et al. 2020) in
56 Guatemala. Erebus volcano (Antartica) also experienced an active explosive activity throughout the
57 Pleistocene and Holocene as testified by tephra layers found up to ~180 km away (Harpel et al.
58 2004).

59 Popocatépetl, with cyclic construction and destruction of lava domes and a large gas flux at the
60 surface may be considered part of the category of open-vent systems as do Arenal and Pacaya that
61 produced homogeneous magma for decades. The cyclic eruptions of high-level magnitude at Fuego
62 (Guatemala), as well as the long-term quasi-steady eruptive pattern at Santiaguito, and Pacaya are
63 other examples of open-vent systems, which are discussed here.

64 The timescales of magma storage, ascent and eruption are now studied through the measurement
65 of the chemical zoning and diffusion patterns in crystals (Costa 2020). Focussing on open-vent
66 volcanoes we note a remarkably high decompression rate of magma and a short time of magma
67 crustal transfer leading to explosive eruptions as retrieved from the modelling of the diffusion

68 profiles of H₂O, CO₂, and S in glass embayments (open-pockets of magma) partly entrapped in
69 crystals. The decompression rate of the magma body that sustained the subplinian eruption (VEI 4)
70 on 17 October 1974 at Fuego reached 0.3–0.5 MPa/s, equivalent to 11–17 m/s ascent velocity
71 (Lloyd et al. 2014), when considering a single-stage decompression. Hence the magma rose
72 from ~10 km depth - its storage region - within the extremely short span of time of 8 to 12 minutes.
73 The total ascent time is between 10 and 35 minutes for a two-stage decompression modelling taking
74 into account different depth ranges of CO₂ and H₂O degassing. At Kilauea, Fergusson et al. (2016)
75 used the same method and report average decompression rates for the magmas that fed the
76 Hawaiian lava fountains to basaltic subplinian eruptions of ~0.05–0.45 MPa per second (Fig. 2a).
77 They calculate ascent timescales from ~5 to ~36 min for these magmas that are ascending from ~2
78 to ~4 km, respectively. The magma decompression rates of 0.1 to ~ 2 MPa/s during the 2017–2018
79 Plinian eruption of Aoba (Ambae; Vanuatu arc) suggest short travel time of less than 2 minutes
80 from ~ 0.5 to 3 km depth (Moussallam et al. 2019).

81 Imbalance between the volume of magma that degassed and the volume of magma is the core of
82 open-vent activity. First observed at basaltic volcanoes and named “endogenous growth” (Francis et
83 al. 1993), it was widely used and debated in literature (Shinohara 2008; Carn et al. 2017). The
84 recent comparison between thermal and SO₂ fluxes suggests that the magma supply rate at Masaya
85 and associated with SO₂ degassing may be 5.5 more than the amount of magma which reaches the
86 surface from thermal fluxes estimated by satellites (Aiuppa et al. 2018).

87 Edmonds et al. (2022) provide a review of the degassing and volcanic activity at open-vent
88 volcanoes producing a wide range of magma compositions from basalts to dacites and rhyolites.
89 They propose that deep-derived volatile phase from magmas accumulating and degassing at crustal
90 depths sustains the persistent degassing at these volcanic systems, which are gas-dominated. It
91 implies the differential transfer of the deep-derived gas phase whereas a major part of the volume of
92 degassing and crystallising magma would be accommodated at depth. As an example, at Masaya the
93 calculated supply rate of tholeiitic magma of 0.19±0.06 km³ per year is suggested to be totally
94 accommodated at depth by extensional tectonic (Zureck et al. 2019). These features are also in
95 agreement with the lack of seismicity other than associated with explosions at Erta 'Ale (Bouche et
96 al. 2010).

97 Persistent degassing at open-vent volcanoes that may have an impact on the health of
98 inhabitants and on agriculture in downwind communities is also a chronic volcanic hazard (see
99 Edmonds et al. 2017 for a review). As an example, the two huge craters Benbow and Marum of
100 Ambrym volcano in Vanuatu, each of them hosting a lava lake until December 2018 (Moussallam
101 et al. 2021), deliver high fluxes of gas rich in trace elements, metals metalloids, halogens (Allard et

102 al. 2016a, 2016b). Human and environmental impacts of halogens concentrate in the downwind
103 western part of the island (Cronin and Sharp 2002; Bani et al. 2009; Allibone et al. 2012). Masaya
104 is one of the strongest degassing sources of SO₂ in the Central America Volcanic Arc (Aiuppa et al.
105 2018), and possibly maintained its steady state behaviour for 30 ka (Zureck et al. 2019). Masaya is
106 also recognised to emit such elements as Hg (Witt et al. 2008). Health and economic hazards
107 associated to Masaya persistent degassing have been long time identified (Delmelle et al. 2002;
108 Williams-Jones and Rymer 2015; Calkins and Delmelle 2021). The 2018 eruption along the lower
109 East Rift Zone (LERZ) at Kilauea produced large quantities of gas and aerosols (i.e., 7.1–13.6 Mt
110 SO₂ and 1.5–2.8 Mt CO₂) in 3 months with significant impacts on air quality (Kern et al. 2020).
111 This aspect of the environmental impacts of the volcanic degassing will not be developed here.

112 In summary, the two main characteristics of open-vent volcanoes are the persistent and excess
113 degassing on one side and on the other side their ability to prevent cooling either by reducing heat
114 losses or by having additional sources of heat at a sufficient rate. We combine here geophysical
115 modelling approach to magma geochemistry to pinpoint key aspects of a selection of well-known
116 open-vent volcanoes. Our goal is to highlight the fundamental properties of these systems, and the
117 rapid improvements of both techniques and modelling for better understanding of their volcanic
118 activity and improvement of their eruption forecasting.

119 We focus on open-vent volcanoes, which cover a range of magma composition and rheology,
120 and show a diversity of activity from persistent degassing to strombolian and vulcanian
121 explosions, up to paroxysmal activity. These volcanoes are monitored and/or have been
122 extensively or more poorly studied, such as Erebus (Antartica), Stromboli (Italy) and Yasur
123 (Vanuatu), respectively. They can host a lava lake (Masaya in Nicaragua, Villarica in Chile,
124 Ambrym in Vanuatu arc, Erta 'Ale and Nyiragongo-Nyamuragira system in Africa) or offer the
125 top of the magma column to air (Stromboli, Yasur, Erebus). In complement Popocatépetl, a dome-
126 forming volcano is considered as one of the largest emitter of SO₂ and Arenal (Costa-Rica), a mid-
127 point in term of magma composition between basalt and dacite, for its long-lasting eruption and
128 the number of studies triggered by its eruption (Mora et al. 2022). Finally three nearby volcanoes
129 from Central American Volcanic Arc (Pacaya, Fuego and Santiaguito) are also selected to discuss
130 the sulphur behaviour in arc-magmas. Kilauea volcano is mostly ignored, due to its enormous
131 number of studies, which are synthetised in a recent special issue of this journal (see Patrick et al.
132 2020 for an introduction).

133 We first discuss the bulk chemical homogeneity of the magma, before presenting basic
134 knowledge necessary to understand the eruptive patterns of our selected volcanoes. We further

135 present the surface activity at lava lakes, including their degassing. We then focus on the
136 strombolian activity of Erebus, Stromboli and Yasur, firstly based on their petrology and magma
137 viscosity and secondly on their surface activity and degassing. We then turn to a summary on
138 vulcanian explosions before reviewing the thermal models, applicable to both lava lakes and
139 conduits. We present the various bi-directional flow models in the conduit and the key
140 informations that can be obtained from sound waves studies. Lastly, we discuss the possible
141 exsolution path of sulphur, firstly on the fate of the sulphur and secondly with the example of
142 Popocatepetl and thirdly on the three nearby volcanoes in Central America, Pacaya, Fuego and
143 Santiaguito.

144

145 **A bulk chemical homogeneity of the magma on the long-term**

146 A relatively homogenous bulk composition but a complex history of the crystal assemblage appear
147 to be shared characteristics of steady-state open-vent volcanoes that may testify to magma recharge
148 and mixing or convection motions without new magma injection.

149 Arenal volcano (Costa Rica) provides a good example of the long-term chemical homogeneity of
150 the bulk lava samples but a complex history recorded by the crystals, involving magma injection,
151 mixing, mineral dissolution and crystallisation (Mora et al. 2022). The distribution of SiO₂ contents
152 of Arenal magma is unimodal and centered on the lavas at about 54 to 57 wt% SiO₂ (Bolge et al
153 2006; Fig. 1). Its mineralogy reveals a complex and diverse growth and mixing histories of the
154 crystal assemblage, although the basaltic-andesitic composition of the extruded magma did not
155 change since 1970 (Streck et al. 2002, Ryder et al. 2006; Parat et al. 2014). The basaltic andesites at
156 Arenal are experimentally reproduced after a minimum of 15% fractional crystallisation at 200 MPa
157 at 1000-1050°C from a basaltic melt (Parat et al. 2014). Streck et al. (2002) suggest, on the basis of
158 mineral zoning and compositions, that recurrent basaltic magma recharges occur with sub-decadal
159 frequency and may predate eruption by months or less. Stromboli is known for its persistent activity
160 at the craters since the eighth century CE (Bertagnini et al. 2011; Rosi et al. 2013). Both the major
161 and trace element of the magma vary in a very restricted range of basaltic-shoshonitic composition
162 (Fig. 1) over the last centuries (Pompilio et al. 2011) while the plagioclase crystals record
163 successive dissolution-crystallisation events (Landi et al. 2006; 2009). Erebus crater hosts a long-
164 lived exposed magma column, often referred to as a “lava lake” fed by a nearly anhydrous phonolite
165 (Giggenbach et al. 1973; Sims et al. 2021), while 1-cm-wide anorthoclase crystals register several
166 (from 1 to 3) complete cycles between the reservoir and the exposed magma column via the conduit
167 (Moussallam et al. 2015). These cycles also imply contrasting flow regimes in reservoir and

168 conduit, with convection in the former (with 1 to 3 cycles of 150 days at a speed of 0.5 mms^{-1}) and
169 more complex cycles of exchange flow and re-entrainment in the latter.

170 In summary, the petrological studies demonstrate the magma chemical homogeneity on
171 several-years time scales, despite the heterogeneous but steady pattern of minerals at the spatial
172 microscale scale.

173 **Basic considerations on degassing and magma viscosity**

174 Two main parameters, namely the degassing pattern and the magma viscosity, are playing a key
175 role in understanding the eruptive regimes. To set the scene for open-vent volcanoes, we discuss
176 here relevant basic informations that will be used later in the paper.

177

178 **Degassing**

179 Degassing at the surface can occur for rising bubbles with various geometries (small, spherical cap
180 and Taylor bubbles (Fig. 3a, 3b and 3c). Laboratory experiments on bubble rise in inviscid to low
181 viscosity fluids have shown that the geometry of rising bubbles depends only on a set of three
182 dimensionless numbers (Clift et al. 1978). These are the Reynolds (Re), Eotvös (Eo) and Morton
183 (Mo) numbers. The Reynolds number, Re , quantifies the respective role of viscous and inertia
184 forces, the Eotvös number that of buoyancy versus surface tension forces and the Morton number
185 (Mo) is the ratio between viscous and surface forces. They can be written as:

$$186 \quad Re = \rho d U / \mu \quad (\text{Eq. 1})$$

$$187 \quad Eo = \rho g D_{\square}^2 / \zeta \sigma \quad (\text{Eq. 2})$$

$$188 \quad Mo = g \mu^4 / \rho \sigma^3 \quad (\text{Eq. 3})$$

189 where ρ and μ are the density (kg m^{-3}) and dynamical viscosity (Pa.s) of the magma, respectively;
190 d is the bubble diameter (m); σ is the surface tension (kg s^{-2}) and U the bubble upwards velocity
191 (m/s). The bubble velocity depends on the shape of the rising bubble for, small bubbles, i.e.

192 called the Stokes velocity (Clift et al. 1978; Eq. 16 in Vergnolle and Jaupart 1986), spherical cap
193 bubbles (Clift et al. 1978; Eq. 5 in Bouche et al. 2010) and Taylor bubbles (Clift et al. 1978; Eq.
194 12 and 17 in Vergnolle and Caplan-Auerbach 2006). Note that the Morton number only depends
195 on the material properties of the magma and the gas, while Reynolds and Eotvös numbers depend
196 on the bubble diameter. The regime diagram displaying the bubble shape during rise is classically
197 used by presenting the Reynolds number as a function of Eotvös number (Clift et al. 1978; Fig. 11
198 in Vergnolle and Jaupart 1986).

199 Bubbles can also be stationary (Fig. 3d), as those accumulated below the crust of a lava lake,
200 creating a foam. Local coalescence within this foam could lead to a long and thin bubble referred

201 to as a flat bubble (Fig. 3d). These flat bubbles have been shown to exist at the Erta 'Ale lava lake
202 (Bouche et al. 2010).

203

204 **Key parameters on magma viscosity**

205 The viscosity of a magma (μ), which is a three phase mixture of melt with dissolved water, crystals
206 and bubbles (Le Losq et al. 2015), is calculated by summing terms as follows:

$$207 \quad \log \mu_{\text{magma}} = \log \mu_{\text{melt}} + X_{\text{water}} + Y_{\text{crystal}} + Z_{\text{bubble}} \quad (\text{Eq. 4})$$

208 where X is the weight fraction of water, and Y and Z the volume fraction of crystals and bubbles,
209 respectively.

210 The respective effects of the temperature (Fig. S1a), the water concentration of the melt (Fig.
211 S1b), the fraction of crystals (Fig. S1c) and of the shape and size of bubbles (Fig. S1d) on the
212 magma viscosity are displayed in the supplementary material.

213 The review paper of Mader et al. (2013) provides an excellent summary of the current models
214 and of the physical processes, which play a role in estimating the magma viscosity at various
215 volcanoes. The first parameter is the crystal volume fraction. The linear approximation of Einstein,
216 who calculates magma viscosity by assuming that the crystal content is small (Mader et al. 2013), is
217 not valid above a crystal volume fraction of 10%. The lowest valid estimate for the viscosity is
218 obtained by Gluth and Gold, from the Taylor expansion of the linear Einstein's equation, made at
219 the second order for the crystal volume fraction (Mader et al. 2013). Some models even predict an
220 exponential increase above a volume fraction exceeding 0.65 (Mader et al. 2013), a case that is
221 never met by our chosen open-vent volcanoes (Tables 1a and 1b).

222 The second parameter to consider is the crystal size and shape and their distributions (Cimarelli
223 et al. 2011; Mueller et al. 2011). The crystal shape is important because it exerts a strong control on
224 the value of the maximum packing fraction, the value for which the viscosity becomes infinite
225 (Mader et al. 2013). This effect is complicated to quantify due to the range of aspect ratios (Mader
226 et al. 2013). The only currently available analysis has to be restricted to that of the average value
227 (Mader et al. 2013) giving a large uncertainty on the final result.

228 The third parameter is the amount of dissolved water in the magma in the conduit, which when
229 large decreases significantly the magma viscosity (Giordano et al. 2008; Fig.S1b). The fraction of
230 dissolved water in magma is drastically changing as the result of gas exsolution when approaching
231 the surface. An accurate prediction of magma viscosity in the conduit requires a good knowledge
232 of the close link between water degassing and crystallisation (Pichavant and MacDonald 2007),
233 both parameters increasing the viscosity close to surface (Fig. S1b and S1c). The depth at which
234 the viscosity starts to increase due to simultaneous loss of dissolved water and increase in the

235 crystal volume fraction is a key ingredient to be known to have a correct view on the physical
236 processes associated to the gas-liquid flow in the conduit, assuming that the crystals passively
237 follow the magma global motion.

238 The fourth parameter is the gas volume fraction, which also increases due to gas exsolution
239 when approaching the surface. The changing gas volume fraction from 0, i.e. small, to 30 and 60%
240 increases the magma viscosity by a factor 2.5 and 10, respectively (Fig. S1c; Mader et al. 2013).
241 The exact calculation of the gas volume fraction is also complex because it depends on whether
242 the small bubbles present within the liquid can move in respect to the liquid, as for a separated gas
243 flow, or are stagnant, as for a homogeneous gas flow (Vergnolle and Jaupart 1986). The
244 consequence of having a separated gas flow is very important for the magma viscosity because the
245 gas volume fraction is significantly reduced when compared to that of a homogeneous gas flow
246 (Fig 5b and 6 in Vergnolle and Jaupart 1986). The first estimates of the gas volume fraction had
247 assumed a homogeneous gas flow (Burton et al. 2007b; Allard et al. 2016b), whereas the
248 framework to calculate the gas volume fraction for a separated gas flow had now been developed
249 (Pioli et al. 2012; Pansino et al. 2019). Three mechanisms can lead to a separated gas flow. The
250 first one is related to the existence of small bubbles sufficiently large, prior to the depth where the
251 gas exsolution starts to be significant, to rise in respect to the melt. The second one is related to the
252 existence of large bubbles and the third one to the existence of bubble clusters, i.e. an aggregate of
253 small bubbles able to rise on its own. Bubble clusters may form in the underlying conduit below
254 lava lakes, as shown to exist at Erta 'Ale (Bouche et al. 2010), and as discussed later in the lava
255 lake section.

256 The fifth parameter is the bubble shape and its effect is displayed, in steady shear, by the
257 Capillary number (Ca) (Mader et al. 2013). This dimensionless number is the ratio between the
258 viscous stress ($\mu\dot{\gamma}$, where $\dot{\gamma}$ is the shear strain-rate) acting on a bubble of diameter d , and the
259 restoring stress supplied by surface tension ($2\sigma/d$), giving:

$$260 \quad Ca = \frac{\mu d \dot{\gamma}}{2\sigma} \quad (\text{Eq. 5})$$

261 The small and non-deformable bubbles increase the magma viscosity by adding some complexity
262 and tortuosity into the path offered to the parcels of moving fluid, while the deformable bubbles
263 decrease the magma viscosity by adding a free slip into the bubbly liquid (Mader et al 2013; Fig.
264 S1d). In both cases, this effect starts to be noticeable for a gas volume fraction of 10 % and is
265 more marked when the gas volume fraction increases. The viscosity of a bubbly magma
266 containing a gas volume fraction of 35 % is either increased by a factor 1.4 for small bubbles or
267 decreased by a factor 0.3 for deformable bubbles (Fig. S1d). The relevance of knowing the bubble

268 shape in the conduit, such as schematically drawn at Santiaguito (Bluth and Rose 2004), might
269 therefore be important. However, looking at the bubble shapes preserved in the ejecta might be
270 misleading due to additional effects associated to expulsion.

271 Another challenging phenomenon arises when a separated gas flow exists in the conduit.
272 Laboratory experiments show that a global liquid motion can result from the bubble motion (Pioli et
273 al. 2012; Pansino et al. 2019). When these conditions are met the small crystals will passively
274 follow the magma motion, thereby decreasing the local crystal volume fraction.

275 In summary, the spatial organisation of the degassing gas bubbles in the conduit is
276 complicated for a magma relatively rich in water, because of the competitive effects of the water
277 content of magma and the gas bubble on the viscosity. The question of the progressive degassing as
278 water is exsolving and how thick an overlying plug can be an interesting question that is addressed
279 further because it requires the knowledge of the dynamics of the magma motion and of its bubbles.

280

281 **Magma supply rate**

282 Two simultaneous pioneer studies, applied to Stromboli (Allard et al. 1994) and Izu-Oshima
283 (Japan; Kazahaya et al. 1994), combined records of SO₂ fluxes with sulphur content prior (melt
284 inclusions) and after (matrix glass) degassing at surface to assess the volume of the degassing
285 magma. An average magma supply rate can be calculated for a given period. This chemical budget
286 does not consider any specific physical process or depth. The only assumption is that the initial
287 sulphur content is quasi-fully lost between depth and surface. This framework had been largely
288 used to assess the magma supply rate at open-vent volcanoes (Tables 1a and 1b) using repetitive
289 measurements of SO₂ fluxes (Tables 2a and 2b).

290

291 **Long-term surface activity at lava lakes**

292 **Lava lakes: pressure gauges of the open-vent systems**

293 Only a few open-vent volcanoes, although distributed all around the world in various geodynamic
294 environments (subduction, rift, and hot spot), host long-lasting lava lakes (6-7 presently known)
295 and/or intermittently active lava lakes (Table 1a). *Sensu stricto*, a lava lake is a natural magma body
296 whose dimensions are large compared to the underlying conduit. In this respect, the so-called "lava
297 lake" at Erebus has a roughly conical shape (Oppenheimer et al. 2009), 40 m across for 30 m depth
298 with 4-10 m wide conduit opening at its base (Dibble 2008; Oppenheimer et al. 2009) and a
299 thickness of a few tens of meters (Jones et al. 2015). Its small diameter and thickness, compared to
300 that of the conduit, suggest it to be the top of a magma column rather than a proper lava lake. It

301 offers a direct view of the underlying conduit when looking from above. For simplicity, we shall
302 refer in the text of Erebus as an exposed magma column.

303 Now, the evidence emerges that most lava lakes have experienced sequences of draining-refilling
304 along their life time that represents major hazards. At Ambrym volcano, several units derived from
305 ponded lava lake bodies were recognised along the Marum crater rim that testifies repeated
306 drainage, excavation or gentle subsidence (Németh and Cronin 2008). Pouclet and Bram (2021)
307 give a detailed review of the activity of the Nyiragongo lava lake, observed since 1948, to have
308 permanent to intermittent and episodic activity with long-term pauses. These authors discuss the
309 mechanisms at the origin of the periodic oscillations of a few tens of minutes for meter-scale level
310 variations. Short-term gas pistoning events and gas release for the rising and the falling phases
311 respectively, modelled by Witham and Llewelin (2006), is discarded because of the absence of
312 relationships between degassing process and oscillatory behaviour of the lava lake (Valade et al.
313 2018), as observed at Kilauea (Patrick et al. 2015). Sudden drops of several tens of meters with
314 strong degassing are ascribed to temporary interruption of the magma convection in the conduit
315 with the lack of fresh magma ascent according to Bobrowski et al. (2017). A draining-refilling
316 model was proposed for Nyamuragira, which involved a gravity-driven drainage of a shallow
317 magma body (or multiple interconnected magma pockets) induced by the eruption of deep
318 undegassed magma along a lateral rift-parallel dike (Coppola et al. 2016).

319 The dynamics of the lava lakes has been intensively studied through the multiparametric
320 measurements of gas and heat fluxes, surface lake motions and flow velocities (Pering et al. 2019,
321 Lev et al. 2019). Measurements have been sporadic or inexistent in the past but they are becoming
322 continuous at a few well-monitored volcanoes. The level of the lava lakes is measured directly at
323 Kilauea (Tilling et al. 1987; Patrick et al. 2015; Fig. 4), Nyiragongo (Burgi et al. 2014; 2020;
324 Barrière et al. 2018; Pouclet and Bram 2021; Fig. 5), Erebus (Jones et al. 2015; Peters et al. 2014a;
325 2018; Fig. 6) or estimated undirectly from satellites (MODIS) at Erta 'Ale (Vergniolle and Bouche
326 2016; Fig. 7) or by measuring the shadow length cast by the crater rim on satellites imagery
327 (Oppenheimer and Francis 1997; Barrière et al. 2018). Unfortunately, the use of satellites is
328 somehow restricted to lava lakes having a funnel shape, such as at Erta 'Ale (Vergniolle and Bouche
329 2016) and Nyiragongo (Burgi et al. 2014), a sufficient radiative surface and a reasonably unfrequent
330 cloud cover.

331 Lava lakes, by being in direct connection with a shallow magma reservoir, offer a unique
332 opportunity to decipher the physical processes at depth. Their level can act as a pressure gauge,
333 making its measurement a key parameter to follow. At Ambrym (Fig. 8), the lava lakes were
334 visually observed to be at a high-level prior the effusive activity of 21 February 2015 (Radebaugh et

335 al. 2016; Hameling and Kilgour 2020; Shreve et al. 2021), as well as that of mid-December 2018
336 (Hameling et al. 2019; Shreve et al. 2019; Moussallam et al. 2021). This shows that the pressure
337 was building up somewhere in the plumbing system prior to these major events. Similarly
338 numerical simulations performed at Nyiragongo, and validated by 30 years of records, have also
339 shown that (i) the level of lava lake rises prior to paroxysmal activity, but (ii) slows down in the
340 preceding months/year (Burgi et al. 2020). Therefore, the fluctuations in the height of a lava lake
341 can track changes in pressure and the dynamics of the magmatic systems.

342 At Masaya (Fig. 9), the lava lake has persisted with varying levels between 2015 to present (C.
343 Wauthier personal communication). Occasionally, these vents have enlarged in dimension, most
344 likely due to magma level increase in the conduit and crater floor collapse, ultimately leading to a
345 lava lake (Aiuppa et al. 2018). Its surface activity had been explained qualitatively, but not
346 quantitatively, by the behaviour of the stable foam accumulated at the top of the reservoir (Stix
347 2007). At Erta 'Ale, the lava lake level was also explained, and modelled, to be controlled by the
348 thickness of the stable foam at the top of the shallow reservoir (Vergniolle and Bouche 2016). The
349 lava lake rises when the underlying gas flux below the foam exceeded that associated to the foam
350 spreading and it falls when the underlying gas flux had stopped (Fig. 10). The foam thickness was
351 modelled with these two different boundary conditions and compared to the level of the lava lake,
352 giving two independent constraints on the plumbing system, namely the area of the shallow magma
353 reservoir and the underlying gas flux (Vergniolle and Bouche 2016). This analysis, done for several
354 years, showed that the gas flux at the top of a magma reservoir could, at time, be oscillatory with a
355 period of 10.8 days, continuous or nonexistent (Vergniolle and Bouche 2016).

356 The connection of the lava lake with a shallow plumbing system is in agreement with the good
357 match observed between the pressure loss, the drop in lava lake level and the deformation pattern
358 (Moore et al. 2019), as at Kilauea (Patrick et al. 2015; Poland and Carbone 2018), Ambrym
359 (Németh and Cronin 2008), Nyiragongo (Pouclet and Bram 2021) and Erta 'Ale (Barnie et al. 2016)
360 with a long-term influence of the regional tectonic activity.

361

362 **Degassing and bubble regimes**

363 We focus first on the present knowledge of lava lakes, which can often be seen from above, when
364 they are not almost entirely covered by a solid crust and hidden as occurring, respectively in
365 December 2004 at Erta 'Ale (Fig. 7c), and in January 2009 at Masaya (Fig. 9b).

366 At Erta 'Ale, the degassing occurs through the breaking of the spherical cap bubbles at a fixed
367 location at the surface of the lava lake (insert in Fig. 7a) or through the flat bubbles (Fig. 3d)
368 located on the incandescent zones, which sometimes separate the few cold plates of the crust

369 (Bouche et al. 2010; Fig. 7a). A spherical cap bubble rising in a conduit in such low viscosity
370 magma can grow a bubbly wake, which periodically detaches from its base upon reaching a
371 maximum volume proportional to that of the driving spherical cap bubble (Bouche et al. 2010).
372 This bubble cluster can then rise in the conduit on its own at a relatively large velocity. The
373 dismantling of these bubble clusters by the return flow of the lava lake is thought to be at the
374 origin of the small bubbles. These small bubbles accumulate below the cooling crust where they
375 can coalesce to produce the flat bubbles (Bouche et al. 2010). Spherical cap bubbles and flat
376 bubbles co-exist and correspond to two different types of degassing. Both types of degassing at
377 Erta 'Ale lead to a weak strombolian activity. However the driving gas overpressure leading to the
378 breaking of spherical cap bubbles is significantly larger than that driving the breaking of the flat
379 bubbles (Bouche et al. 2010). On some occasions, these bubbly clusters remain attached to their
380 driving spherical cap bubbles until very close to the surface of the lava lake, and burst at the
381 surface as small lava fountains (Bouche et al. 2010).

382 Is the rise of the large bubbles at other lava lakes sufficiently turbulent to grow a wake at the
383 surface or in the conduit? Can this bubbly wake detach and incorporate small bubbles as proposed
384 by Bouche et al. (2010)? The key point of such a mechanism is that some magma is rapidly
385 brought to the surface, travelling at the velocity of the driving large bubble or that of a bubble
386 cluster when within a detached bubbly wake. This depends on the value of the Reynolds number
387 (Eq. 1). For a value above 30, a wake, a vortex zone initially attached to the driving large bubble,
388 exists and can attract small bubbles in it (Fig. 15 in Vergnolle and Ripepe 2008; Fig. 27.11 in
389 Taddeucci et al 2015). Above a value of 70-100, the wake becomes open, with strong interactions
390 between the fluid around the bubble and the wake itself. This laminar wake is also unstable, hence
391 can detach and rebuild. At Reynolds numbers exceeding 2000, the detachment of the wake, fully
392 turbulent, occurs periodically upon reaching a critical volume, proportional to the volume of the
393 driving bubble (Bouche et al. 2010). In this latter regime, the quantification of the volume of
394 magma within the detached bubbly wake is possible, providing a knowledge of the volume of the
395 driving bubble and the gas volume fraction within the bubbly wake. The magma might be
396 sufficiently fluid at a depth where the amount of dissolved water is considered as partly or fully
397 undegassed. This allows the large bubbles to rise at relatively high Reynolds number, despite their
398 compression in gas volume with depth. In this case, the degassing is organised at depth with large
399 driving bubbles and their detached bubbly wakes. Large bubbles and detached bubbly wakes can
400 then rise towards the surface and potentially have their Reynolds number decreasing, despite their
401 increase in gas volume, due to the rapid increase in the gas volume fraction existing in the magma
402 containing stagnant bubbles. If the Reynolds number becomes below the critical value of 70-100,

403 the values estimated for the large bubbles at the surface do not reflect anymore the fact that the
404 detached bubbly wakes were previously formed in the conduit and had already led to a proper
405 separated gas flow at depth. If a separated gas flow is organised at depth, the newly gas exsolved
406 above this depth is likely to mainly diffuse into the small bubbles already present in the separated
407 gas flow, enhancing their differential velocity in respect to the magma, hence the vigour of the
408 separated gas flow.

409 One should then consider the Reynolds number (Eq. 1) to decide on the existence of the
410 detached bubbly wakes somewhere in the conduit. For simplicity, we considered here the depth
411 where the magma is still rich in dissolved water to be 500 m below the surface for all the selected
412 lava lakes, based on the calculation of the gas volume fraction at Ambrym and its relatively high
413 dissolved water content (Allard et al. 2016b). Assuming that the magma is fully degassed, the
414 Reynolds number calculated a depth of 100 m, is reduced by a multiplicative factor of 0.19 (Table
415 3). It would be reduced by a factor of 0.087 at 500 m due to gas compression when assuming, for
416 the sake of the argument, a fully degassed magma.

417 We are now going to discuss specific examples, using the Giordano's model (2008) unless
418 specifically given elsewhere and the relevant parameters (Table 3). For each example, we discuss
419 the final magma viscosity when adding crystals or small bubbles whenever possible.

420 The Reynolds number of the driving spherical caps at Erta 'Ale, is 1840 and 8000 at the surface
421 when using an updated value of the magma viscosity of 22-27 Pa.s (Table 3). It is still well above
422 the threshold value for which the detachment of the bubbly wake exists and is periodic. Again, this
423 example illustrates the importance of the viscosity on the bubble regime as the value of 10 Pa.s
424 used by Bouche et al. (2010) could have led to a different scenario. The formation of detached
425 bubbly wakes (Fig. 11a), which is a mechanism at work even during a period of very low activity
426 of the lava lake (Bouche et al. 2010; Vergnolle and Bouche 2016), is hence a persistent feature of
427 its degassing (Fig. 11).

428 Similarly, the large bubbles observed at Nyiragongo, 10 m in diameter (Tazieff 1996), led to
429 relatively high values of the Reynolds number at the surface, between 3152 and 822 (Table 3), for
430 a magma viscosity from 56 Pa.s to 230 Pa.s (Burgi et al. 2014; 2018; 2020), respectively, a value
431 also sufficient to produce detached bubbly wakes. The Reynolds number at a depth of 500 m is
432 also sufficiently high, 306 and 71 for a magma viscosity of 56-230 Pa.s, respectively, (Table 3) to
433 lead to a fully separated gas flow in the conduit, organised with driving spherical cap bubbles and
434 their bubbly wakes (Fig. 11a).

435 The Reynolds number of the spherical cap bubbles observed at Villarica is between 65 and 232
436 at the surface (Table 3), with gas volumes between 200 m³ and 2500 m³ (Gurioli et al. 2008),

437 respectively, and a magma viscosity of 1780 Pa.s, calculated by assuming a crystal volume
438 fraction of 38 vol% obtained with stagnant crystals (Witter et al. 2004). Such a value of the
439 Reynolds number is again mostly compatible with the formation of bubbly wakes and their
440 detachment close to the surface. The very high Reynolds number at a depth of 500 m, 20000-
441 71500 and 556-1990, when assuming a negligible crystal volume fraction and a magma viscosity
442 of 0.5 Pa.s and 18 Pa.s, respectively, obtained for a dissolved water content of 4 wt% and 1 wt%
443 (Witter et al. 2004; Table 3), clearly show that the driving spherical cap bubbles are organised at
444 depth similarly to that of Erta 'Ale close to the surface (Fig. 11a), with a periodic detachment of
445 the bubbly wake onto reaching a maximum wake volume of 4-6 that of the driving spherical cap
446 (Bouche et al. 2010).

447 The bubbles observed at the surface of Ambrym lava lakes were very large, plurimetric (Allard
448 et al. 2016b) with a diameter of 5-10 m at Benbow on 5 October 2008 (P. Allard, pers. com. on 25
449 October 2021) and even larger at Marum in May 2014, 12 to 16 m in diameter (Radebaugh et al.
450 2016). The Reynolds number of these bubbles at the surface is between 318 and 1820, for a bubble
451 diameter of 5 and 16 m in diameter, respectively, and a magma viscosity between 170 and 250
452 Pa.s (Table 3). The conditions are therefore met to have the large bubbles rising in the lava lake
453 and at the origin of detached bubbly wakes at the surface. However, the above calculation of the
454 magma viscosity does not consider the gas volume fraction of small bubbles potentially suspended
455 in the magma, a limit case for which most of the bubbles, even small, can move in respect to the
456 liquid, hence in a separated gas flow. In contrast, the gas volume fraction has been estimated by
457 combining records from open-path Fourier transform infrared spectroscopy of gas emissions at
458 Ambrym, with the laws of the gas exsolution of H₂O, CO₂ and SO₂ from the melt at equilibrium,
459 while all the newly produced gas is organised into small bubbles passively following the melt
460 phase (Allard et al. 2016b). In these conditions, the magma viscosity is increased by a factor 10
461 (Fig. S1c; Mader et al. 2013) as soon as it reaches the threshold value, for which the small bubbles
462 are touching one another, which occurs at a depth of 160 m (Allard et al. 2016b). In this case, the
463 degassing at the surface of the lava lake at Ambrym does not present detached bubbly wakes for
464 the smallest observed bubbles, 5 m in diameter (Fig. 11b). However the detached bubbly wakes
465 can exist if the diameter of the driving large bubble exceeds 8.5 m (Fig. 11c), such as for the
466 largest bubbles on 5 October 2008 (P. Allard, pers. com. 25 October 2021) and for the entire range
467 of bubble diameters seen in May 2014 (Radebaugh et al. 2016).

468 The bubble diameters are relatively small at Masaya, with a median value of 2.6 m and a range
469 of 0.6-8.5 m, even during a period of vigorous activity (Pering et al. 2019). The Reynolds number
470 of a bubble, whose diameter is 2.6 m, is 156 and 30 at the surface and a depth of 100 m,

471 respectively, (Table 3) for a magma viscosity between 140 and 180 Pa.s. The Reynolds number at
472 the surface, calculated above with a negligible gas volume fraction, could be below the threshold
473 of 70-100, if the magma viscosity is multiplied by 2.5, such as for a gas volume fraction exceeding
474 a value of 30 % (Fig. S1c). The Reynolds number at a depth of 500 m, equal to 78 if we assume
475 that the magma still contains 1.45 wt% of dissolved water (Table 3), is just above the lowest value
476 for starting an open wake and initiating a separated gas flow. However, the magma at Masaya,
477 being richer in dissolved water, 1.45 wt%, than that at Ambrym, 1.2 wt%, may have partially lost
478 its initial dissolved water at a depth below than 500 m, up to a significant value. In this case, the
479 magma viscosity at this depth increases, thereby decreasing the Reynolds number. It may then
480 lead to a Reynolds number below the threshold value of 70-100, preventing both the formation of
481 open wakes and that of a separated gas flow at this depth. If we consider that the depth at which
482 the magma is still rich in dissolved water, 1.45 wt%, is 700 m rather than 500 m, the driving
483 spherical cap bubble at Masaya cannot grow an unstable wake at the lowest possible value of the
484 magma viscosity. This is even more the case if the depth, where part of the dissolved water is
485 significantly lost, is larger than 700 m, invalidating the possibility to have a separated gas flow by
486 this mechanism at any depth below 500 m.

487

488 **Small lava fountains: detached bubble wakes**

489 The existence of small lava fountains, which have been interpreted at Erta 'Ale as the surface
490 expression of newly detached bubbly wakes, could be used as an independent constrain in favour
491 of the existence of detached bubbly wakes at the surface (Bouche et al. 2010). Small lava
492 fountains have also been observed at Nyiragongo (Burgi et al. 2014; 2018), Villarica (Palma et al.
493 2008) and Ambrym (Radebaugh et al. 2016). This suggests that a mechanism based on the
494 existence of detached bubbly wakes is possible at the surface of these lava lakes, in agreement
495 with relatively high values of the Reynolds number of their spherical cap bubbles close to the
496 surface (Table 3). Furthermore, the results from the sulphur isotopes, which have shown that the
497 degassing at Erta 'Ale occur in disequilibria (De Moor et al. 2013), also reinforce our proposed
498 mechanism of spherical cap bubbles already existing at 500 m and sufficiently large to be able to
499 produce detached bubbly wakes even when the activity at the lava lake is very low (Bouche et al.
500 2010).

501 Small lava fountains have been observed at Ambrym at a time where the bubbles were 12-16 m
502 in diameter (Radebaugh et al. 2016). Their Reynolds numbers (Table 3) are either 1190-1820 or
503 119-182, when considering that the small bubbles suspended in the liquid phase move separately
504 and at a low gas volume fraction or together with the liquid at a gas volume fraction of 60 %,

505 respectively. These Reynolds numbers, well above the value of 70-100, cannot be used to give an
506 indication on the gas volume fraction at the surface.

507 The lack of small lava fountains at Masaya during all periods of observations (P. Delmelle, pers.
508 com., 2 November 2021) suggests that the Reynolds number at the surface is always below 70.
509 The Reynolds number of the typical bubble observed during a vigorous period, 2.6 m in diameter
510 (Pering et al. 2019), is equal to 156 when assuming a negligible gas volume fraction (Table 3).
511 This suggests that the gas volume fraction at the surface must always exceed 30 %. Such a value
512 can easily be explained by the richness in volatiles of the magma. The degassing at Masaya
513 (Martin et al. 2010) has been shown to be at equilibrium, when using the sulphur isotopes during a
514 period of very low activity (De Moor et al. 2013). The degassing at equilibrium is in agreement
515 with the lack of open wakes below a depth of 700 m and a large gas volume fraction close to the
516 surface. But we do not know whether the degassing at equilibrium is only occurring at periods of
517 low activity or is persistent at the lava lake.

518

519 **Homogeneous versus separated gas flow?**

520 We now discuss Ambrym and Masaya as typical examples. The records from open-path Fourier
521 transform infrared spectroscopy of gas emissions at Ambrym suggest that two types of degassing
522 exist. The first one is associated to a separated gas flow, corresponding to the large bubbles
523 observed at the surface and shown to exist already at depth (Allard et al. 2016b). This is in
524 agreement with our proposed model of spherical cap bubbles and their detached bubbly wakes
525 already existing at a depth of 500 m (Fig. 11b and 11c). The second type of degassing at Ambrym
526 is due to a coupled magma-gas ascent, leading to a very shallow degassing of puffs, hence a
527 separated gas flow, possibly occurring at depths above several tens of meters below the surface
528 (Allard et al. 2016b), i.e. within the lava lake. The coupled degassing, and its resulting separated
529 gas flow within puffs, can easily be produced if the gas volume fraction associated to the small
530 bubbles is large, thereby favouring a local bubble coalescence or their simultaneous breaking at
531 the surface. The relatively frequent multimeteric CO₂-rich bubbles, 4 detected during 1h20min, on
532 5 October 2008 during a moderate period of activity (Allard et al. 2016b), suggests that the
533 separated gas flow may play a significant role in the degassing pattern, thereby reducing the gas
534 volume fraction in the conduit from that estimated by assuming gas exsolution within a fully
535 homogenous gas flow.

536 The Reynolds number of the bubbles, with a diameter of 5-10m at a depth of 100 m, 61-172 is
537 just slightly below the value of 70-100 (Table 3), suggesting that most of the time an open wake
538 can also exist at 100 m depth during this period. The existence of detached bubble wakes at 100 m

539 depth is even less questionable within the framework of the model proposed by Bouche et al.
540 (2010) and the value used for the magma viscosity, when the bubbles are larger, 12-16 m in
541 diameter (Radebaugh et al. 2016), due to their relatively large Reynolds number, 226-348,
542 respectively (Table 3). We therefore propose that the degassing at Ambrym is mostly driven by a
543 separated gas flow, induced below a depth of 500 m (Fig. 11b and 11c).

544 In the same line of reasoning, we could explore at other lava lakes the consequences of having
545 large bubbles at a depth of 500 m on the degassing pattern in the conduit. The calculation of the
546 Reynolds numbers is particularly revealing as it can show whether a wake can exist or no with a
547 threshold value of 70-100 and whether a wake is closed and laminar or open and turbulent (Fan
548 and Tsuchiya 1990). Among our choice of lava lakes, we note that the lava lake at Villarica
549 presents the largest values of the Reynolds numbers associated to driving large bubbles, even for
550 the largest value of the viscosity associated to the undegassed magma, 18 Pa.s (Table 3). The
551 Reynolds numbers of 556-1990 are slightly below the transition for a fully turbulent rise for the
552 large bubble, 2000 (Bouche et al. 2010). It only requires a decrease in viscosity by a factor 2 to
553 place a typical driving large bubble, such as those observed (Gurioli et al. 2008), in the fully
554 turbulent regime. This could perhaps be envisioned, as the maximum value of the initial dissolved
555 water is very high, 4 wt% (Witter et al 2004).

556 In summary, the main restriction is related to the assumption of equilibrium degassing, shown
557 to be appropriate at Masaya and incorrect at Erta 'Ale (De Moor et al. 2013). This is perhaps a
558 possibility to consider or discard in the future, given the suggestion that the mixing of fluids
559 between the degassing and degassed magma is turbulent at Villarica in contrast to Erebus and
560 Kilauea (Moussallam et al. 2016).

561 The calculation of the Reynolds numbers, associated to a given period during which the
562 measurements of the bubble volumes are performed, is dependent of the vigour of the lava lake,
563 which can anywhere between quiet or vigorous. This variation in activity emphasises the need for
564 continuous measurements. However, the technology to set continuous measurements even at low-
565 danger lava lakes is complicated and/or costly, as for the records from open-path Fourier
566 transform infrared spectroscopy, or the data analysis is very long to perform automatically and
567 requires enormous amount of computer memory and storage, as for the video's measurements in
568 the visible, infra-red or ultra-violet range of recordings.

569

570 **Strombolian activity at Erebus, Stromboli and Yasur**

571 **Petrology and magma viscosity**

572 Erebus, Yasur and Stromboli are textbook examples of open-vent volcanoes that maintained long-
573 term steady-state behaviour (centuries). As the magma is continuously degassing and losing
574 temperature at the vents it crystallises and its viscosity significantly varies.

575 At Erebus, the mineral assemblage found in phonolitic lavas and tephra has not changed in
576 composition for at least ~17 ka (Kelly et al. 2008). At $950 \pm 25^\circ\text{C}$, the anorthoclase bearing
577 phonolite is almost dry ($\text{H}_2\text{O} < 0.2 \text{ wt}\%$ versus 1-2 wt% in the parental basanite) (Moussallam et al.
578 2013; 2015; Sims et al. 2021), its viscosity is calculated to be $10^{6.3} \text{ Pa}\cdot\text{s}$ (Le Losq et al. 2015) for 30
579 vol% anorthoclase, an amount of megacrystals that is kept constant through time (Kelly et al. 2008).

580 The temperature of the anorthoclase-bearing phonolite at Erebus is relatively high with respect to
581 those of water-rich phonolites. Values of $760\text{-}780^\circ\text{C}$ and $840\text{-}870^\circ\text{C}$ are reported for the phonolitic
582 magma of Laacher See (Rout and Wörner 2020) having 4.0-3.6 wt% H_2O (Harms and Schmincke
583 2000); $800\text{-}850^\circ\text{C}$ for 3.0-2.5 wt% H_2O at Tenerife, 935°C for 3 wt% H_2O at Tambora; and
584 $815 \pm 10^\circ\text{C}$ for the 79AD phonolite having 6.2 wt% H_2O at Vesuvius and even lower ($785\text{-}800^\circ\text{C}$)
585 for the other Vesuvius phonolites for a range of H_2O content between 7.5 and 3.5 wt% H_2O
586 (Andùjar and Scaillet 2012). Moussallam et al. (2015) propose that the CO_2 flux sustains the
587 convective motion observed at Erebus with recycling of degassed magma in accordance with a bi-
588 directional flow model in the conduit (see details in separated section). This is in agreement with
589 the coexistence of two magma batches differing by their temperature and viscosity in a single
590 conduit up to a depth of ~30 m, where the descending cold magma could be at least 100°C colder
591 than the ascending flow of bubbly magma coming from 2-3 km (Molina et al. 2015). A temperature
592 range from 950°C to $1000\text{-}1050^\circ\text{C}$ would signify a change in viscosity of at least one order of
593 magnitude ($10^{6.3}\text{-}10^{5.3} \text{ Pa}\cdot\text{s}$ and possibly as high as $10^7 \text{ Pa}\cdot\text{s}$) (Le Losq et al. 2015.)

594 At Yasur, Firth et al. (2014) suggested that strombolian-style activity has persisted in its current
595 form for the last 630–850 years from their study of recently exposed tephra sequences. They show
596 that the emission rate is constant with $\sim 5.7 \times 10^5 \text{ kg}$ per day expelled magma volume of basaltic
597 trachyandesitic magma. Neither the crystallisation temperatures nor the major and trace element
598 composition of Yasur magma vary significantly over nearly 800 years activity (Firth et al. 2014).
599 The magma supply rate, calculated on the basis of the SO_2 flux and the sulphur content of olivine
600 hosted melt inclusions (Tables 1 and 2), achieves nearly 0.05 km^3 per year (Métrich et al. 2011;
601 Woitischek et al. 2020). Woitischek et al. (2020) propose when assuming equilibrium conditions,
602 that the degassed shallow conduit at Yasur consists of a crystal-rich region with a thickness of at
603 least 0.6 and up to 2 km, if extensive crystallisation is driven by H_2O degassing at equilibrium
604 following Métrich et al. (2011). In these conditions, the proportion of crystals increases from 10 to
605 32 vol% on degassing. Calculations, using a software called MELTS (Ghiorso and Gualda 2015),

606 indicate that the bulk magma effective viscosity would vary from 5.8×10^2 Pa.s prior to degassing to
607 1.5×10^5 Pa.s after degassing and crystallisation, with H₂O from 1.1 wt% to 0.2 wt% respectively
608 (Woitischek et al. 2020). While the trachyandesitic magma at Yasur is degassing and crystallising,
609 the SiO₂ concentration of the residual melt changes to reach 59 wt% (Métrich et al. 2011).
610 Simultaneously, its viscosity becomes $10^{3.4}$ Pa.s for a water concentration of 0.3-0.2 wt% and using
611 Giordano et al.'s model (2008). A volume fraction of crystals of ~ 30 % increases the viscosity by
612 0.5-1.0 log unit depending on their aspect ratio (Mader et al. 2013; Le Losq et al. 2015). It means
613 that the Yasur conduits may be capped by a relatively viscous magma in agreement with
614 equilibrium calculation of Woitischek et al. (2020).

615 At Stromboli, a magma supply rate of ~ 0.1 km³ per year is needed to sustain the long-term
616 average of SO₂ flux (220-260 tons per day (Allard et al. 2008) (Tables 1 and 2). The major element
617 compositions of most degassed shoshonitic pyroclasts vary in a very restricted range (Pompilio et
618 al. 2011) as do the percentage of crystals (Landi et al. 2004; 2006; 2009). In contrast, a complex
619 zoning of phenocrysts, particularly of plagioclase, has been reported for a long time, supporting
620 processes of magma mixing and up and down motion. As an example, the modal analysis of a series
621 of 12 crystal-rich scoriae samples covering a period from 1986 to 2000 indicates 48 to 55 vol%
622 crystals made of plagioclase (27-38 vol%), clinopyroxene (16-10 vol%) and olivine (2-5 vol%)
623 (Landi et al. 2004). Modal analysis performed on 9 lava samples of the 2002-2003 lava flow
624 provide similar results with 41 to 54 vol% (38 vol% in one sample) and similar proportions of
625 plagioclase (23-34 vol%), clinopyroxene (5-19 vol%), olivine (2-8 vol%) (Landi et al. 2006). In the
626 2007 lava samples (9 samples analysed) the proportion of phenocrysts varies from 45 to 51 vol%
627 (plagioclase 29-33 vol%; clinopyroxene 11-14 vol%; 4-5 vol%) (Landi et al. 2009). The melt
628 viscosity reaches $10^{2.7}$ Pa.s at 1100°C, when using Giordano et al.'s model (2008) and a water
629 concentration of 0.3-0.2 wt%.

630 Erebus, Yasur and Stromboli conduits may be capped by degassed and relatively viscous
631 magmas (10^4 Pa.s) when assuming equilibrium conditions. They contain a significant proportion of
632 crystals from nearly 30 vol% (Yasur, Erebus) up to 55 vol% (Stromboli), for temperature range
633 from 950°C (Erebus) to 1110-1120°C (Yasur, Stromboli). At Stromboli, a crystal content of 45 vol
634 % corresponds to an increase in viscosity by a factor of 0.6-0.9 log unit, while a crystal content of
635 55 vol% leads to an increase by 1.2 to nearly 1.8 orders of magnitude (Fig. S1c). In these
636 conditions, the magma existing during the classical strombolian activity has a viscosity of 500-820
637 Pa.s and 650-1000 Pa.s for 45 vol% and 55 vol% of crystals, respectively.

638

639 **Input from surface measurements**

640 Erebus, Stromboli and Yasur are well-studied strombolian volcanoes.

641 The description and quantification of the surface activity at Erebus, which can safely be
642 observed from above (Fig. 6) are superbly done either using gas studies (Oppenheimer and Kyle
643 2008; Oppenheimer et al. 2009; 2011; Boichu et al. 2010; Ilanko et al. 2015a; 2015b) and/or
644 geophysical studies, which include videos, infrasound, seismicity and radars (Rowe et al. 2000;
645 Dibble et al. 2008; Johnson et al. 2008; Jones et al. 2008; Aster et al. 2003; 2008; Gerst et al.
646 2008; 2013). The degassing at Erebus (Dibble et al. 1988; Rowe et al. 2000; Dibble et al. 2008) is
647 also mainly two-fold. It takes the form of rare explosions (Johnson et al. 2008; Peters et al.
648 2014b), whose gas is initially strongly overpressurised, here called active degassing, and of more
649 frequent (each 11 min) and much smaller gas releases, associated to a very small gas overpressure
650 (blue cloud on photo small bubble breaking on Fig. 6; Oppenheimer et al. 2009; Peters et al.
651 2014b; Ilanko et al. 2015a and 2015b), hence here called passive degassing, and similar gas
652 puffing. Gas studies have been restricted to short continuous periods, the longest lasting 10 hours
653 (Fig. 6d; Oppenheimer et al. 2009) and mostly mostly focused on the passive degassing
654 (Oppenheimer and Kyle 2008; Peters et al. 2014b, 2018; Ilanko et al. 2015a) rather than on the
655 explosions, which only occurred on average 3-6 times a day (Jones et al. 2008; Oppenheimer et al.
656 2009; Oppenheimer et al. 2011; Ilanko et al. 2015b). In contrast, infrasonic, seismic and radar
657 measurements, which have been run continuously for several days, were able to constrain many
658 physical parameters, such as velocities and gas volumes, and mechanisms occurring at the vent
659 (Johnson et al. 2008; Jones et al. 2008; Aster et al. 2003; 2008; Gerst et al. 2008; 2013). Estimates
660 of gas volume from explosions have been obtained from infrasonic measurements to vary between
661 10^3 and 3×10^4 m³ (Johnson et al. 2008; Table 3). Gas puffing, although markedly smaller than
662 explosions (Fig. 6d), could nevertheless significantly contribute to the gas fluxes due to their
663 occurrence (Oppenheimer and Kyle 2008; Peters et al. 2014b, 2018; Ilanko et al. 2015a). Aster et
664 al. (2003; 2008) showed that the Very Long Period of the seismic records (VLP) at Erebus could
665 be very well explained by the response of the magma column to the ascent of a Taylor bubble
666 (Fig. 3c) and its subsequent disequilibrium, in agreement with the laboratory experiments (Ripepe
667 et al. 2001). The moment tensor inversion of the VLP events provided an estimate of the average
668 displaced mass of magma, 8×10^7 kg for an acceleration of 1 m²/s (Aster et al. 2008). This mass
669 can be contained in a conduit radius of 5.6 m, when assuming a magma column height of 400 m
670 (Aster et al. 2008), in perfect agreement with observations of the conduit radius at the surface, 5-
671 10 m (Dibble et al. 2008; Oppenheimer et al. 2009). The oscillation in volume of the rising Taylor
672 bubble (Fig. 3c), detected by using an array of 3 radars, showed that most of their gas overpressure

673 in the conduit is released by these precursory oscillations rather than during their bursting (Gerst et
674 al. 2013). They also show that the sound of the explosion is related to the bursting rather than by
675 the bubble volume oscillation, in contrast to what had been proposed at Stromboli (Vergniolle and
676 Brandeis 1994; 1996). The difference in the bursting mechanism of large bubbles between Erebus
677 and Stromboli is likely to result from the large differences in magma viscosity, which are $10^{6.3}$ Pa.s
678 (Le Losq et al. 2015) and $10^{2.7}$ Pa.s calculated using Giordano et al. (2008), respectively. The case
679 of Erebus illustrates the importance of having an accurate estimate of the magma viscosity. The
680 Taylor bubbles (Fig. 3c) associated to the explosions have been considered to be able to grow a
681 wake at their bottom, when using the viscosity previously estimated to be ~ 1600 Pa.s (Kyle et al.
682 1992; Calkins et al. 2008), a value now considered as too low (Le Losq et al. 2015). However, this
683 mechanism is now shown to be impossible when using the updated value of the magma viscosity
684 of $10^{6.3}$ Pa.s (Le Losq et al. 2015), because their Reynolds number is very small (Table 3). This
685 drastic change in the interpretation of the degassing pattern, at the surface and in the conduit,
686 shows the key role of magma viscosity in understanding the eruptive behaviour. The result
687 associated to this updated magma viscosity is in perfect agreement with the finding of
688 Oppenheimer et al. (2009) and Moussallam et al. (2016), who have suggested that the degassing at
689 Erebus is driven by a stable bi-directional flow, in which the new batch of magma regularly
690 replaces the degassed sinking magma.

691 The degassing at Stromboli has been extensively described (Fig. 12) and quantified by gas and
692 geophysical studies (Harris and Ripepe 2007; Ripepe et al. 2008; Ripepe et al. 2005; Del Donne
693 and Ripepe 2012; Pering et al. 2020; Thivet et al. 2021). The main techniques, which have been
694 used separately or simultaneously, consist into 1) videos in the visible and infrared range and
695 rarely high-speed cameras (Patrick et al. 2007; Harris et al. 2012; Taddeucci et al. 2012a, b; Harris
696 et al. 2013; Gaudin et al. 2014a; 2014b; Bombrun et al. 2015; Gaudin et al. 2017); 2) DOAS,
697 multi-gas, open-path Fourier transform infrared spectroscopy, ultraviolet-cameras for gas studies
698 (Burton et al. 2007; Aiuppa et al. 2010; Tamburello et al. 2012), 3) infrasound, seismicity and
699 radar for geophysical studies (Weill et al. 1992; Vergniolle and Brandeis 1994; 1996; Chouet et al.
700 1999; 2003; Scharff et al. 2008; Genco and Ripepe 2010; Del Donne et al. 2016; Patanè et al.
701 2017) and 4) laboratory experiments and models (Lane et al. 2013; Del Bello et al. 2012; 2015). It
702 is now well understood that the degassing at Stromboli is also mainly two-fold, with the weak
703 puffs, which occurs quasi-permanently at the central vents but can also exist at times at the
704 northeastern and southwestern vents (Harris and Ripepe 2007; Gaudin et al. 2017; Pering et al.
705 2020) and the explosions, whose physical parameters, such as ejecta and gas velocities or gas
706 volumes, are now well known (Harris and Ripepe 2007; Patrick et al. 2007; Harris et al. 2012;

707 Taddeucci et al. 2012a, b; Gaudin et al. 2014a; 2014b; Bombrun et al. 2015; Thivet et al. 2021).
708 Gas volumes from explosions have been estimated to be 2-100 m³ (Vergnolle and Brandeis 1996),
709 20-35 m³ (Ripepe and Marchetti 2002), 400 m³ (Tamburello et al. 2012) whereas the gas volumes
710 in the puffs only reach 19-211 m³ (Harris and Ripepe 2007), 1.4-21.5 m³ (Tamburello et al. 2012),
711 1-100 m³ (Gaudin et al. 2017). The occurrence of puffs, each 1 to 2 seconds, is responsible for the
712 major contribution of passive degassing to the total gas flux, > 95 %, (Ripepe and Marchetti 2002;
713 Ripepe et al. 2008; Gaudin et al. 2017). Explosions and puffs at Stromboli differ significantly in
714 their gas overpressure, large or small for explosions and puffs, respectively, and in a lesser extent
715 on their gas volumes, large or small for explosions and puffs, respectively. They also differ in their
716 depth of formation, 3 km for the deepest explosions and very shallow (11-150 m), for puffs
717 (Burton et al. 2007). Hence explosions correspond to active degassing while puffs belong to the
718 passive degassing.

719 To a lesser extent among the well-studied volcanoes, there is Yasur (Fig. 13a). Gas studies
720 (Bani and Lardy 2007; Bani et al. 2012; Oppenheimer et al. 2006; Woitischek et al. 2020), visible,
721 thermal and high speed videos (Bani et al. 2013; Gaudin et al. 2014a; 2014b; Gomez and Kennedy
722 2017) together with seismic, infrasonic and radar measurements (Nabyl et al. 1997; Battaglia et al.
723 2012; 2016a, b; Kremers et al. 2013; Marchetti et al. 2013; Spina et al. 2016; Meier et al. 2016;
724 Jolly et al. 2017; Iezzi et al. 2019; Simmons et al. 2020; Perring et al. 2019; Fee et al. 2021) have
725 in the past 20 years help to constrain the eruptive pattern. Some of these studies have also shown
726 two classes of degassing (Oppenheimer et al. 2006; Bani et al. 2013; Meier et al. 2016; Kremers et
727 al. 2013; Marchetti et al. 2013; Spina et al. 2016; Simmons et al. 2020; Fee et al. 2021), although
728 in practice a continuum of degassing events may exist (Gaudin et al. 2017). The frequent and
729 weakly overpressurised events on one side and the less frequent but strongly overpressurised
730 events on the other side are also examples of passive and active degassing, referred by Spina et al.
731 (2016) as minor and major events. Explosions at Yasur are very frequent, one per 1-2 min (Spina
732 et al 2016; Woitischek et al. 2020), while the minor events occurs as frequently as one event each
733 1-5 min (Bani et al. 2013; Fee et al. 2021) to 40 per min (Spina et al. 2016). The gas volumes of
734 the strong explosions have been estimated for at 5-80x10³ m³ from infrasound modelling during a
735 vigorous period (Iezzi et al. 2019) and on average at 14.25x10³ m³ from open-path Fourier
736 transform infrared spectroscopy combined with SO₂ flux measurements during an average period
737 (Woitischek et al. 2020).

738 These three laboratory open-vent volcanoes clearly show that degassing consists in both a
739 strong and a weak degassing, here referred to as active and passive degassing, respectively. In this

740 respect, the active degassing at Erta 'Ale (spherical cap bubble; Fig. 3a) shares a similar origin
741 than explosions at Stromboli and Erebus and to the major explosions at Yasur.

742 The strength of active degassing can be quantified by the maximum gas flux. Here we report
743 values that can be compared together because they all derive from modelling the acoustic waves.
744 The maximum gas fluxes reach 510 m³/s at Erta 'Ale (Bouche et al. 2010), 680 m³/s at Stromboli
745 (Vergnolle and Brandeis 1996), 3x10³ - 6x10⁴ m³/s at Yasur (Iezzi et al. 2019), and 7x10³ - 7x10⁴
746 m³/s at Erebus (Johnson et al 2008). It is tempting to relate the difference in strength to the
747 respective viscosities of undegassed and degassed magma that range from 22-27 Pa.s (Erta 'Ale),
748 500 - 10³ Pa.s (Stromboli), 5.8 ×10² - 1.5 ×10⁵ Pa.s (Yasur), up to 10^{6.3} Pa.s (Erebus). Similarly,
749 the small gas release at Erebus (blue cloud; Fig. 6) should be compared to the puffs of Stromboli,
750 to the minor events at Yasur or to the flat bubbles at Erta 'Ale, although at Erta 'Ale additional
751 effects exist because of the cold crust.

752 This interpretation of the strombolian activity with a well identified two-fold degassing could
753 be applied more broadly. Therefore time series need to be much larger than the typical return time
754 of active degassing, if the goal is to assess its associated eruptive pattern. This may become a
755 challenge at Erta 'Ale, from the relatively short time series possible in gas studies (Sawyer et al.
756 2008), as well as at Erebus, due to rarity of explosions, 4-6 per day (Rowe et al. 2000; Burgisser et
757 al. 2012; Jones et al. 2015) and at Villarica (Sawyer et al. 2011; Moussallam et al. 2016).

758

759 **Vulcanian activity at open-vent volcanoes**

760 Our selection of open-vent volcanoes, associated to intermediate to high-silica magma
761 compositions, may present short vulcanian explosions. It occurs at Arenal (Mora et al. 2022; Fig.
762 13b-d), Fuego (Morrissey et al. 2008; Marchetti et al. 2009; Diaz-Moreno et al. 2020),
763 Popocatepetl (Schaaf et al. 2005; Fig. 14a-b) and Santiaguito (Fig. 14c; Rose 1972; Rose et al.
764 1987; Harris et al. 2002; 2003; Bluth and Rose 2004; Johnson et al. 2004b; Sahetapy-Engel et al.
765 2008; Sahetapy-Engel and Harris 2009a, 2009b; Marchetti et al. 2009; Johnson et al. 2011; Scott
766 et al. 2013). A vulcanian explosion can be produced by the disruption of a solid cap suddenly
767 failing under a significant underlying gas overpressure. The overpressurised gas is suddenly
768 released and often leads to the formation of small eruptive columns of a few kilometers high or
769 above and sometimes with pyroclastic dense flows (Clarke et al. 2013). The gas ejection at the
770 vent is short compared to the rising time of the eruptive columns, making the initial injection of
771 the gas in the atmosphere sustained by an initial pulse of overpressurised gas rather than by a
772 continuous gas flow feeding the eruptive column.

773 The pre-eruption pressure and ejection velocity are relatively high, <1-10 MPa and 400 m/s
774 (Morrissey and Chouet 1997; Arciniega-Ceballos et al. 1999, 2012; Chouet et al. 2005; Clarke et
775 al. 2013). A shock wave, i.e. a pressure discontinuity, is produced in air upon disruption of the
776 plug and travels into the atmosphere at a velocity exceeding that of the sound, while a
777 decompression-induced fragmentation propagates down into the conduit (Kieffer 1981; Turcotte et
778 al. 1990; Woods 1995). This fragmentation, inducing the formation of ejecta, only occurs in the
779 shallowest portion of the conduit (Clarke et al. 2013). The magma left in the conduit cools until
780 being sufficiently cold and rigid to seal the top of the magma column. Meanwhile, some
781 vesiculation occurs below, inducing the building-up of pressure, ultimately responsible for the
782 next vulcanian explosion (Clarke et al. 2013).

783 Several volcanoes, such as Arenal (Mora et al. 2022), sometimes Fuego (Martin and Rose
784 1981; Morrissey and Mastin 2000), and perhaps Santiaguito with the small and strong ash-and-gas
785 explosions, are able to switch between periods of vulcanian explosions and periods of strombolian
786 explosions. This implies that a drastic change of conditions, between a mechanically sealed vent
787 and an open vent, can occur at the vent, although perhaps one vent can be sealed while another
788 one is simultaneously unsealed, as recently proposed for Arenal (Mora et al. 2022). The
789 conditions, which prevail at such transitions, have not yet been clearly identified. Alternatively,
790 Clarke et al. (2013) had proposed that the difference between strombolian and vulcanian
791 explosions results in the bubble motion, largely separated or stagnant in the magma, respectively.

792 Popocatépetl is also remarkably surprising because the dome prior to a vulcanian explosion is
793 seen rising and growing into the conduit (R. Campion, pers. com., 7 July 2021; Fig. 14a and 14b),
794 invalidating the conditions of a fully sealed vent. Furthermore the SO₂ flux is always quite high,
795 (Table 2b; Campion et al. 2018). This high SO₂ flux exists not only during vulcanian explosions
796 but also between 2 successive vulcanian explosions. This observation also appears to be
797 incompatible with the condition of a fully mechanically sealed vent. The detection by a thermal
798 camera of one or two circular hot zones, of 20-50 m in diameter, is likely to be associated to the
799 gas percolation (R. Campion, pers. com., 7 July 2021).

800 In contrast, Santiaguito, which mostly display dacitic domes and sometimes, vulcanian
801 explosions (Yamamoto et al. 2008; Scharff et al. 2012) as at Popocatépetl, has a surprisingly low
802 SO₂ flux (Table 2b). The classification of explosions at Santiaguito is still a matter to debate, from
803 a closed vent prior to explosions to a fully open vent. Explosions are considered as weak vulcanian
804 explosions (Johnson et al. 2011), or referred to as small to moderate gas-and-ash explosions (De
805 Angelis et al. 2019; Wallace et al. 2020), rather than strombolian explosions (Bluth and Rose
806 2008), while the vent is sometimes considered as fully open for degassing (Holland et al. 2011).

807 The level of the dome at the conduit varies at different periods (Lamb et al. 2019; Gottschammer
808 et al. 2021). To our knowledge, no photographic evidence exists of a high-level dome being
809 systematically emplaced prior to a vulcanian explosion. But the dome extrusion, often cyclic, is a
810 frequent feature of its long-lasting eruption (Rose 1972; Rose et al. 1987; Harris et al. 2002;
811 2003). The initiation of a vulcanian explosion had been beautifully caught by a video taken from
812 above, showing that an explosion starts with a very weakly overpressurised degassing on an
813 annulus prior to the entire disruption of the solid cap in one unit from the center of this circle, as
814 initially quantified by Bluth and Rose, (2008). This may be indicative that the eruptive pattern is
815 similar at Popocatepetl and Santiaguito, although with two contrasting SO₂ fluxes (Table 2b) and
816 perhaps different amplitudes in the variations of level of magma in the conduit. The strength in the
817 explosions is also different at Popocatepetl and Santiaguito, typical and weak, respectively
818 (Marchetti et al. 2009; Johnson et al. 2011; Scharff et al. 2012).

819 The differences between vulcanian and strombolian explosions have been tentatively quantified
820 by looking at the simultaneous thermal and infrasonic records performed at Villarica, Stromboli,
821 Fuego and Santiaguito (Marchetti et al. 2009). Strombolian explosions at Stromboli and Villarrica
822 present relatively low values of thermal radiation energy, consistent with the short explosive
823 events of these two volcanoes. In contrast, the longer-lasting thermal waveforms observed for
824 explosions at Santiaguito and Fuego result in the longer ash plume dynamics, which corresponds
825 to high values of thermal radiation energy. However, Santiaguito and Villarrica share similar
826 infrasonic energies, both being lower than the values produced by explosions at Stromboli and
827 Fuego (Marchetti et al. 2009). This may be associated to the very low level of activity both at
828 Villarrica and Santiaguito during this period. The relationship between infrasonic energy, used as
829 a proxy of gas thrust, and the difference between infrasonic and thermal energies, used as a proxy
830 of buoyancy, shows that strombolian and vulcanian explosions are organised in two very different
831 clusters of points, suggesting a method to fully quantified these types of activity (Marchetti et al.
832 2009). Furthermore, combining thermal and infrasonic records on open-vent volcanoes opens an
833 avenue for a quantified description of surface activity. These joined records could be used for
834 deciding whether the vent is properly sealed or open and also for understanding how the
835 transitions between regimes can occur at a single volcano.

836

837 **Thermal models**

838 Open-vent volcanoes must release both gas and heat in order to maintain a persistent activity and
839 one key ingredient to maintain an open-vent volcano active is to reduce the heat loss. We discuss

840 below three mechanisms by which heat transfer can occur, mainly conduction, thermal convection
841 and arrival of hot magma through bubbly wakes.

842

843 **Thermal models of lava lakes**

844 The radiated heat output had been measured at several volcanoes, mostly at the surface of lava lakes
845 in relatively close proximity, such as at Erta 'Ale (Burgi et al. 2002; Harris et al. 2005; Spampinato
846 et al. 2008), Erebus (Calkins et al. 2008), Nyiragongo (Spampinato et al. 2013) and Kilauea
847 (Spampinato et al. 2012). But thermal measurements have also been done by satellites (Ramsey and
848 Harris 2013), and routinely such as by MODIS (Harris et al. 1999; Copola et al. 2016; Vergniolle
849 and Bouche 2016; Wright 2016; Aiuppa et al. 2018; Naismith et al. 2019) or by SEVERI (Field et
850 al. 2012).

851 Thermal models of lava lakes, initially performed without considering the convection (Peck et al.
852 1977), aimed at modelling the cooling of lava lakes, thereby estimating the thickness of the crust as
853 a function of time and quantifying the role of small bubbles in stopping of convection (Worster et
854 al. 1993; Davaille 1993). The quantification of the heat budget of a lava lake or a magma reservoir
855 requires the knowledge of the in and out heat fluxes. The heat transfer occurs by conduction for thin
856 lava lakes as well as by thermal convection, if its thickness exceeds a critical value (Davaille 1993).
857 The cooling is very slow for a sole thermal conduction, such as for the thinnest lava lakes at Kilauea
858 (Davaille 1993) and at Erebus, whose magma depth in the crater area is only of a few tens of meters
859 (Jones et al. 2015). Once the thermal convection sets in, the heat losses are drastically enhanced.
860 Several additional factors can prevent thermal convection to exist, such as a gas volume fraction
861 exceeding 0.6 vol% (Davaille 1993), as for the cooling of the Makaopuhi lava lake (Hawaii), or the
862 settling of large crystals (Carrigan 1987) as for the Kilauea Iki lava lake (Helz, 1987; Davaille
863 1993; Jellinek and Kerr 2001). Additionally, the thickness of the solid crust growing at the surface
864 has been modelled under the assumption of a strong thermal convection within the lava lake
865 (Worster et al. 1993).

866 The temperature contrast between the magma within the lava lake and its surroundings rocks
867 should lead to its cooling if given a sufficient time. This occurs briefly at the lava lake of Erta 'Ale
868 for several months around December 2004 (Fig. 7c). At this time, the degassing occurred at the site
869 of the 3 hornitos, located above the underlying conduits (Fig. 7c; Vergniolle and Bouche 2016).
870 Furthermore, the existence of hornitos, which could result from the local accumulation of ejecta
871 able to reach the surface of the partially encrusted lava lake rather than falling back within the lava
872 lake, showed that the Strombolian explosions were still ongoing at this time. Therefore, lava lakes
873 never cooled entirely, hence could restart as a hot lava lake when the solid crust disappeared.

874 The lava lake at Villarrica, when encrusted, has small openings by which the degassing can
875 occur (Gurioli et al. 2008; Goto and Johnson 2011; Johnson et al. 2018). The comparison between
876 Villarrica and Erta 'Ale lava lakes suggests that the openings at Villarrica may be located above
877 the underlying conduits. However the lack of a small structure around the openings at Villarrica
878 suggests that the level of the underlying lava lake is further away from its solid crust than that at
879 Erta 'Ale, as also suggested from acoustic records (Johnson et al. 2018).

880 The observed lack of cooling of lava lakes has been first explained by the arrival of hot magma
881 brought to the surface by convective processes, driven by a density difference between a volatile-
882 rich magma and a degassed magma. This model, here referred to as a bi-directional flow model
883 (Fig. 15) considers that the hot and gas-rich magma rises while the degassed and cold magma falls
884 back in the conduit (Francis et al. 1993; Kazahaya et al. 1994; Stevenson and Blake 1998;
885 Oppenheimer and Francis 1998; Harris et al. 1999; Oppenheimer et al. 2004; Witter et al. 2004;
886 Harris et al. 2005; Jones et al. 2006; Huppert and Hallworth 2007; Harris 2008; Palma et al. 2011;
887 Beckett et al. 2011; 2014). The bi-directional flow models of Stevenson and Blake, (1998; Fig.
888 15a) and Huppert and Hallworth, (2007; Fig. 15c) were used at Nyiragongo to estimate both the
889 conduit diameter and the net magma flux necessary to maintain its giant lava lake ($> 15 \times 10^6 \text{ m}^3$) in
890 a molten state (Burgi et al. 2014; 2020).

891 Alternatively the heat could be transferred from depth to the lava lake by the arrival of bubble
892 clusters, initially formed in the wake produced at the bottom of the driving spherical cap bubbles
893 during their rise in the conduit (Bouche et al. 2010; Fig. 11). The heat brought to the lava lake is
894 provided by the interstitial magma initially present in the bubbly wake prior to its fragmentation in
895 the lava lake (Bouche et al. 2010) rather than that solely brought by the series of small hot
896 bubbles, as incorrectly deduced for Villarrica and Kilauea (Moussallam et al. 2016). The key point
897 of the qualitative thermal model of Bouche et al. (2010) is that the hot magma added to the lava
898 lake had been kept hot because it had travelled from depth to the surface at a relatively large
899 velocity, that of the driving spherical cap bubble. The second point is that this mechanism for heat
900 transfer is only possible if the rise of the large bubbles is sufficiently vigorous to grow an instable
901 wake, laminar or a turbulent for Reynolds number of 70(100) - 2000 and >2000 , respectively
902 (Bouche et al. 2010). At Erebus, the large bubbles responsible for explosions cannot grow a wake
903 when using the updated value of the viscosity $10^{6.3} \text{ Pa.s}$ (Le Losq et al. 2015), in agreement with
904 the findings that the behaviour of the lava lake is governed by a magma exchange rather than by
905 an underlying gas flux from the reservoir (Peters et al. 2014b). The heat at Erebus is therefore
906 provided either by magma upwards motion in a bi-directional flow in the conduit (Oppenheimer et
907 al. 2009, 2011; Moussallam et al. 2015) or by the enthalpy of the shallow reservoir (Aster et al.

908 2003), located either at 400 m (Aster et al. 2008) or between 80 m and 1300 m, when assuming
909 that the volatile species are at equilibrium (Burgisser et al. 2012), or by a combination of the two.
910 A source of heat, which combined the enthalpy of the shallow reservoir with a bi-directional flow
911 in the conduit, is our preferred interpretation, given the comparatively large conduit diameter at
912 Erebus, 4-10 m (Dibble et al. 2008; Oppenheimer et al. 2009), which exceeds the value of 1 m
913 proposed to balance the heat loss from the conduit walls with the assumed magma supply rate in
914 the conduit at Stromboli (Giberti et al. 1992).

915 It is particularly important to realise that lava lakes, which expose large hot areas to the surface,
916 have a sole or an additional source of heat, which is provided by the existence of the detached
917 bubbly wakes (Fig. 11), when compared to open-vent volcanoes only presenting tops of magma
918 columns. The thermal effect at lava lakes, associated to the possible existence of detached bubbly
919 wakes, is complicated to calculate in detail because it requires to know both the occurrence of the
920 driving large bubbles on a long time scale, due to fluctuations in the level of activity, and the local
921 gas volume fraction in the conduit.

922 Several main types of degassing at lava lakes can exist. On one side, the existence of detached
923 bubbly wakes at depths of > 1 km and > 500 m-1 km at Erta 'Ale and Nyiragongo, respectively
924 (Table 3; Fig. 11a), suggests that their heat could be a significant source over the entire length of
925 the conduit up to 1 km. Hence it would promote efficient exchange of heat between this depth and
926 the surface during the rise of the driving large bubbles. On the other side, the detached bubbly
927 wakes may mostly exist at depths and be partially or fully suppressed in the conduit, such as at
928 Villarrica and Ambrym at times (Table 3; Fig. 11b and 11c), respectively, but still play a key role
929 in providing heat or in decreasing the gas volume fraction by favouring the separated gas flow.

930

931 **Thermal models in conduit**

932 The first model considered that the magma undergoes thermal convection in the conduit (Carrigan
933 1983). In this case, ascending hot (possibly gas-rich) magma mixes with the magma residing in the
934 conduit and the cooling occurs at the expense of the reservoir enthalpy (Carrigan 1983). The second
935 model that was applied to Stromboli suggested that thermal convection could be ignored due to both
936 the small diameter of the conduit and the constant rise of large bubbles in the conduit (Giberti et al.
937 1992). They suggested that the only communication between magma reservoir and conduit occurs
938 after an explosion when the magma level in the conduit had returned to its equilibrium value, an
939 interpretation fully validated by laboratory experiments (Ripepe et al. 2001) and by the location of
940 the tremor and Very Long Period events (Chouet et al. 1999; 2003). The numerical model of Giberti
941 et al. (1992), which considers a large reservoir located below a small conduit, showed that the

942 persistent state of Stromboli could be very well be explained by a shallow reservoir at a few
943 hundreds of meters below the vent, a result entirely validated by further independent studies
944 (Chouet et al. 1999; 2003; Harris and Ripepe 2007). The same model could be partly applicable to
945 Erebus, which presents a shallow reservoir at a depth of 400 m (Aster et al. 2003; 2008), and a
946 conduit slightly larger than twice that at Stromboli (Dibble et al. 2008; Oppenheimer et al. 2009).

947

948 **Bi-directional flow models in conduit**

949 Another potential convective mechanism, that may occur in the conduit, is driven by the density
950 difference between a hot and volatile-rich magma, light and rising, and a cold and volatile-poor
951 magma, hence dense, flowing in opposite direction (Fig. 15a). This mechanism is based on an
952 exchange flow in the conduit (Kazahaya et al. 1994; Harris and Stevenson 1997; Stevenson and
953 Blake 1998). The excess degassing observed at the surface of Stromboli, estimated when comparing
954 the volumes expelled by gas and magma during strombolian explosions (Chouet et al 1974; Ripepe
955 et al. 1993; Patrick et al. 2007; Ripepe et al. 2008; Delle Donne and Ripepe 2012; Harris et al.
956 2012; Harris et al. 2013; Gaudin et al. 2014b), had been explained by the existence of such a flow
957 loop. This bi-directional flow is a potential mechanism for explaining both the persistent outgassing
958 and providing heat for the thermal budget of conduits and lave lakes.

959

960 **Existing models**

961 Several models, now referred as bi-directional flow models (Fig. 15), were developed with various
962 assumptions detailed below. Several studies use this model to explain the behaviour of several
963 open-vent volcanoes, without any clear indication on how such a flow loop could be initiated in the
964 conduit and maintained for very long periods. The rising magma is degassing on its way towards
965 the surface due to gas exsolution, thereby increasing its positive buoyancy. Laboratory experiments
966 of exchange flows in vertical pipes, performed in conditions for which the net volume flux of
967 ascending magma is matched by the volume flux of the descending magma, have shown the key
968 role of the ratio of viscosities, between that of the more viscous fluid divided by that of the less
969 viscous fluid (Stevenson and Blake 1998; Huppert and Hallworth 2007; Beckett et al. 2011; Palma
970 et al. 2011). Models describing the spatial organisation of the upwards and downwards magma
971 flows in the conduit had been called bi-directional flow models (Fig. 15).

972 The pioneer quantitative work of Stevenson and Blake (1998) used laboratory experiments to
973 show that the bi-directional flow is a core-annular flow, in which the less viscous fluid flows in the
974 center and the more viscous flows in an annulus close to conduit walls (Fig. 15a). They present a

975 theoretical model for the core-annular flow, which is used to give a reasonable estimate of conduit
976 radius at Stromboli (Stevenson and Blake 1998) and Villarrica (Witter et al. 2004). Burton et al.
977 (2007b) added to the core-annular flow (Fig. 15b) the degassing path at each depth along the
978 conduit, constrained by petrology data and SO₂ flux at Stromboli but ignore the crystallisation path.
979 The rising magma is modelled to be degassing at equilibrium due to the gas exsolution. The area
980 available for the rise of the degassing magma is calculated by assuming that its velocity is
981 maximum (Burton et al. 2007b), an assumption later shown to be incorrect (Beckett et al. 2011;
982 Suckale et al. 2018). Nevertheless, this early model gave an estimate of the radius and the velocity
983 of the rising degassing magma at each depth, as well as those of the falling degassed magma
984 (Burton et al. 2007b). They also provide an estimate of the conduit radius, in agreement with radius
985 observed at the surface.

986 This model was later refined by laboratory experiments (Fig. 15c), performed for both
987 vertical and inclined conduits, and a dimensionless analysis, which included lateral gradients in
988 magma viscosity and density (Palma et al. 2011). But the properties of the rising and degassed
989 magma were taken to be constant during transport (Palma et al. 2011). This model was used to
990 constrain the degassing and ascent rates of volatile-rich magma, which, when combined with
991 petrologic data on magmatic volatile content at Villarrica, led to an estimate of the conduit radius
992 (Palma et al. 2011). Palma et al. (2011) only consider the flow in the lowest conduit, in which the
993 degassing occurs with stagnant CO₂-bubbles and ignore the shallowest conduit for which the
994 bubbles become sufficiently large to have a separated gas flow in respect to the magma, on which a
995 significant exsolution of water is added.

996 The model of Huppert and Hallworth, (2007), carefully and extensively performed to assess the
997 effects of each physical parameter, showed that the core-annular flow is the most frequent regime
998 (Fig. 15d). They also noted that the fluid may be highly irregular and may present a varicose
999 instability, sometimes leading to the fragmentation of the degassing hot magma in many discrete
1000 blobs (Huppert and Hallworth 2007). When this situation occurs, the flow of the degassing magma
1001 is not organised in the conduit as a continuous stream but as a discontinuous series of vertically
1002 spaced blobs of degassing magma. A coefficient flux, defined by a ratio of two dimensionless
1003 numbers, is used to analyse the flux of the exchange flow (Huppert and Hallworth 2007; Palma et
1004 al. 2011). This coefficient was experimentally estimated for vertical and inclined flows (Palma et al.
1005 2011). Note that these laboratory experiments were performed with fluid reservoirs at the end of the
1006 pipes to ensure a longer duration for the bi-directional flow in the conduit (Huppert and Hallworth
1007 2007; Beckett et al. 2011; Palma et al. 2011).

1008

1009 When the ratio of viscosities exceeds 75, the bi-directional flow is organised with an
 1010 axisymmetric core-annular flow (Fig. 15d), in which the less viscous fluid occupies a cylindrical
 1011 core and the denser and more viscous fluid flows downwards in an annulus (Huppert and Hallworth
 1012 2007; Beckett et al. 2011). The bi-directional flow is a side-by-side flow, for which both fluids are
 1013 in contact with the conduit walls and there is a single interface between them (Fig. 15 d), for a ratio
 1014 of viscosities less than 117 (Beckett et al. 2011). The side-by-side flow is transitional (Fig. 15d) for
 1015 a ratio of viscosities between 5 and 59 and presents simultaneously both a core-annular flow and a
 1016 side-by-side flow at different depths (Beckett et al. 2011). In this case, the flow of the degassing
 1017 magma is not a continuous stream from depth to the surface (Fig. 15d).

1018 Huppert and Hallworth (2007) use a dimensionless analysis for quantifying the flux of the dense
 1019 fluid, referred with index u for upper fluid in equations, as a function of the ratio of the two
 1020 viscosities, γ , and the Reynolds number of the upper fluid, Re_U . The dimensionless number, called
 1021 the transport number for exchange flow, Te , is defined by:

$$1022 \quad Te = \mu_u Q / (g \Delta \rho R^4) \quad (\text{Eq. 6})$$

1023 where Q , $\Delta \rho$ and g are the volume flux in either fluid in the tube of radius R , the difference in
 1024 density between the denser and the lighter fluids and the acceleration of gravity, respectively. For
 1025 low Reynolds number, two equations allow the calculation of the transport number Te as a function
 1026 of the viscosity ratio
 1027 γ

1028 (μ_u / μ_b fluid divided by that of the less viscous fluid). The coefficient is estimated from laboratory
 1029 experiment scaled by a dimensionless analysis.

$$1031 \quad Te = 0.01 \gamma \quad (\gamma \ll 1) \quad (\text{Eq. 7a})$$

$$1032 \quad Te = 0.125 \quad (\gamma \gg 1), \quad (\text{Eq. 7b})$$

1033 whereas for large Reynolds number, the transport number, Te , depends on is the value of the
 1034 Reynolds number of the upper fluid, Re_U as :

$$1035 \quad Te = 0.556 Re_U^{-1} \quad (Re_U \gg 1) \quad (\text{Eq. 8})$$

1036 where Re_U is the Reynolds number of the upper fluid.

1037 Beckett et al. (2014) showed a similar relationship, for an axisymmetric core-annular flow,
 1038 between the net magma flux of the ascending magma, Q , and the viscosity ratio between the
 1039 degassed and the volatile-rich buoyant magma components, β :

$$1040 \quad Q = 0.059 \beta^{-0.74} (g \Delta \rho R^4 / 2 \mu_b) \quad (\text{Eq. 9})$$

1041 where $\Delta\rho$ is their difference in density, μ_b is the dynamic viscosity of the buoyant component, g is
1042 gravitational acceleration and R is the effective conduit radius.

1043
1044 This model had been applied to Stromboli and combined to the degassing and crystallisation
1045 paths of the ascending and descending magmas, constrained by gas flux and melt inclusion data
1046 (Beckett et al. 2014). They propose, based on their choice of viscosity ratio, that the bi-directional
1047 flow below a depth of 3 km is a core-annular flow, in which the degassing magma rises in the center
1048 while the degassed magma flows around it (Beckett et al. 2014). Above a depth of 3 km, they
1049 suggest that the bi-directional flow is a side-by-side flow, with both ascending and descending
1050 magma adjacent to a portion of the conduit walls (Beckett et al. 2014). In this model, the degassing
1051 due to gas exsolution is assumed to occur at equilibrium and with an implicit assumption that the
1052 small bubbles embodied in the magma are stagnant (Beckett et al. 2014). The implications of such a
1053 hypothesis, also used previously at Stromboli (Burton et al. 2007b) and later at Ambrym (Allard et
1054 al. 2016b), are strong, as previously discussed. No theoretical relationship between the exchange
1055 flux and the pressure gradient so far exists (Beckett et al. 2014), limiting volcanological
1056 applications to the use of empirical laws, such as the coefficient flux (Huppert and Hallworth 2007;
1057 Palma et al. 2011) or that of Beckett et al. (2014) used at Ambrym (Allard et al. 2016b). The core-
1058 annular flow, the most common flow configuration, is also shown to be inherently bistable, i.e. able
1059 to switch between two steady states, and the regime at work cannot be predicted solely from the
1060 material properties of the fluids and the tube geometry alone (Suckale et al. 2018).

1061 The spatial configuration of a bi-directional flow can only be organised as discussed above if
1062 no large bubble rises in the conduit and perturb the flow field. The existence of large bubbles rising
1063 in the conduit as spherical cap bubbles or Taylor bubbles (Fig. 3b and 3c), and the potential
1064 formation of detached bubbly wakes (Bouche et al. 2010; section lava lakes; Fig. 11) at several lava
1065 lakes, can erase and replace the above bi-directional flow models when the driving large bubbles are
1066 very frequent in the conduit. The above bi-directional flow models can be solely at work in between
1067 the rise of two successive large bubbles, 1 hr at lava lake of Erta 'Ale (Bouche et al. 2010).

1068
1069 **Implications and examples of bi-directional flows**

1070 By definition, a bi-directional flow involves a rising degassing magma and the descending degassed
1071 magma, hence is a form of convection. Their relative velocity in the conduit cannot be estimated
1072 directly. In the past, it has been derived from the direct measurements of surface velocity at lava
1073 lakes, as summarised in Lev et al. (2019). A notable exception is the case of Kilauea, where ejecta
1074 were directly sampled during the enhanced activity of 9 April 2008 (Carey et al. 2013). They

1075 allowed the first quantification of the convective velocity and the height of the convective cell in the
1076 conduit (Fig. 15e) to be, 0.02-0.8 m/s and 100-300 m, respectively, from the dimensions of the halo
1077 of re-dissolving bubbles within the downward flow of magma (Carey et al. 2013).

1078 Modelling the bi-directional flow in a conduit implies to know the relative areas of the rising
1079 degassing magma and the descending degassed magma. They vary with depth as a consequence of
1080 increasing the gas volume fraction within the degassing magma due to gas exsolution. The
1081 velocities of the rising and degassed magma were estimated at each depth based on the magma
1082 supply rate when assuming equilibrium conditions and full gas exsolution (Burton et al. 2007). The
1083 calculation of the gas volume fraction in the conduit, as estimated for Stromboli (Burton et al.
1084 2007b) and Ambrym (Allard et al. 2016b) is based on two implicit assumptions, one is that the
1085 bubbles are small, hence cannot move in respect to the liquid, and the second is that gas and its
1086 surrounding magma are in chemical equilibrium for degassing.

1087 A certain amount of small bubbles may be produced in the rising magma mainly due to gas
1088 exsolution when approaching to the surface. Alternatively the excess in volatiles can migrate with
1089 gas diffusion towards pre-existing bubbles. These bubbles, if small, can either be moving with the
1090 rising magma, such as in a homogeneous gas flow, or have their own differential velocity in respect
1091 to the liquid, as in a separated gas flow. In the first case, the calculation of the magma viscosity,
1092 used by Beckett et al (2014), should consider the gas volume fraction in the magma as part of single
1093 phase while in the second case, the magma viscosity should only consider the magma without the
1094 small bubbles, which are flowing on their own. The first consequence of a separated gas flow is to
1095 reduce the gas volume fraction (Vergnolle and Jaupart 1986), by allowing a larger gas flux in the
1096 conduit. The second consequence is that a separated gas flow can enhance the disequilibrium
1097 between dissolved and exsolved gas, due to the relatively fast transport of exsolved gas towards the
1098 surface. In this respect, the sulphur isotopes could be used to assess the amount of chemical
1099 disequilibrium in volatiles, shown to exist at Erta 'Ale in contrast to Masaya (De Moor et al. 2013).

1100 The bubbles present in the rising degassing magma may be sufficiently large to behave as a
1101 separated gas flow, or drift flow, in regards to that of the liquid (Vergnolle and Jaupart 1986). In
1102 this case, the gas volume fraction should be calculated from the superficial velocity of the gas phase
1103 and the drift velocity of a bubble, which depends on both the bubble diameter and the liquid
1104 viscosity (Vergnolle and Jaupart 1986; Pioli et al. 2012; Pansino et al. 2019). These calculations
1105 rely on a good knowledge of the magma viscosity, estimated without the bubbles present in the
1106 separated gas flow, and of the conduit radius, a second key parameter (Pansino et al. 2019).
1107 Quantifying the gas volume fraction at the surface also requires the independent determination of
1108 the flux of the rising magma and the total gas flux. The magma supply rate derives from the SO₂

1109 flux and the melt sulphur content, which implies full magma degassing from depth to surface. The
1110 total gas flux used by Pansino et al. (2019) combines the ratios of di-atomic gases such as CO₂/SO₂
1111 and H₂O/ SO₂, with the SO₂ flux at several volcanoes. However, the total gas flux, i.e. obtained by
1112 adding CO₂, H₂O, SO₂ fluxes, and the magma supply rate are not independent, invalidating the use
1113 of the estimates of gas volume fractions obtained by Pansino et al. (2019). Nevertheless, a proper
1114 estimate of the gas volume fraction should consider whether the small bubbles are flowing in a
1115 homogenous flow, i.e. moving together with the liquid, or in a separated gas flow. Because of the
1116 key role of the viscosity in understanding the physical process at work in a given volcano, these two
1117 limit cases must be considered, unless being able to measure independently whether the gas flow of
1118 the small suspended bubbles, induced by gas exsolution, is homogeneous or separated.

1119

1120 **The key informations derived from sound waves studies**

1121 Studies on infrasonic (<20 Hz) and acoustic (>20 Hz) sound waves, applied for the first time to
1122 volcanoes in the 1990's (Vergnolle and Brandeis 1994; 1996; Vergnolle et al. 1996; Garcès et al.
1123 1996; Johnson et al.,1998), can also provide constraints on eruptive patterns. The use of broad-
1124 band sensors such as microbarographs (a few tenths of Hz to 200 Hz) have been developed to run
1125 continuously, in contrast to microphones (0.1 and 4 kHz) more complicated to protect outdoor.
1126 This technique is now expanding significantly for monitoring the volcanic activity, particularly at
1127 open-vent volcanoes with an “easy” access. The main interest of acoustic measurements is to
1128 provide a remote way to monitor the surface of the magma column and to locate the source of
1129 sound when using an array. The location of the source of the sound, often due to degassing at the
1130 vent (e.g., Johnson 2005; Johnson et al. 2011; Colo et al. 2010; Marchetti et al. 2013; Kondo et al.
1131 2019), can also be produced by the front of a lahar, such as at Santiaguito (Johnson et al. 2011) or
1132 at Villarica, thereby providing an estimate of the flow front in time (Johnson and Palma 2015;
1133 Johnson et al. 2015). The frequency of the infrasound had been used at Villarica as a mean of
1134 following the level of the lava lake (Goto and Johnson 2011; Richardson et al. 2014), which rises
1135 2 days before the paroxysmal phase of 2015 (Johnson et al. 2018). However, this analysis was
1136 only possible because of a very specific geometry of the lava lake, mostly encrusted with a small
1137 opening in the crust (Johnson et al. 2018). The satellite SAR imagery at Nyiragongo, which can
1138 constrain the lava lake by measuring the length of the shadow cast by the rim of the pit crater
1139 hosting the lava lake, can be joined to the analysis of a seismic and infrasonic records to deduce
1140 the lava lake level in the future from a single seismic and infrasonic station (Barrière et al. 2018).
1141 Combining infrasonic and thermal measurements allows the recognition of vulcanian and

1142 strombolian explosions (Marchetti et al. 2009), whereas it can be difficult from acoustic records
1143 alone (Mora et al. 2022). This approach could be particularly relevant in the future for open-vent
1144 volcanoes with a high-silica magma composition, if run continuously. These volcanoes can either
1145 produce vulcanian explosions when the vent is mechanically sealed, strombolian explosions when
1146 the vent is mechanically open, and small to moderate gas-and-ash explosions as shown at
1147 Santiaguito (De Angelis et al. 2019; Wallace et al. 2020). But transitions exist at times between
1148 vulcanian and strombolian explosions, as at Arenal (Mora et al. 2022) and Fuego (Diaz-Moreno et
1149 al. 2020; Brill et al. 2022). This requires continuous measurements for a better modelling of this
1150 transition.

1151 Various models exist to explain the sound produced by strombolian explosions, each being
1152 driven at the vent by the breaking of a Taylor bubble (Fig. 3c). These models are based on the: 1)
1153 oscillations in volume of a large bubble prior to its bursting (Vergniolle and Brandeis 1994; 1996);
1154 2) resonances of a rigid cavity opened by a small hole as for Helmholtz resonators (Vergniolle and
1155 Caplan-Auerbach 2004); 3) formation of a hole piercing the magma layer overlying a small
1156 bubble, either with an extremely thin and inviscid liquid film, as for soap bubbles in water (Vidal
1157 et al. 2010; Sanchez et al. 2014) or in a viscous fluid (Koyabashi et al. 2010). The observations
1158 that the source of the sound is mostly monopolar had led Johnson et al. (2008) and Gerst et al.
1159 (2013), to estimate the gas volume and the gas flux under this assumption for some strombolian
1160 explosions at Erebus, with further validation from comparison with video records, at least for the
1161 beginning of the explosion (Witsil and Johnson 2018). The robust assumption of a monopole
1162 source is valid for any type of explosion (strombolian and vulcanian) providing that the sound
1163 propagation is linear, hence not associated to shock waves. The effect of the topography had also
1164 been included on the inversion of acoustic waveforms recorded with an array, giving estimates of
1165 gas flux and gas volume at Yasur (Iezzi et al. 2019, Fee et al. 2021). The use of a single acoustic
1166 sensor, set at a proximal distance from the vent and with an unobstructed line-of sight, provides
1167 reasonable estimates of gas fluxes and gas volumes when using the geometrical spreading of a
1168 monopole source and ignoring the topography (Johnson and Miller 2014). Furthermore, the use of
1169 a monopole approximation to recover the source parameters, such as maximum gas flux and gas
1170 volume, is more useful for monitoring purposes than just using the maximum radiated acoustic
1171 pressure, sometimes seen to be poorly correlated with the height of the eruptive column (Johnson
1172 and Miller 2014). Topography effects can sometimes affect the infrasonic waveforms, such as at
1173 Fuego (De Angelis 2019), but the perturbation can be much reduced by the use of an infrasonic
1174 array and inversions of waveforms (Iezzi et al. 2019; Diaz-Moreno et al. 2020). However, the use
1175 of a single sensor, located at a proximal distance and with unobstructed line-of-sight to the vent,

1176 had been proven to give a reasonable estimate of the source parameters also for vulcanian
1177 explosions when using a simple monopole source (Johnson and Miller 2014). Inversions of
1178 infrasonic waveforms done for small and moderate gas-and-ash explosions at Santiaguito provides
1179 the time history of mass eruption rates in good agreement with thermal or visible imagery,
1180 validating the use of acoustic measurements for estimates of gas volumes and gas fluxes (Johnson
1181 et al. 2010; De Angelis et al. 2016). The radiation pattern of the strombolian explosions at Yasur
1182 was also measured by using infrasound sensors aboard a tethered aerostat above the crater area,
1183 showing that both path effects from crater walls and source directionality could play a role in the
1184 infrasonic waveforms (Jolly et al. 2017).

1185 Non-linear effects in the sound propagation, such as existing during blast waves and shock
1186 waves, have been reported for the most vigorous strombolian explosions, with a velocity just
1187 slightly above the sound wave at Yasur (Marchetti et al. 2013; Taddeucci et al. 2014; Maher et al.
1188 2022) or well-marked during vulcanian explosions and during the 2018 paroxysm at Fuego
1189 (Morrissey et al. 2008; Diaz-Moreno et al. 2020). The modelling using strong shock waves could
1190 be applicable to weak shock waves produced by volcanoes (Medici, et al. 2014). Blast waves can
1191 often be distinguished from linear sources of sound based on their specific shape and amplitudes
1192 exceeding several hundreds of Pa within a few hundred metres from the source and also by their
1193 characteristic N-shape acoustic waveforms at a far distance (De Angelis et al. 2019). However,
1194 specific acoustic waveforms, asymmetrical with the larger compressive peak in comparison with
1195 its following rarefaction peak, are sometimes associated to shock waves and supersonic fluid flow,
1196 can be easily obtained for subsonic flows (Brogi et al. 2018), for which the monopole
1197 approximation holds. Furthermore, a recent study, also discussing supersonic jet flows, had shown
1198 that the sound associated to volcanic vortices and jet noise could be used to retrieve vent size and
1199 eruption parameters at open-vent volcanoes (Taddeucci et al. 2021).

1200 In addition, gas velocity and gas volume were also estimated by using the infrasonic power on
1201 a subplinian basaltic eruptive column at Shishaldin (USA; Vergnolle and Caplan-Auerbach 2006)
1202 and during the 2006 eruption of Augustine (USA; Caplan-Auerbach et al. 2010). However care
1203 should be used due to the multiphase nature (solid particles and liquid droplets carried by a hot
1204 gas) of the volcanic eruptive cloud when simplifying the acoustic source produced by a sustained
1205 eruptive column to a simple dipole or quadrupole (Matoza et al. 2009; 2013). The temporal
1206 evolution of the infrasonic power was also used to locate the depth of the reservoir at Shishaldin
1207 (Vergnolle and Caplan-Auerbach 2006), at 3.9 km in agreement with melt inclusions ($> 3\text{km}$)
1208 (Rasmussen et al., 2018), and the rise in the lava lake prior to the paroxysm at Villarica (Johnson
1209 et al. 2018).

1210 The sole use of infrasonic records to estimate the gas volumes at strombolian volcanoes often
1211 leads to an underestimate on the total gas volume, as infrasonic records can only record the
1212 unsteady gas flow (Johnson 2003) or that of the overpressurised gas expanding at the surface
1213 (Vergniolle and Brandeis 1994, 1996). The difference in total gas volumes deduced from
1214 infrasonic records with that obtained from records of videos in the visible or infrared or ultra-
1215 violet range, open-path Fourier transform infrared spectroscopy and radar is noticeable (see
1216 discussion in Vergniolle and Gaudemer 2015). The cause of this discrepancy is mainly a
1217 consequence of the significant amount of passive degassing associated to each explosion, keeping
1218 in mind that any technique, which cannot measure directly at the vent but above the vent, is also
1219 measuring air entrained within the volcanic cloud, such often the case with video, open-path
1220 Fourier transform infrared spectroscopy and radar techniques. The existence of passive degassing
1221 associated to explosions at Erebus is very clear from the comparison between videos and
1222 infrasonic records, in full agreement in the early part of explosion (gas decompression at the vent)
1223 but not later (Witsil and Johnson 2018). Although passive degassing could sometimes be
1224 associated to a bubbly wake attached to the bursting of the large bubble driving the explosion, the
1225 large viscosity of Erebus magma, $10^{6.3}$ Pa.s (Le Losq et al. 2015), prevents such a mechanism to
1226 be called for. It is then likely that the passive degassing expelled during an explosion at Erebus is
1227 induced by the bursting of numerous small bubbles present in the shallowest part of the magma
1228 column and made to burst by the rarefaction wave induced by the explosion and propagating down
1229 in the conduit. The active degassing, even if not major in term of gas volume at the vent in
1230 comparison with passive degassing, needs to be estimated because is a key to unravel the eruptive
1231 pattern, and in particular estimate the gas flux at depth. The comparison between videos and
1232 infrasonic records also shows the strong potential of combining various techniques at open-vent
1233 volcanoes to assess the extent of both passive and active degassing, hence to obtain a refined
1234 estimate of the gas flux.

1235

1236 **Sulphur evolution path**

1237 **The fate of the sulphur**

1238 New inventory and detection of new and unquantified sources of SO₂ passive emissions in volcanic
1239 arcs (Aleutian, Papouasie New Guinea, Indonesia) (Carn et al. 2017), and a better evaluation of the
1240 budgets of global volcanic SO₂ and CO₂ emissions (Fisher et al. 2019) have benefited from the
1241 advances in space-borne instruments, data treatments, and the combination of satellite-derived
1242 measurements with ground-based techniques and networks. It is recognised that the Nyiragongo –

1243 Nyamuragira system significantly contributes to the CO₂ volcanic flux of continental rift (Fisher et
1244 al. 2019), and to the global emissions of SO₂ (Carn et al. 2017), after Ambrym (Allard et al. 2016a,
1245 b). Since 2012, Nyamuragira strongly contributes to the global budgets of bromine (18–35% Br_{total})
1246 and iodine (8–18% I_{total}) (Bobrowski et al. 2017). It is characterised by an “excess” of sulphur
1247 degassing during effusive activity (Bluth and Carn 2008). A comparison between the SO₂ emissions
1248 inferred from the melt inclusion data for the 1986 and 2006 eruptions with satellite based records is
1249 compatible with pre eruption gas loss and gas accumulation together with degassing of unerupted
1250 shallow magma (Head et al. 2011). However, such an excess degassing is questioned and could not
1251 be the rule at Nyamuragira (Coppola et al. 2013). Hence the sulphur-degassing budget remained
1252 difficult to be constrained because of its multi-valence states and dependence on such parameters as
1253 fO_2 , fS_2 , pressure and magma composition (e.g., Wallace and Edmonds 2011; Métrich 2021).

1254 Erebus is another case where the sulphur evolution path can be tricky. The phonolitic magma
1255 that fills the magma at the top of the column is derived from the extensive differentiation of a
1256 parental basanite, after the removal of 75 % of crystals (Kyle et al. 1992). The parental melt may
1257 contain up 0.25 wt% S versus 0.03–0.06 wt% S in the phonolite as measured in melt inclusions of
1258 olivine and anorthoclase, respectively (Moussallam et al. 2014). A part of this sulphur is locked in
1259 the sulphide globules described in melt inclusions of their host crystals (Moussallam et al. 2016) as
1260 well as in the lava mineralogy (Kelly et al. 2008). A very rough estimation of the magma volume
1261 that is sustaining the low SO₂ flux at Erebus during passive degassing could be tentatively derived
1262 from the dissolved S content (610 ppm the highest S content in anorthoclase) and the SO₂ flux (on
1263 average 52t/d; Oppenheimer et al. 2004; Sawyer et al. 2008; de Moor et al. 2013). The volume of
1264 magma that sustained the passive SO₂ emissions at Erebus would be 0.25 m³/s (7.6 10⁻³ km³/yr,
1265 Tables 1 and 2).

1266 New strategies now involve Unmanned Aerial Aircraft Systems (drone), in complement to
1267 satellite based-SO₂ flux measurements (Tropospheric Ozone Monitoring Instrument (TROPOMI);
1268 Ozone Mapping and Profiler Suite (OMPS)), to provide large scale and repeated measurements of
1269 volcanic gas emissions, and they have been proved to be efficient for almost inaccessible volcanoes
1270 (Lui et al. 2020). Manam in Papua New Guinea whose vents have been active for several decades is
1271 an example of a newly identified contributor to the global volcanic fluxes of CO₂ and SO₂ (Lui et al.
1272 2020; Edmonds et al. 2021). Observed correlations between the molar CO₂/SO₂ ratios of surface gas
1273 emissions and incompatible trace element ratios in bulk rocks (i.e., Ba/La; Sr/Nd) of bulk rocks
1274 (Aiuppa et al. 2019) represent a major step forward towards a better quantification of the volcanic
1275 gas fluxes. Such an approach has been tested at Pacaya, regarded as the strongest degassing source
1276 in Central America (Battaglia et al. 2018), and used to predict the CO₂/SO₂ emissions of so called

1277 “unmeasured” volcanoes, as Fuego and Santiaguito in Guatemala (Aiuppa et al. 2019). In Japan six
1278 persistently active volcanoes (Miyakejima, Sakurajima, Satsuma-Iwojima, Asama, Aso,
1279 Suwanosejima) dominate the annual SO₂ flux (Shinohara 2013) and produce CO₂-poor gas
1280 emissions that mirror to the low amount of carbon in subducted sediments (Aiuppa et al. 2019).

1281

1282 **The example of Popocatépetl volcano in Mexico**

1283 Popocatépetl volcano provides a good example of passive degassing (Delgado-Granados et al.
1284 2001) as a large part of the magma that supports the surface SO₂ emissions is not erupting and
1285 continued to degas at depth while crystallising (Witter et al. 2005; Roberge et al. 2009).
1286 Popocatépetl is observed to be in a state of permanent open-vent activity since 1994 with cycles of
1287 building and destruction (associated to vulcanian explosions) of dacitic lava domes (Gómez-
1288 Vazquez et al. 2016; Taquet et al. 2019) and strong gas emissions (5000 tons/d SO₂ as measured on
1289 28/2/2019) from the central part of the dome (Campion et al. 2018). The activity renewed after ~70
1290 years of repose time, the last eruption occurred in 1920 and lasted 7 years (Delgado-Granados
1291 2001). Campion et al (2018) report a 4-year average SO₂ flux of 45 kg/s (3888 t/d against an
1292 average value of 1658±893 tons per day (1σ) given by Carn (2017) from SO₂ camera measurements
1293 between 2013 and 2016, during which degassing dominates (>95% of the time). They place
1294 Popocatépetl as one of the strongest permanent emitters of volcanic SO₂ over this period together
1295 with Ambrym (100 kg/s; Allard et al. 2016a, b), Kilauea (10–60 kg/s; Nadeau et al. 2015), and
1296 Nyamuragira (20–60 kg/s; Coppola et al. 2016).

1297 From March 1996 to 1st January 1998, the total SO₂ emissions achieved 9 Mt (9-13 kt/d) that is 4
1298 times higher than the SO₂ flux during the inter-eruption period (2-3 kt/d; Delgado-Granado et al.
1299 2001). Roberge et al (2009) conclude to a recharge of a minimum of 0.8 km³ (equivalent of a
1300 magma supply rate of 0.285 kg per year over this period) of mafic magma (for a magma containing
1301 2000 ppm S) for sustaining this high discharge amount of SO₂, rather than convection of magma in
1302 the uppermost part of the system. It would imply an initial CO₂ content of 1 wt% (Roberge et al.
1303 2009). They propose a model of decompression and degassing of magma (with up to 5 wt% H₂O) at
1304 150-350 MPa, with only a small portion of this magma reaching the surface, while being mixed
1305 with the silicic shallow magma. The effect of H₂O loss promotes crystallisation and increases the
1306 mixture viscosity that may slow down the convection. They thus suggest a mechanism based on the
1307 intrusion and degassing of a mafic magma batch at the origin of these emissions rather than one
1308 based of convection in the shallowest part of the subvolcanic conduits. On the basis of the presence
1309 of Mg-rich olivine together with textural and compositional evidence for mixing, Schaaf et al.

1310 (2005) propose dominant recharge of olivine-bearing basaltic andesite magma with relatively high
1311 volatile content.

1312 Long-time series of the gas composition at Popocatépetl between 2012 and 2016, after the 2011
1313 magma reinjection, indicate variation of the SO₂ flux between 1990 to 3680 tons per day (Table 2b)
1314 with the highest value corresponding active activity with magma extrusion and the lowest quiet
1315 period, and an average for the whole period of 2790 tons per day (Taquet et al. 2019). Following the
1316 approach developed by Roberge et al. (2009), we have tentatively calculated the magma supply rate
1317 for the 2012-2016 period using Taquet et al. (2019) SO₂ flux of 2790 tons per day. The magma
1318 supply rate could achieve 0.1 km³ per year while Campion et al. (2018) obtained a value of 0.16
1319 km³ (Table 1b) from a compilation of the SO₂ flux since 1995, including periods of high and low
1320 activity.

1321

1322 **Persistent degassing and sulphur behaviour at open-vent volcanoes in Central American** 1323 **Volcanic Arc**

1324 Pacaya, Fuego and Santiaguito are three open-vent volcanoes in Guatemala and are located at the
1325 triple junction of the North American, Cocos, and Caribbean tectonic plates that have sustained
1326 persistent degassing activity during several decades (Battaglia et al. 2018).

1327 The case of these three volcanoes provide the opportunity of discussing the sulphur behaviour in
1328 arc related basalts able to ascent before extensive crystal fractionation at Pacaya, to basalt and
1329 basaltic andesites at Fuego and dacitic magmas that are the final products of differentiation of such
1330 basaltic melts. Their magmas share comparable Ba/La ratios (on average 44-52) and CO₂/S_{total} ratio
1331 of 1-1.5 at Pacaya; 1.5±0.75 at Fuego, and 1.4±0.75 at Santiaguito (Aiuppa et al. 2017; Battaglia et
1332 al. 2019). According to these authors they thus share similar nature of slab component with
1333 dominant aqueous fluids derived from the slab dehydration, and small amount of carbonate in
1334 subducted sediments.

1335 Pacaya volcano, resumed Strombolian activity in 1961, after 200 years of rest and produced lava
1336 flow and pyroclastic explosive eruptions over nearly 50 years of activity, with flank eruptions that
1337 possibly emptying the upper most parts within the cone (Rose et al. 2013b). Violent explosive
1338 eruptions and lava fountains are reported in January and February 2000, and in 2010 (Rose et al.
1339 2013b). Pacaya produced homogeneous crystal-rich high-Al basalt having between nearly 30 to 50
1340 vol% phenocrysts with an average eruption rate for Pacaya of 0.17 ± 0.04 m³/s (78 kg/s) from 1961
1341 to 2001 (Rose et al. 2013b). The rapid ascent and crustal transfer of magma could have been
1342 facilitated by local extensional regime (Cameron et al. 2002; et al. 2018).

1343 Time series of in-situ (Multi-GAS) and remote (ultra-violet camera) plume measurements carried
1344 out in January 2016, during a period of relatively mild-strombolian activity at Pacaya, provide a
1345 SO₂ flux of 885±550 t/d (Battaglia et al. 2019). In contrast, it has fluctuated since the onset of the
1346 ongoing eruptive period in 1965, from 260-290 tons/day in the period of 1972-1992 (Andres et al.
1347 1993). It peaked at 1350 t/d within the 1999–2002 time period of higher level of explosive activity
1348 and reached 1570 tons per day while a lava lake is observed at the crater from August 2000 until
1349 May 2002 (Rodríguez et al. 2004). These observations led Rodríguez et al. (2004) to propose that
1350 Pacaya has a substantial convecting and circulating magma body near the surface that is degassing
1351 high-Al basalt, only partially extruded.

1352 A magma production rate of $0.17 \pm 0.04 \text{ m}^3/\text{s}$ (equivalent to $5 \times 10^{-3} \text{ km}^3$ per year) would imply an
1353 initial concentration of sulphur $\gg 1 \text{ wt}\%$ for a flux of varying from 260 to 1350 t/d that is
1354 unrealistic. The initial concentration of sulphur in parental basalt is not accurately known since only
1355 a few values are available ($\leq 0.17 \text{ wt}\% \text{ S}$; Walker et al. 2003). Considering the highest value of 0.17
1356 wt% S measured by Walker et al. (2003), that could be underestimated, would imply a volume ratio
1357 between the degassed and extruded magma of the order of 7, for an intermediate SO₂ flux of 885 t/d
1358 (Table 2b), with thus excess of sulphur degassing as concluded by Rose et al. (2013).

1359
1360 Fuego is regarded as the most dangerous volcano in Central America known, since 1524, for its
1361 Subplinian eruptions (volcanic explosivity index 4), as occurred in October 1974 (Rose et al 1978;
1362 Chesner and Rose 1984) after periods of repose times that lasted years or decades as reviewed by
1363 Naismith et al. (2019). The October 1974 Subplinian eruption produced hybrid magma from
1364 basaltic (crystal-poor) to basaltic andesite (crystal-rich) magmas (Rose et al. 1978). It was sustained
1365 by an influx of $\sim 0.1 \text{ km}^3$ H₂O-rich high-alumina basaltic magma (Rose et al. 1978; 2008). Low-
1366 level Strombolian activity persisted until 1979 (Martin and Rose 1981) and from 1980 to 1999
1367 Fuego had irregularly spaced subplinian (volcanic explosivity index 1-2) events with periods of
1368 repose (Lyons et al. 2010). The magma erupted in 1999 and 2003, after two decades of quiescence
1369 (Lyons et al. 2010), is partly residual from 1974 (Berlo et al. 2012). During 2 years of continuous
1370 observations (2005–2007) Fuego was persistently active, with a repeating cycle of activity: 1)
1371 passive lava effusion and minor strombolian explosion, followed by 2) paroxysmal eruptions, and
1372 finally 3) degassing explosions without lava effusion (Lyons et al. (2010). One of Fuego's largest
1373 eruptions in the period 1999–present occurred on 13th September 2012 whereas the most
1374 destructive eruption occurred on 3 June 2018 (Naismith et al. 2019; Liu et al. 2020). This explosive
1375 eruption was preceded by 5-month hiatus in activity that was proposed to be sufficient a time for

1376 crystallisation of a shallow low permeability plug and by the flowing of hot and high-speed lava
1377 flows (Liu et al. 2020).

1378 It is found to be part of a 45-year cycle of high-energy eruption that produced a magma volume
1379 of $0.04 \pm 0.01 \text{ km}^3$ (dense rock equivalent) and 130 ktons of SO_2 (IASI satellite data) that could
1380 have involved the influx of basaltic magma (Pardini et al. 2019). This SO_2 flux would imply a
1381 concentration of sulphur of nearly 500 ppm a value by far lower than the S dissolved amount in the
1382 1974 olivine-hosted melt inclusions up to 2250 ppm (Lloyd et al. 2014) and ~ 2500 ppm (Berlo et al.
1383 2012).

1384 The hybrid magma body erupted in between 14 and 23 October 1974 was proposed to reflect the
1385 contribution of several magma rather than a single magma composition, the basaltic magma (0.60
1386 wt% K_2O) standing at >10 km depth and a second basaltic andesite magma (0.90 wt% K_2O) at 3–8
1387 km depth (Roggensack 2001). Accordingly, the observed variability is a reflection of magma
1388 hybridization immediately before the eruption and that the pre-mixing water contents of basaltic
1389 magma were likely 4–5 wt%. Lloyd et al. (2014) measured in the 1974 melt inclusions 4.5 wt%
1390 H_2O . Most data of 1974 olivine-hosted melt inclusions of Fuego can be reproduced by
1391 decompression-crystallisation trend between 1010°C and 1100°C in a vertically extended reservoir
1392 (Cashman and Edmonds 2019). According to these authors, the high Al_2O_3 content recorded in MIs
1393 (4.5 wt% H_2O ; Lloyd et al. 2014) prior to late-stage plagioclase crystallisation supports a high
1394 proportion (50%) of crystal fractionation (olivine and clinopyroxene) from a parental melt possibly
1395 having up to 7.6–9.6 wt%. Ion-probe analysis of S, H_2O and CO_2 diffusion profile in open glassy
1396 gulfs (embayments) in olivine crystals still connected to the carrier magma indicate a
1397 decompression rate 0.24 to 0.60 MPa/s (~ 8 –21 m/s) of the magma erupted on 17 October 1974
1398 (Lloyd et al. 2014).

1399 Liu et al. (2020) proposed a top-down decompression of magma in the conduit as the triggering
1400 mechanism of the eruption of 3 June 2018, shallow crystallised magma acting as a plug. Liu et al.
1401 (2020) also showed that the frequency of paroxysms at Fuego is broadly proportional to the gas
1402 supply rate.

1403 Low sulphur concentration (~ 500 ppm) corresponds to the sulphide saturated melt, which has
1404 lost H_2O (Wade et al. 2006). Pyrrhotite is actually observed in association with titanomagnetite
1405 (Rose et al 1978, Berlo et al. 2012). Comparatively basaltic-andesite magma at Arenal contains
1406 similar S concentrations (2500 ppm), and becomes sulphide saturated as it is degassing and
1407 crystallising (Wade et al. 2006). Hence, low SO_2 flux reflects the degassing of crustal magma that is
1408 losing water and crystallising, a part of sulphur being locked in segregated sulphide globules.

1409

1410 Santiago complex consists of four domes, along an East-West trending fracture. The activity
1411 of dome-building began in 1922 within the crater formed during the cataclysmic 1902 eruption of
1412 Santa María (Rose 1972, 1987, 2013; Scott et al. 2012, 2013) and continues today. The longevity
1413 and continuous activity of Santiaguito are unusual among historic dome eruptions (Scott et al.
1414 2013). Magma extrusion rates have shown a cyclicity with 3–6-year-long periods of higher
1415 extrusion ($0.6\text{--}2.1\text{ m}^3\text{ s}^{-1}$), which are separated by 4- to 11-year-long periods of lower ($\sim 0.2\text{ m}^3\text{ s}^{-1}$)
1416 extrusion rate (Rose 1987; Harris et al. 2003, 2004). The activity at Santiaguito since 1975 is
1417 characterised by effusion of blocky lava flows and small-to-moderate gas-rich explosions (Harris et
1418 al. 2003) reaching up to 1.5 km above the vent with explosions occurring at different intervals, from
1419 a few minutes up to ~ 6 days (Carter et al. 2020). Santiaguito dacitic rocks are typically porphyritic,
1420 with a phase assemblage dominated by plagioclase (~ 20 to ~ 30 modal%) (Scott et al. 2013). Dacitic
1421 magma is found to be derived from the andesite via ~ 20 to 25% fractional crystallisation (Scott et
1422 al. 2013). Singer et al. (2011) propose that the dacite erupted in 1902 and during the early dome-
1423 forming cycles of Santiaguito lavas resulted from ~ 25 ka of fractional crystallisation in a closed
1424 system. The erupted magma has become progressively less evolved over time, with a decrease in
1425 whole rock SiO_2 from ~ 66 to ~ 62 wt% from 1922 to 2002 (Scott et al. 2013) with magma being
1426 extracted progressively from a chemically-stratified lower crustal (~ 12 to ~ 25 km) storage zone
1427 thought to have formed during the ~ 25 ka of quiescence that preceded the 1902 eruption.
1428 Santiaguito is by some aspect comparable to Colima for its cyclic emissions of SO_2 , with low
1429 background and high emissions of gas (1/3 of the emissions) leading to a range of SO_2 flux and
1430 explosion phenomenology (Lamb et al. 2019).

1431 Battaglia et al. (2018) report time-averaged SO_2 fluxes of 127 ± 58 tons/day at Santiaguito (Table
1432 2b), which reflects a very shallow magma degassing. Santiaguito parental melt have most likely
1433 similar parental basaltic magma, rich in water and sulphur as shown for Pacaya and Fuego. Whereas
1434 at Pacaya the SO_2 flux is sustained by high-alumina basalt degassing, dacitic magma evolution
1435 requires long-term fractional crystallisation (Singer et al. 2011), it thus implies titanomagnetite
1436 crystallisation, magma degassing and thus change in the redox conditions promoting melt sulphide
1437 saturation.

1438 In summary, these examples highlight the great need to combine time-series data, geochemical
1439 and petrological approaches as the necessity of having good geochemical modeling of depth-
1440 dependent magma redox.

1441

1442 **Concluding points**

1443 Combining time series infrasonic data and measurements of gas fluxes on well monitored open-vent
1444 volcanoes on the field is essential for the interpretation and modelling of the degassing pattern at the
1445 surface and in the conduit and understanding the eruptive activity. However, it cannot be
1446 dissociated from the good knowledge of the texture of the erupted products, the depth-evolution of
1447 the dissolved amount of water in the melt and thus its crystallinity owing to the key role of magma
1448 viscosity in modelling the bubbles and magma motions. Key advances could be made by any
1449 techniques constraining the in-situ bubble diameters and the gas volume fraction of the small
1450 bubbles, as one way to view the different eruptive regimes at basaltic and explosive volcanoes is a
1451 consequence of the ability of their largest bubbles to rise with a differential velocity in respect to the
1452 liquid or be stagnant, respectively. An accurate modelling of the magma viscosity itself combining
1453 physical and thermodynamic parameters is thus a challenge.

1454 A better modelling of the processes at the vent could be obtained by the joined and systematic use
1455 of thermal and infrasonic records. The inputs, which could be offered by imagery of the surface
1456 activity, possibly at high-speed, such as in the visible, infra-red or UV range, are enormous for our
1457 understanding, as these open-vent volcanoes remain an open window onto a deeper plumbing
1458 system, in which the future activity at the surface is being prepared. Similarly, be able to measure
1459 systematically and continuously the level of the magma column in the conduit or in the lava lake
1460 could be used as a key to detect pressure changes at depth and/or be used as a precursory signal of
1461 an enhanced activity. The case of Masaya shed lights on the interest to record simultaneous thermal
1462 and SO₂ fluxes to quantify the magma supply rate.

1463 Another interesting avenue to explore is that provided by the analysis of long-time series as open-
1464 vent volcanoes show sudden or progressive changes in behaviour. Several observatories across the
1465 world obtain these data but so far continuous long-time series are mainly restricted to geophysical
1466 methods.

1467 Additionally, a key parameter to know for a better quantification of the SO₂ flux in term of volume
1468 of degassed magma is the magma redox evolution during its crustal evolution and crystallisation.
1469 The fate of the degassed magma is also important, as it may remain at depth, be forcefully intruded
1470 into the edifice or be partly recycled by a convective loop in the conduit, i.e. the bi-directional flow
1471 at work at the less viscous open-vent volcanoes.

1472

1473 **Acknowledgements:** Many beautiful photographs had been given by colleagues, who we would
1474 like to thank warmly for making our paper visually captivating (P. Allard, O. Aragon, J-M
1475 Bardintzeff, T. Boyer, R. Campion, S. Carn, P. Delmelle, A. Finizola, Y Moussallam, C
1476 Oppenheimer, M. Patrick, T. Ricci, G. Sartoris, B. Smets, T. Staudacher). We would also like to
1477 thank authors, who had provided original figures for us to redraw (F Beckett, M. Burton, R. Carey,
1478 DJ Ferguson, C. Le Losq, J Palma, D. Patanè, A. Pouclet, H. Mader). We also would like to thank
1479 Y. Gaudemer, the reviewers (unknown and M. Patrick) and the associated editor, J. Taddeucci, who
1480 help us to improve significantly the clarity of the text.

1481

1482

1483 **References**

- 1484 Aiuppa A, Bertagnini A, Métrich N, Moretti R, Di Muro A, Liuzzo M, Tamburello G (2010) A
1485 model of degassing for Stromboli volcano. *Earth Planet Sci Lett* 295: 195–204
- 1486 Aiuppa A, Bitetto M, Delle Donne D, Paolo La Monica F, Tamburello G, Coppola D, Della Schiava
1487 M, Innocenti L, Lacanna G, Laiolo M, Massimetti F, Pistolesi M, Silengo M C, Ripepe M (2021)
1488 Volcanic CO₂ tracks the incubation period of basaltic paroxysms. *Sci Adv* 7:38
1489 <https://doi.org/eabh0191>
- 1490 Aiuppa A, Bitetto M, Francofonte V, Velasquez, G, Parra, CB, Giudice G, Liuzzo M, Moretti R,
1491 Moussallam Y, Nials P, Tamburello G, Valderrama OA, Curtis A (2017) A CO₂-gas precursor to
1492 the March 2015 Villarrica volcano eruption. *Geochem Geophys Geosyst* 18:2120–2132.
1493 <https://doi.org/10.1002/2017GC006892>
- 1494 Aiuppa A, Fisher TP, Plank T, Bani P (2019) CO₂ flux emissions from Earth's most actively
1495 degassing volcanoes 2005-2015. *Sci Rep* 9:5442. <https://doi.org/10.1038/s41598-019-41901-y>
- 1496 Allard P, Aiuppa A, Burton M, Caltabiano T, Federico C, Salerno G, La Spina A (2008) Crater gas
1497 emissions and the magma feeding system of Stromboli volcano. In: Calvari S, Inguaggiato S,
1498 Puglisi G, Ripepe M and Rosi M (eds), *Learning from Stromboli*. Amer Geophys Union
1499 *Geophys Monograph* 182:65-80
- 1500 Allard P, Aiuppa A, Bani P, Métrich, N, Bertagnini A, Gauthier, P-J, Shinohara H, Sawyer G,
1501 Parello F, Bagnato E, Pelletier B, Garaebiti E (2016a) Prodigious emission rates and magma
1502 degassing budget of major, trace and radioactive volatile species from Ambrym basaltic volcano,
1503 Vanuatu island Arc. *J Volcanol Geotherm Res* 322:119-143, in Special issue Understanding

1504 volcanoes in Vanuatu arc (Eds. S. Vergnolle and N. Métrich).
1505 <https://doi.org/10.1016/j.jvolgeores.2015.08.022>

1506 Allard P, Burton M, Sawyer G, Bani P (2016b) Degassing dynamics of basaltic lava lake at a top-
1507 ranking volatile emitter: Ambrym volcano, Vanuatu arc. *Earth Planet Sci Lett* 448:69-80.
1508 <http://dx.doi.org/10.1016/j.epsl.2016.05.014>

1509 Allibone R, Cronin SJ, Charley DT, Neall VE, Stewart RB, Oppenheimer C (2012) Dental fluorosis
1510 linked to degassing of Ambrym volcano, Vanuatu: a novel exposure pathway. *Environ Geochem*
1511 *Health* 34 (2):155–170. <https://doi.org/10.1007/s10653-010-9338-2>.

1512 Andres RJ, Rose WI, Stoiber R., Williams SN, Matías O, Morales R, (1993) A summary of sulfur
1513 dioxide emission rate measurements from Guatemalan volcanoes. *Bull Volcanol* 55:379-388

1514 Andújar J, Scaillet B (2012) Relationships between pre-eruptive conditions and eruptive styles of
1515 phonolite–trachyte magmas. *Lithos* 152:122-131. <https://doi.org/10.1016/j.lithos.2012.05.009>

1516 Arciniega-Ceballos A, Chouet B, Dawson P (1999) Very long-period signals associated with
1517 vulcanian explosions at Popocatepetl volcano, Mexico. *Geophys Res Lett* 26: 3013-3016

1518 Arciniega-Ceballos A, Dawson P, Chouet BA (2012) Long period seismic source characterization at
1519 Popocatépetl volcano, Mexico. *Geophys Res Lett* 39:L20307.
1520 <https://doi.org/10.1029/2012GL053494>

1521 Aster R, Mah S, Kyle P, McIntosh W, Dunbar N, Johnson J, Ruiz M, McNamara S (2003) Very
1522 long period oscillation of Mount Erebus volcano. *J Geophys Res* 108/(11).
1523 <https://doi.org/10.1029/2002JB002101>

1524 Bani P, Oppenheimer C, Tsanev VI, Carn SA, Cronin SJ, Crimp R, Calkins JA, Charley D, Lardy
1525 M, Roberts TR (2009) Surge in sulphur and halogen degassing from Ambrym volcano, Vanuatu.
1526 *Bull Volcanol* 71(10):1159–1168

1527 Bani P, Harris AJL, Shinohara H, Donnadiou F (2013) Magma dynamics feeding Yasur’s explosive
1528 activity observed using thermal infrared remote sensing. *Geophys Res Lett* 40:3830–3835

1529 Bani P, Oppenheimer C, Allard P, Shinohara H, Tsanev V, Carn S, Lardy M, Garaebiti E (2012)
1530 First estimate of volcanic SO₂ budget for Vanuatu island arc. *J Volcanol Geotherm Res* 211-
1531 212:36-46. <https://doi.org/10.1016/j.jvolgeores.2011.10.005>

1532 Barnie TD, Oppenheimer C, Pagli C (2016) Does the lava lake of Erta ‘Ale volcano respond to
1533 regional magmatic and tectonic events? An investigation using Earth Observation data. From:
1534 Wright TJ, Ayele, A, Ferguson DJ, Kidane T, Vye-Brown C (eds) 2016. *Magmatic Rifting and*
1535 *Active Volcanism*. *Geol Soc London Spec Pub* 420:181–208. <https://doi.org/10.1144/SP420.15>

- 1536 Barrière J, d'Oreye N, Oth A, Geirsson H, Mashagiro N, Johnson JB, Smets B, Samsonov S,
1537 Kervyn F (2018) Single-Station Seismo-Acoustic Monitoring of Nyiragongo's Lava Lake
1538 Activity (D.R. Congo). *Front Earth Sci* 6:82
- 1539 Battaglia, J, Métaxian, JP, Garaebiti, E (2012) Earthquake-volcano interaction imaged by coda
1540 wave interferometry. *Geophys Res Lett* 39:11
- 1541 Battaglia J, Métaxian, J-P, Garaebiti E (2016a) Short term precursors of Strombolian explosions at
1542 Yasur volcano (Vanuatu). *Geophys Res Lett* 43:1-6, doi:10.1002/2016GL067823
- 1543 Battaglia J, Métaxian, J-P, Garaebiti E (2016b) Families of similar events and modes of oscillation
1544 of the conduit at Yasur volcano (Vanuatu). *J Volcanol Geotherm Res*, Special issue on
1545 Understanding volcanoes in the Vanuatu arc, 322:196--211
- 1546 Battaglia A, Bitetto M, Aiuppa A, Rizzo AL, Chigna G, Watson IM, D'Aleo R, Juárez Cacao FJ, de
1547 Moor M (2018) The magmatic gas signature of Pacaya Volcano, with implications for the
1548 volcanic CO₂ flux from Guatemala. *Geochem Geophys Geosyst*. 19:667-692.
1549 <https://doi.org/10.1002/2017GC007238>
- 1550 Beckett FM, Mader HM, Phillips JC, Rust AC, Witham F (2011) An experimental study of low-
1551 Reynolds-number exchange flow of two Newtonian fluids in a vertical pipe. *J Fluid Mech*
1552 682:652-670
- 1553 Beckett FM, Burton M, Mader HM, Phillips JC, Polacci M, Rust AC, Witham F (2014) Conduit
1554 convection driving persistent degassing at basaltic volcanoes. *J Volcanol Geotherm Res*
1555 283:19-35
- 1556 Berlo K, Stix J, Roggensack K, Ghaleb B (2012) A tale of two magmas, Fuego, Guatemala. *Bull*
1557 *Volcanol* 74(2):377–390. <https://doi.org/10.1007/s00445-011-0530-8>
- 1558 Bertagnini A, Di Roberto A, Pompilio M (2011) Paroxysmal activity at Stromboli: lessons from the
1559 past. *Bull Volcanol* 73:1229-1243. <https://doi.org/10.1007/s00445-011-0470-3>
- 1560 Bluth GJS, Carn SA (2008) Exceptional sulphur degassing from Nyamuragira volcano, 1979–2005.
1561 *Int J Remote Sens* 29:6667–6685. <https://doi.org/10.1080/01431160802168434>
- 1562 Bobrowski N, Giuffrida GB, Arellano S, Yalire M, Liotta M, Brusca L, Calabrese S, Scaglione S,
1563 Rüdiger J, Castro JM, Galle B, Tedesco D (2017) Plume composition and volatile flux of
1564 Nyamulagira volcano, Democratic Republic of Congo, during birth and evolution of the lava
1565 lake, 2014–2015. *Bull Volcanol* 79-90. <https://doi.org/10.1007/s00445-017-1174-0>
- 1566 Bolge LL, Carr MJ, Feigenson MD, Alvarado GE (2006) Geochemical stratigraphy and magmatic
1567 evolution at Arenal Volcano, Costa Rica. *J Volcanol Geotherm Res* 34-48.
1568 <https://doi.org/10.1016/j.jvolgeores.2006.03.036>

1569 Bouche E, Vergniolle S, Staudacher T, Nercessian A, Delmont JC, Frogneux M, Cartault F, Le
1570 Pichon A (2010) The role of large bubbles detected from acoustic measurements on the
1571 dynamics of Erta'Ale lava lake (Ethiopia). *Earth Planet Sci Lett* 295:37-48

1572 Brill KA, Waite GP, Carn S, Chigna G, Palma R (2022) Long term stability of conduit dynamics
1573 at Fuego volcano, Guatemala, 2008-2015 84:37 this issue

1574 Brogi F, Ripepe M, Bonadonna C (2018) Lattice Boltzmann modeling to explain volcano acoustic
1575 source. *Sci Rep* 8:9537. <https://doi.org/10.1038/s41598-018-27387-0>

1576 Buckingham MJ, Garcès MA (1996) A canonical model of volcano acoustics. *J Geophys Res*
1577 101:8129-8151

1578 Burgi P-Y, Caillet M, Haefeli S (2002) Field temperature measurements at Erta' Ale lava lake,
1579 Ethiopia. *Bull Volcanol* 64(7):472-485

1580 Burgi P-Y, Caillet M, Haefeli S (2002) Field temperature measurements at Erta' Ale lava lake,
1581 Ethiopia. *Bull Volcanol* 64(7):472-485

1582 Burton MR, Oppenheimer C, Horrocks LA, Francis PW (2000) Remote sensing of CO₂ and H₂O
1583 emission rates from Masaya volcano, Nicaragua. *Geology* 28(10):915-918

1584 Burton M, Allard P, Muré F, La Spina A (2007) Magmatic gas composition reveals the source
1585 depth of slug-driven strombolian explosive activity. *Science* 317:227-230

1586 Burton M, Sawyer G, Bani P (2016) Degassing dynamics of basaltic lava lake at a top-ranking
1587 volatile emitter: Ambrym volcano, Vanuatu arc. *Earth Planet Sci Lett* 448:69-80.
1588 <https://doi.org/10.1016/j.epsl.2016.05.014>

1589 Calkins J, Oppenheimer C, Kyle PR (2008) Ground-based thermal imaging at Erebus volcano,
1590 Antarctica. *J Volcanol Geotherm Res* 177:695-704

1591 Calkins JA, Delmelle P (2021) Quantitative analysis of persistent volcanic fluoride risk reveals
1592 differential exposure pathways for adults and children downwind of Masaya Volcano,
1593 Nicaragua. *Bull Volcanol* 83:83 <https://doi.org/10.1007/s00445-021-01504-w> this issue

1594 Cameron BI, Walker JA, Carr MJ, Patino LC, Mat O, Feigenson MD (2002) Flux versus
1595 decompression melting at stratovolcanoes in southeastern Guatemala. *J Volcanol Geotherm Res*
1596 119:21-50

1597 Champion R (2014) New lava lake at Nyiamuragira volcano revealed by combined ASTER and OMI
1598 SO₂ measurements. *Geophys Res Lett* 41:7485-7492. <https://doi.org/10.1012/2014GL061808>

1599 Champion R, Delgado-Granados H, Legrand D, Taquet N., Boulesteix T, Pedraza-Espitía S Lecocq
1600 T (2018) Breathing and Coughing: The Extraordinarily High Degassing of Popocatepetl Volcano
1601 Investigated With an SO₂ Camera. *Front Earth Sci* 6:163. [https://doi.org/](https://doi.org/10.3389/feart.2018.00163)
1602 [10.3389/feart.2018.00163](https://doi.org/10.3389/feart.2018.00163)

1603 Caplan-Auerbach J, Bellesiles A, Fernandes JK (2010) Estimates of eruption velocity and plume
1604 height from infrasonic recordings of the 2006 eruption of Augustine Volcano, Alaska. *J Volcanol*
1605 *Geotherm Res* 189:12–18

1606 Carrigan, CR (1983) A heat pipe model for vertical, magma-filled conduits. *J Volcanol Geotherm*
1607 *Res* 16, 279-298

1608 Carrigan C R (1987) The magmatic Rayleigh number and time dependent convection in cooling
1609 magma. *Geophys Res Lett* 14 9:915-918

1610 Carn SA, Fioletov VE, McLinden CA, Li C, Krotkov NA (2017) A decade of global volcanic SO₂
1611 emissions measured from space. *Sci Rep* 7:44095. <https://doi.org/10.1038/srep44095>.

1612 Cashman KV, Edmonds M (2019) Mafic compositions: a record of magma storage conditions,
1613 mixing and ascent. *Phil Trans R Soc A* 377:20180004. <https://doi.org/10.1098/rsta.2018.0004>

1614 Chesner CA, Rose WI (1984) Geochemistry and evolution of the Fuego volcanic complex,
1615 Guatemala. *J Volcanol Geotherm Res* 21:25–44

1616 Chouet B, Dawson P, Arciniega-Ceballos A (2005) Source mechanism of Vulcanian degassing at
1617 Popocatepetl Volcano, Mexico, determined from waveform inversions of very long period
1618 signals. *J Geophys Res* 110:B07301. <https://doi.org/10.1029/2004JB003524>

1619 Cigolini C, Borgia A, Casertano L (1984) Intra-crater activity, AA-block lava, viscosity and flow
1620 dynamics: Arenal volcano, Costa Rica. *J Volcanol Geotherm Res* 20:155-176

1621 Cimarelli C, Costa A, Mueller S, Mader HM (2011), Rheology of magmas with bimodal crystal size
1622 and shape distributions: Insights from analog experiments. *Geochem Geophys Geosyst*,
1623 12:Q07024. <https://doi.org/10.1029/2011GC003606>

1624 Clarke AB (2013) Unsteady vulcanian explosions. *Modeling Volcanic Processes: The Physics and*
1625 *Mathematics of Volcanism*, eds. SA Fagents, TKP Gregg, and RMC Lopes. 27:129-152
1626 Cambridge University Press

1627 Clarke AB, TE Ongaro, A Belousov (2015) Vulcanian explosions. *The Encyclopedia of Volcanoes*,
1628 2nd edition, 28:505-518 Academic Press

1629 Clift R., JR Grace, ME Weber (1978) Bubbles, drops and particles. Academic press, London, 1-380

1630 Coppola D, Champion R, Laiolo M, Cuoco E, Balagizi C, Ripepe M, Cigolini C, Tedesco D (2016)
1631 Birth of a lava lake: Nyamulagira volcano 2011-2015. *Bull Volcanol* 78:20.
1632 <https://doi.org/10.1007/s00445-016-1014-7>

1633 Coppola D, Laiolo M, Massimetti F, Cigolini C (2019) Monitoring endogenous growth of open-
1634 vent volcanoes by balancing thermal and SO₂ emissions data derived from space. *Sci Rep*
1635 9:9394. <https://doi.org/10.1038/s41598-019-45753-4>

- 1636 Costa F, Shea T, Ubide T (2020) Diffusion chronometry and the timescales of magmatic processes
1637 Nature Reviews Earth and Environment 1:201-214
- 1638 Cronin SJ, Sharp DS (2002) Environmental impacts on health from continuous volcanic activity at
1639 Yasur (Tanna) and Ambrym, Vanuatu. *Int J Environ Health Res* 12:109-123
- 1640 De Angelis S, A Diaz-Moreno, L Zuccarello (2019) Recent Developments and Applications of
1641 Acoustic Infrasound to Monitor Volcanic Emissions. *Remote Sens* 11:1302.
1642 <https://doi.org/10.3390/rs11111302>
- 1643 Delgado-Granados H, Cárdenas-González L, Piedad-Sánchez N (2001) Sulphur dioxide emissions
1644 from Popocatepetl volcano (Mexico): case study of a high-emission rate, passively degassing
1645 erupting volcano. *J Volcanol Geotherm Res* 108:107-120
- 1646 Delmelle P, Stix J, Baxter P, Garcia-Alvarez, J, Barquero J (2002) Atmospheric dispersion,
1647 environmental effects and potential health hazard associated with the low-altitude gas plume of
1648 Masaya volcano, Nicaragua. *Bull Volcanol* 64(6):423–434
- 1649 De Moor JM, Fischer TP, Sharp ZD, King PL, Wilke M, Botcharnikov RE, Cottrell E, Wilke
1650 Zelenski M, Marty B, Klimm K, Rivard C, Ayalew D, Ramirez C, Kelley KA (2013) Sulfur
1651 degassing at Erta Ale (Ethiopia) and Masaya (Nicaragua) volcanoes: Implications for the
1652 degassing processes and oxygen fugacities of basaltic systems. *Geochem Geophys Geosyst*
1653 14:4076-4108. <https://doi.org/10.1002/ggge.20255>
- 1654 Diaz-Moreno A, Roca A, Lamur A, Munkli BH, Ilanko T, Pering TD, Pineda A, De Angelis S
1655 (2020) Characterization of Acoustic Infrasound Signals at Volcán de Fuego, Guatemala: A
1656 baseline for volcano monitoring. *Front Earth Sci* 8:54977.
1657 <https://doi.org/10.3389/feart.2020.549774>
- 1658 Edmonds M, Wallace P (2017) Volatiles and exsolved vapor in volcanic systems. *Elements* 13:29-
1659 34. <https://doi.org/10.2113/gselements.13.1.29>
- 1660 Edmonds M, Liu EJ, Cashman KV (2022) Open-vent volcanoes fuelled by depth-integrated magma
1661 degassing. *Bull Volcanol* 84:28. <https://doi.org/10.1007/s00445-021-01522-8> this issue
- 1662 Fan L-S, Tsuchiya K (1990) Bubble wake dynamics in liquids and liquid-solid suspensions.
1663 Butterworth-Heinemann series in chemical engineering, Boston, 1-363
- 1664 Fee D, Izbekov P, Kim K, Yokoo A, Lopez T, Prata, F, Kazahaya R, Nakamichi H, Iguchi M
1665 (2017) Eruption mass estimation using infrasound waveform inversion and ash and gas
1666 measurements: evaluation at Sakurajima Volcano, Japan. *Earth Planet Sci Lett* 480:42–52.
1667 <https://doi.org/10.1016/j.epsl.2017.09.043>
- 1668 Fee D, Toney L, Kim K, Sanderson RW, Iezzi AM, Matoza RS, De Angelis S, Jolly AD, Lyons JJ,
1669 Haney MM (2021) Local Explosion Detection and Infrasound Localization by Reverse Time

1670 Migration Using 3-D Finite-Difference Wave Propagation. *Front Earth Sci* 9:620813.
1671 <https://doi.org/10.3389/feart.2021.620813>

1672 Ferguson DJ, Gonnermann HM, Ruprecht P, Plank T, Hauri EH, Houghton BF, Swanson DA
1673 (2016) Magma decompression rates during explosive eruptions of Kīlauea volcano, Hawaii,
1674 recorded by melt embayments. *Bull Volcanol* (2016) 78:71

1675 Field L, Barnie T, Blundy J, Brooker RA, Keir D, Lewi E, Saunders K (2012) Integrated field,
1676 satellite and petrological observations of the November 2010 eruption of Erta Ale. *Bull*
1677 *Volcanol*. <https://doi.org/10.1007/s00445-012-0660-7>

1678 Firth CW, Handley HK, Cronin SJ, Turner SP (2014) The eruptive history and chemical
1679 stratigraphy of a post-caldera, steady-state volcano: Yasur, Vanuatu. *Bull Volcanol* 76:837
1680 <https://doi.org/10.1007/s00445-014-0837-3>

1681 Fischer TP, Arellano S, Carn S, Aiuppa A, Galle B, Allard P, Lopez T, Shinohara H, Kelly P,
1682 Werner C, Cardellini C, Chiodini G (2019) The emissions of CO₂ and other volatiles from the
1683 world's subaerial volcanoes. *Sci Rep* 9:8716. <https://doi.org/10.1038/s41598-019-54682-1>

1684 Francis P, Oppenheimer C, Stevenson D (1993) Endogenous growth of persistently active
1685 volcanoes. *Nature* 366:554–557. <https://doi.org/10.1038/366554a0>

1686 Gaudin, D, Moroni, M, Taddeucci, J, Scarlato, P, Shindler, L (2014a) Pyroclast Tracking
1687 Velocimetry: A particle tracking velocimetry-based tool for the study of Strombolian explosive
1688 eruptions. *J. Geophys. Res.* 119, 5369-5383. <https://doi.org/10.1002/2014JB011095>

1689 Gaudin, D, Taddeucci, J, Scarlato, P, Moroni, M, Freda, C, Gaeta M, Palladino DM (2014b)
1690 Pyroclast Tracking Velocimetry illuminates bomb ejection and explosion dynamics at Stromboli
1691 (Italy) and Yasur (Vanuatu) volcanoes. *J Geophys Res* 119:5384-5397.
1692 <https://doi.org/10.1002/2014JB01109>

1693 Gaudin D, Taddeucci J, Scarlato P, Harris A, Bombrun M, Del Bello E, Ricci T (2017)
1694 Characteristics of puffing activity revealed by ground-based, thermal infrared imaging: the
1695 example of Stromboli Volcano (Italy). *Bull Volcanol* 79: 24. [https://doi.org/10.1007/s00445-](https://doi.org/10.1007/s00445-017-1108-x)
1696 [017-1108-x](https://doi.org/10.1007/s00445-017-1108-x)

1697 Genco R, Ripepe M (2010) Inflation-deflation cycles revealed by tilt and seismic records at
1698 Stromboli volcano. *Geophys. Res. Lett.* 37, L12302. <https://doi.org/10.1029/2010GL04292>

1699 Gerst A, Hort M, Aster RC, Johnson JB (2013) The first second of volcanic eruptions from the
1700 Erebus Volcano lava lake, Antarctica - Energies, pressures, seismology, and infrasound. *J*
1701 *Geophys Res* 118:1–23

1702 Ghiorso MS, Gualda GA (2015) An H₂O–CO₂ mixed fluid saturation model compatible with
1703 rhyolite-MELTS. *Contrib Mineral Petrol* 169:5

- 1704 Giberti G, Jaupart C, Sartoris G (1992) Steady-state operation of Stromboli Volcano, Italy:
1705 Constraints on the feeding system. *Bull Volcanol* 54:535-541.
1706 <https://doi.org/doi:10.1007/BF00569938>
- 1707 Giggenbach WF, Kyle PR, Lyon GL (1973) Present volcanic activity on Mount Erebus, Ross
1708 Island, Antarctica. *Geology* 1(3):135-136
- 1709 Giordano D, Russell J, Dingwell D (2008) Viscosity of magmatic liquids: a model. *Earth Planet Sci*
1710 *Lett* 271:123–134
- 1711 Global Volcanism Program. Report on Pacaya (Guatemala) (2021) In Sennert SK (ed) Weekly
1712 volcanic activity Report 31 March-6 April 2021. Smithsonian Institution and US Geol Survey
- 1713 Guth E, Gold O (1938) On the hydrodynamical theory of the viscosity of suspensions. *Phys Review*
1714 53:322.
- 1715 Gomez C, B Kennedy (2017) Capturing volcanic plumes in 3D with UAV-based photogrammetry
1716 at Yasur Volcano – Vanuatu. *J Volcanol Geotherm Res* 350:84-88
- 1717 Gómez-Vazquez A, De la Cruz-Reyna S, Mendoza-Rosas AT (2016) The ongoing dome
1718 emplacement and destruction cyclic process at Popocatepetl volcano, central Mexico. *Bull*
1719 *Volcanol* 78:2–15
- 1720 Goto A, Johnson JB (2011) Monotonic infrasound and Helmholtz resonance at Volcan Villarrica
1721 (Chile), *Geophys Res Lett* 38:L06301. <https://doi.org/10.1029/2011GL046858>.
- 1722 Goto A, Ripepe M, Lacanna G (2014) Wideband acoustic records of explosive volcanic eruptions at
1723 Stromboli: New insights on the explosive process and the acoustic source. *Geophys Res Lett*
1724 41:3851–3857. <https://doi.org/10.1002/2014GL060143>
- 1725 Hagerty MT, Schwartz SY, Garcés MA, Protti M (2000) Analysis of seismic and acoustic
1726 observations at Arenal volcano, Costa Rica, 1995-1997. *J Volcanol Geotherm Res* 101:27-65
- 1727 Harms E, Schmincke H-U (2000) Volatile composition of the phonolitic Laacher See magma
1728 (12,900 yr BP): implications for syn-eruptive degassing of S, F, Cl and H₂O. *Contrib Mineral*
1729 *Petrol* 138:84-98
- 1730 Harpel CJ, Kyle PR, Caldwell DA, McIntosh WC, Esser RP (2004) ⁴⁰Ar/³⁹Ar dating of the eruptive
1731 history of Mount Erebus, Antarctica: summit flows and caldera collapse. *Bull Volcanol* 66:687-
1732 702
- 1733 Harris AJL, DS Stevenson (1997) Magma budget and steady-state at Stromboli and Vulcano.
1734 *Geophys Res Lett* 24 9:1043-1046
- 1735 Harris AJL, Flynn LP, Rothery DA, Oppenheimer C, Sherman SB (1999) Mass flux measurements
1736 at active lava lakes: implication for magma recycling. *J Geophys Res* 104:B4:7117-7136

- 1737 Harris AJL, Flynn LP, Matias O, Rose WI (2002) The thermal stealth flows of Santiaguito:
1738 implications for the cooling and emplacement of dacitic block lava flows. *Geol Soc Am Bull*
1739 114:533-546
- 1740 Harris AJL, Rose WI, Flynn LP (2003) Temporal trends in lava dome extrusion at Santiaguito
1741 1922–2000. *Bull Volcanol* 65:77-89
- 1742 Harris AJL, Flynn LP, Matias O, Rose WI, Julio Cornejo J (2004) The evolution of an active silicic
1743 lava flow field: an ETM+ perspective. *J Volcanol Geotherm Res* 135:147-168
- 1744 Harris AJL, Carniel R, Jones J (2005) Identification of variable convective regime at Erta 'Ale
1745 lava lake. *J Volcanol Geotherm Res* 142:207-223
- 1746 Harris AJL, Ripepe M (2007) Temperature and dynamics of degassing at Stromboli, *J Geophys*
1747 *Res* 112:B03205. <https://doi.org/doi:10.1029/2006JB00439>
- 1748 Harris AJL, Ripepe M, Hughes EA (2012) Detailed analysis of particle launch velocities, size
1749 distributions and gas densities during normal explosions at Stromboli. *J Volcanol Geothermal*
1750 *Res* 231-232:109-131
- 1751 Harris AJL, Delle Donne D, Dehn J, Ripepe M, Worden AK (2013) Volcanic plume and bomb
1752 field masses from thermal infrared camera imagery, *Earth Planet Sci Lett* 365:77-85
- 1753 Head EM, Shaw AM, Wallace PJ, Sims KWW, Carn SA (2011) Insight into volatile behavior at
1754 Nyamuragira volcano (D.R. Congo, Africa) through olivine hosted melt inclusions. *Geochem*
1755 *Geophys Geosyst* 12:Q0AB11. <https://doi.org/10.1029/2011GC003699>
- 1756 Helz RT (1987) Diverse olivine types in lava of the 1959 eruption of Kilauea volcano and their
1757 bearing on eruption dynamics. In *Volcanism in Hawaii, US. Geol Surv Prof Pap* 1350:691-722
- 1758 Holland PAS, Watson MI, Phillips JC, Caricchi L, Dalton MP (2011) Degassing processes during
1759 lava dome growth: Insights from Santiaguito lava dome, Guatemala, *J Volc Geotherm Res*
1760 202:153–166. <https://doi.org/10.1016/j.jvolgeores.2011.02.004>
- 1761 Huppert HE, Hallworth M (2007) Bi-directional flows in constrained systems. *J Fluid Mech*
1762 578:95-112
- 1763 Iezzi AM, Fee D, Kim K, Jolly AD, Matoza RS (2019) Three-Dimensional Acoustic Multipole
1764 Waveform Inversion at Yasur Volcano, Vanuatu. *J Geophys Res Solid Earth* 124:8679–8703.
1765 <https://doi.org/10.1029/2018JB017073>
- 1766 Ilanko T, Oppenheimer C, Burgisser A, Kyle PR (2015a) Cyclic degassing of Erebus volcano,
1767 Antarctica. *Bull Volcanol* 77:56. <https://doi.org/10.1007/s00445-015-0941-z>
- 1768 Ilanko T, Oppenheimer C, Burgisser A, Kyle P (2015b) Transient degassing events at the lava lake
1769 of Erebus volcano, Antarctica: Chemistry and mechanisms. *Geo Res J* 7:43–58

1770 Jellinek MA, Kerr RC (2001) Magma dynamics, crystallization, and chemical differentiation of the
1771 1959 Kilauea Iki lava lake, Hawaii, revisited. *J Volc Geotherm Res* 110:235-263

1772 Johnson JB (2003) Generation and propagation of infrasonic airwaves from volcanic explosions *J*
1773 *Volcanol Geotherm Res* 121:1-14

1774 Johnson JB, Lees JM, Gordeev EI (1998) Degassing explosions at Karymsky Volcano, Kamchatka.
1775 *Geophys Res Lett* 25:3999-4002

1776 Johnson JB (2004a) Volcanic eruptions observed with infrasound. *Geophys Res Lett* 31:L14604

1777 Johnson JB, Harris AJL, Sahetapy-Engel S, Wolf RE, Rose WI (2004b) Explosion dynamics of
1778 pyroclastic eruptions at Santiaguito, Guatemala. *Geophys. Res. Lett.* 31 (L06610)

1779 Johnson JB (2005) Source location variability and volcanic vent mapping with a small-aperture
1780 infrasound array at Stromboli Volcano, Italy. *Bull Volcanol* 67:1-14.
1781 <https://doi.org/10.1007/s00445-004-0356-8>

1782 Johnson JB, Sanderson R, Lyons J, Escobar-Wolf R, Waite G, Lees JM (2009) Dissection of a
1783 composite volcanic earthquake at Santiaguito, Guatemala. *Geophys Res Lett* 36:L16308

1784 Johnson JB, Lees JM, Varley N (2010) Characterizing complex eruptive activity at Santiaguito
1785 Volcano, Guatemala using infrasound semblance in networked arrays. *J Volc Geotherm Res*
1786 199:1-14

1787 Johnson JB, Lees J, Varley N (2011) Characterizing complex eruptive activity at Santiaguito,
1788 Guatemala using infrasound semblance in networked arrays. *J Volcanol Geotherm Res* 199:1–14

1789 Johnson JB, Miller AJC (2014) Application of the Monopole Source to Quantify Explosive Flux
1790 during Vulcanian Explosions at Sakurajima Volcano (Japan). *Seismol Res Lett* 85:1163-1176

1791 Johnson JB, Palma JL (2015), Lahar infrasound associated with Volcán Villarrica's 3 March 2015
1792 eruption. *Geophys Res Lett* 42:6324–6331. <https://doi.org/10.1002/2015GL065024>

1793 Johnson JB, Watson, LM, Palma JL, Dunham EM, Anderson JF (2018) Forecasting the Eruption of
1794 an Open-Vent Volcano Using Resonant Infrasound Tones. *Geophys Res Lett* 45:2213-2018

1795 Jolly AD, Matoza RS, Fee D, Kennedy BM, Iezzi AM, Fitzgerald, RH, Austin A, Johnson R (2017)
1796 Capturing the acoustic radiation pattern of strombolian eruptions using infrasound sensors
1797 aboard a tethered aerostat, Yasur volcano, Vanuatu. *Geophys Res Lett* 44:9672–9680.
1798 <https://doi.org/10.1002/2017GL074971>

1799 Jones LK, Kyle PR, Oppenheimer C, Frechette JD, Okal MH (2015) Terrestrial laser scanning
1800 observations of geomorphic changes and varying lava lake levels at Erebus volcano, Antarctica.
1801 *J Volcanol Geotherm Res* 295:43–54. <https://doi.org/10.1016/j.jvolgeores.2015.02.011>

1802 Kazahaya K, Shinohara H, Sato G. (1994) Excessive degassing of Izu-Oshima volcano: magma
1803 convection in a conduit. *Bull Volcanol* 56:207-216

- 1804 Kelly PJ, Kyle PR, Dunbar NW, Sims KWW (2008) Geochemistry and mineralogy of the phonolite
1805 lava lake, Erebus volcano, Antarctica: 1972-2004 and comparison with older lavas. *J Volcanol*
1806 *Geotherm Res* 177:589-605
- 1807 Kern C, Lerner AH, Elias T, Nadeau PA, Holland L, Kelly PJ, Werner CA, Clor LE, Cappos M
1808 (2020) Quantifying gas emissions associated with the 2018 rift eruption of Kīlauea volcano using
1809 ground-based DOAS measurements. *Bull Volcanol* 82:55. [https://doi.org/10.1007/s00445-020-](https://doi.org/10.1007/s00445-020-01390-8)
1810 01390-8
- 1811 Kieffer SW (1981) Fluid dynamics of the May 18 blast at Mount St. Helens. *US Geol Surv Prof Pap*
1812 1250:379
- 1813 Kim K, Fee D, Yokoo A, Lees JM (2015) Acoustic source inversion to estimate volume flux from
1814 volcanic explosions. *Geophys Res Lett* 42:5243–5249. <https://doi.org/10.1002/2015GL064466>
- 1815 Komorowski J-C, Tedesco D, Kasereka M, Allard P, Papale P, Vaselli O, Durieux J, Baxter P,
1816 Halbwachs M, Akumbe M, Baluku B, Briole P, Ciraba M, Dupin J-C, Etoy O, Garcin D,
1817 Hamaguchi H, Houlié N, Kavotha KS, Lemarchand A, Lockwood J, Luckaya N, Mavonga G, De
1818 Michele M, Mpore S, Mukambilwa K, Munyololo F, Newhall C, Ruch J, Yalire M, Wafula M
1819 (2004) The January 2002 flank eruption of Nyiragongo volcano (Democratic Republic of
1820 Congo): chronology, evidence for a tectonic rift trigger, and impact of lava flows on the city of
1821 Goma. *Acta Vulcanol* 14-15:27–62. <https://doi.org/10.1400/19077>
- 1822 Kondo G, Aoyama H, Nishimura T, Ripepe M, Lacanna G, Genco R, Kawaguchi R, Yamada T,
1823 Miwa T, Fujita E (2019) Gas flux cyclic regime at an open vent magmatic column inferred from
1824 seismic and acoustic records. *Sci. Rep. Nature* 9:5678. [https://doi.org/10.1038/s41598-019-](https://doi.org/10.1038/s41598-019-42033-z)
1825 42033-z
- 1826 Kremers S, Wassermann J, Meier K, Pelties C, van Driel M, Vasseur J, Hort M (2013) Inverting the
1827 Source Mechanism of Strombolian Explosions at Mt. Yasur, Vanuatu, using a Multi-Parameter
1828 Dataset. *J Volcanol Geotherm Res* 262:104-122
- 1829 Kyle PR, Moore JA, Thirlwall MF (1992) Petrologic evolution of anorthoclase phonolite lavas at
1830 Mount Erebus, Ross Island, Antarctica. *J Petrol* 33:849–875. [http://dx.doi.](http://dx.doi.org/10.1093/petrology/33.4.849)
1831 [org/10.1093/petrology/33.4.849](http://dx.doi.org/10.1093/petrology/33.4.849)
- 1832 Lamb OD, Lamur A, Díaz-Moreno A, De Angelis S, Hornby AJ, von Aulock FW, Kendrick JE,
1833 Wallace PA, Gottschämmer E, Rietbrock A, Alvarez I, Chigna G, Lavallée Y (2019) Disruption
1834 of Long-Term Effusive-Explosive Activity at Santiaguito, Guatemala. *Front Earth Sci* 6:253.
1835 <http://dx.doi.org/10.3389/feart.2018.00253>
- 1836 Landi P, Corsaro RA, Francalanci L, Civetta L, Miraglia L, Pompilio M, Tesoro R (2009) Magma
1837 dynamics during the 2007 Stromboli eruption (Aeolian Islands, Italy): Mineralogical,

1838 geochemical and isotopic data. *J Volcanol Geotherm Res* 182:255–268
1839 <https://doi.org/10.1016/j.jvolgeores.2008.11.010>

1840 Landi P, Francalanci L, Pompilio M, Rosi M, Corsaro RA, Petrone CM, Nardini I, Miraglia L
1841 (2006) The December 2002–July 2003 effusive event at Stromboli volcano, Italy: an insight into
1842 the shallow plumbing system by petrochemical studies. *J Volcanol Geotherm Res* 155:263–284

1843 Landi P, Métrich N, Bertagnini A, Rosi, M (2004) Dynamics of magma mixing and degassing
1844 recorded in plagioclase at Stromboli (Aeolian Archipelago, Italy). *Contrib Mineral Petrol*
1845 147:213–227

1846 Le Losq C, Neuville DR, Moretti R, Kyle PR, Oppenheimer C (2015) Rheology of phonolite
1847 magmas: the case of the Erebus lava lake. *Earth Planet Sci Lett* 411:53–61.
1848 <http://dx.doi.org/10.1016/j.epsl.2014.11.042>

1849 Liu EJ, Cashman KV, Miller E, Moore H, Edmonds M, Kunz KE, Jenner F, G Chigna (2020)
1850 Petrologic monitoring at Volcán de Fuego, Guatemala. *J Volcanol Geotherm Res* 405:107044.
1851 <https://doi.org/10.1016/j.jvolgeores.2020.107044>

1852 Lui EJ, Aiuppa A, Alan A, Arellano S, Bitetto M, Bobrowski N, Carn S, Clarke R, Corrales E, de
1853 Moor JM, Diaz JA, Edmonds M, Fischer TP, Freer J, Fricke GM, Galle B, Gerdes G, Giudice G,
1854 Gutmann A, Hayer C, Itikarai I, Jones J, Mason E, McCormick Kilbride BT, Mulina K, Nowicki
1855 S, Rahilly K, Richardson T, Rüdiger J, Schipper CI, Watson IM, Wood K 2020 Aerial strategies
1856 advance in volcanic gas measurements at inaccessible, strongly degassing volcanoes. *Sci Adv*
1857 6:eabb9103

1858 Lyons JJ, Waite GP, Rose WI, Chigna G (2010) Patterns in open vent, strombolian behaviour at
1859 Fuego volcano, Guatemala, 2005-2007. *Bull Volcanol* 72:1-15.
1860 <http://dx.doi.org/10.1007/s00445-009-0305-7>

1861 Mader HM, Llewellyn EW, Mueller SP (2013) The rheology of two-phase magmas: A review and
1862 analysis. *J Volcanol Geotherm Res* 257:135-158

1863 Maher SP, RS Matoza, C de Groot-Hedlin, KL Gee, Fee D (2022) Evidence for near-source
1864 nonlinear propagation of volcano infrasound from strombolian explosions at Yasur volcano,
1865 Vanuatu (2022). *Bull Volc* 84:41 this issue

1866 Marchetti E, Ripepe M, Delle Donne D, Genco R, Finizola A, Garaebiti E (2013) Blast waves from
1867 violent explosive activity at Yasur Volcano, Vanuatu. *Geophys Res Lett* 40:5838-5843.
1868 <https://doi.org/10.1002/2013GL057900>

1869 Martin DP, Rose WI (1981) Behavioral patterns of Fuego volcano, Guatemala. *J Volcanol*
1870 *Geotherm Res* 10:67–81

1871 Martin RS, Sawyer GM, Spampinato G, Salerno GG, Ramirez C, Ilyinskaya I, Witt MLI, Mather
1872 TA, Watson IM, Phillips JC, Oppenheimer C (2010) A volatile inventory for Masaya Volcano,
1873 Nicaragua. *J Geophys Res* 115, B09215

1874 Matoza RS, Fee D, Neilsen K, Gee L, Ogden DE (2013) Aeroacoustics of volcanic jets: Acoustic
1875 power estimation and jet velocity dependence. *J Geophys Res Solid Earth* 118:6269–6284.
1876 <https://doi.org/10.1002/2013JB010303>.

1877 Matoza RS, Fee D, Garcès MA, Seiner JM, Ramón PA, Hedlin MAH (2009) Infrasonic jet noise
1878 from volcanic eruptions, *Geophys Res Lett* 3: L08303. <https://doi.org/10.1029/2008GL036486>

1879 Medici EF, Allen JS, Waite GP (2014) Modeling shock waves generated by explosive volcanic
1880 eruptions. *Geophys Res Lett* 41:414–421. <https://doi.org/10.1002/2013GL058340>

1881 Meier K, Hort M, Wassermann J, Garaebiti E (2016) Strombolian surface activity regimes at Yasur
1882 volcano, Vanuatu, as observed by Doppler radar, infrared camera and infrasound. *J Volcanol*
1883 *Geotherm Res*, Special issue, on Understanding volcanoes in the Vanuatu arc 322:184-195

1884 Métrich N, Allard P, Aiuppa A, Bani P, Bertagnini A, Shinohara H, Parello F, Di Muro A, Garaebiti
1885 E, Belhadj O, Massare D (2011) Magma and volatile supply to post-collapse volcanism and
1886 block resurgence in Siwi caldera (Tanna island, Vanuatu arc). *J Petrol* 51:603-626.
1887 <https://doi.org/10.1093/petrology/egr019>

1888 Métrich N, Bertagnini A, Pistolesi M (2021) Paroxysms at Stromboli volcano (Italy): source,
1889 genesis and dynamics. *Front Earth Sci* 9:593339. <https://doi.org/10.3389/feart.2021.593339>

1890 Métrich N. (2021) Redox state of volatiles and their relationships with iron in silicate melts:
1891 Implications for magma degassing. In *Magma redox geochemistry* (Moretti R and Neuville D
1892 eds). Monograph, Amer Geophys Union 266:215-230.
1893 <https://doi.org/10.1002/9781119473206.ch11>

1894 Michon L, Di Muro A, Villeneuve N, Saint-Marc C, Fadda P, Manta F (2013) Explosive activity of
1895 the summit cone of Piton de la Fournaise volcano (La Réunion island): A historical and
1896 geological review. *J Volcanol Geotherm Res* 264:117-133.
1897 <https://doi.org/10.1016/j.jvolgeores.2013.06.012>

1898 Molina I, Burgisser A, Oppenheimer C (2015) A model of the geochemical and physical
1899 fluctuations of the lava lake at Erebus volcano, Antarctica. *J Volcanol Geotherm Res* 308:142-
1900 157. <http://dx.doi.org/10.1016/j.jvolgeores.2015.10.027>

1901 Mora MM, Lesage P, Taylor-Castillo W, Vergnion S, Fourel L, Soto GJ (2022) Retrospective of
1902 an open-vent eruption at Arenal volcano (Costa Rica, 1968-2010): evolution, dynamics, what we
1903 learned, and future perspectives. *Bull Volc* 84:66 this issue. [https://doi.org/10.1007/s00445-022-](https://doi.org/10.1007/s00445-022-01570-8)
1904 [01570-8](https://doi.org/10.1007/s00445-022-01570-8)

1905 Morrissey M, Garcés M, Ishihara K, Iguchi M (2008) Analysis of infrasonic and seismic events
1906 related to the 1998 Vulcanian eruption at Sakurajima. *J Volcanol Geotherm Res* 175:315-324

1907 Morrissey MM, Chouet B (1997) A numerical investigation of choked flow dynamics and its
1908 application to the triggering mechanism of long-period events at Redoubt Volcano, Alaska. *J*
1909 *Geophys Res* 102(B4):7965-7983

1910 Morrissey MM, Mastin LG (2000) Vulcanian eruptions. *Encyclopedia of volcanoes*, first edition,
1911 Academic Press, 463-475

1912 Morrison AA, Whittington A, Smets B, Kervyn M, Sehlke A (2020) The Rheology of Crystallizing
1913 basaltic lavas from Nyiragongo and Nyamuragira volcanoes, D.R.C. *Volcanica* 3(1):1-28.
1914 <http://dx.doi.org/10.30909/vol.03.01.0128>

1915 Moussallam Y, Oppenheimer C, Scaillet B, Kyle P (2013) Experimental Phase-equilibrium
1916 Constraints on the Phonolite Magmatic System of Erebus Volcano, Antarctica. *J Petrol* 54:1285-
1917 1307. <https://doi.org/10.1093/petrology/egt012>

1918 Moussallam Y, Bani P, Curtis A, Barnie T, Moussallam M, Peters N, Schipper CI, Aiuppa A,
1919 Giudice G, Amigo A, Velasquez G, Cardona C (2016) Sustaining persistent lava lakes:
1920 Observations from high-resolution gas measurements at Villarrica Volcano, Chile. *Earth Planet*
1921 *Sci Lett* 454:237–247

1922 Moussallam Y, Rose-Koga EF, Koga KT, Médard E, Bani P, Devidal J-L, Tari D (2019) Fast ascent
1923 rate during the 2017–2018 Plinian eruption of Ambae (Aoba) volcano: a petrological
1924 investigation. *Contrib Mineral Petrol* 174:90. <https://doi.org/10.1007/s00410-019-1625-z>

1925 Moussallam Y, Médard E, Georgeais G, Rose-Koga EF, Koga KT, Pelletier B, Bani Ph, Shreve TL,
1926 Grandin TL, Boichu M, Tari D, Peters N (2021) How to turn off a lava lake? A petrological
1927 investigation of the 2018 intra-caldera and submarine eruptions of Ambrym volcano. *Bull*
1928 *Volcanol* 83:36, this issue. <https://doi.org/10.1007/s00445-021-01455-2>

1929 Moussallam Y, Oppenheimer C, Scaillet B, Buisman I, Kimball C, Dunbar N, Burgisser A, Schipper
1930 CI, Andújar J, Kyle P (2015) Megacrystals track magma convection between reservoir and
1931 surface. *Earth Planet Sci Lett* 413:1-12. <http://dx.doi.org/10.1016/j.epsl.2014.12.022>

1932 Moussallam Y, Oppenheimer C, Scaillet B, Gaillard F, Kyle P, Peters N, Hartley M, Berloe K,
1933 Donovana A (2014) Tracking the changing oxidation state of Erebus magmas from mantle to
1934 surface driven by magma ascent and degassing. *Earth Planet Sci Lett* 393:200–209.
1935 <http://dx.doi.org/10.1016/j.epsl.2014.02.055>

1936 Mueller S, Llewellyn EW, Mader HM (2011) The effect of particle shape on suspension viscosity
1937 and implications for magmatic flows. *Geophys Res Lett* 38:L13316.
1938 <https://doi.org/10.1029/2011GL047167>

- 1939 Nabyl A, Dorel J, Lardy M (1997) A comparative study of low-frequency seismic signals recorded
1940 at Stromboli volcano, Italy, and at Yasur volcano, Vanuatu. *New Zeal J Geol and Geophysics*
1941 40:549-558
- 1942 Nadeau PA, Werner C A, Waite G P, Carn, SA, Brewer, ID, Elias T, Sutton AJ, Kern C (2015)
1943 Using SO₂ camera imagery and seismicity to examine degassing and gas accumulation at Kilauea
1944 volcano, May 2010. *J Volcanol Geotherm Res* 300:70–80.
1945 <https://doi.org/10.1016/j.jvolgeores.2019-03.014>
- 1946 Naismith AK, Watson IM, Escobar-Wolf R, Chigna G, Thomas G, Coppola G, Chun C. (2019)
1947 Eruption frequency patterns through time for the current (1999–2018) activity cycle at Volcán de
1948 Fuego derived from remote sensing data: Evidence for an accelerating cycle of explosive
1949 paroxysms and potential implications of eruptive activity. *J Volcanol Geotherm Res* 371:206-
1950 219. <https://doi.org/10.1016/j.jvolgeores.2019.01.001>
- 1951 Németh K, Cronin SJ (2011) Drivers of explosivity and elevated hazard in basaltic fissure
1952 eruptions: The 1913 eruption of Ambrym Volcano, Vanuatu (SW-Pacific). *J Volcanol Geotherm*
1953 *Res* 201:194-209. <https://doi.org/10.1016/j.jvolgeores.2010.12.007>
- 1954 Németh K, Cronin SJ (2008) Volcanic craters, pit craters and high-level magma-feeding systems of
1955 a mafic island-arc volcano: Ambrym. *Geol Soc London Spec Pub* 302:87-102.
1956 <https://doi.org/10.1144/SP302.6>
- 1957 Oppenheimer C, Lomakina AS, Kyle PR, Kingsbury NG, Boichu M (2009) Pulsatory magma
1958 supply to a phonolite lava lake. *Earth Planet Sci Lett* 284:392-398.
1959 <https://doi.org/10.1016/j.epsl.2009.04.043>
- 1960 Oppenheimer C, Moretti R, Kyle PR, Eschenbacher A, Lowenstern JB, Hervig RL, Dunbar, NW
1961 (2011) Mantle to surface degassing of alkalic magmas at Erebus volcano, Antarctica. *Earth*
1962 *Planet Sci Lett* 306:261-271. <https://doi.org/10.1016/j.epsl.2011.04.005>
- 1963 Pansino S, Calder E, Menand T (2019) Experimental analysis of bubble-driven magma motion in
1964 the conduit, for persistently active, open vent volcanoes. *Bull Volcanol* 81:12.
1965 <https://doi.org/10.1007/s00445-019-1339-0>
- 1966 Parat F, Streck MJ, Holtz F, Almeev R (2014) Experimental study into the petrogenesis of crystal-
1967 rich basaltic to andesitic magmas at Arenal volcano. *Contrib Mineral Petrol* 168(2):1040.
1968 <https://doi.org/10.1007/s00410-14-1040-4>
- 1969 Pardini F, Queiße M, Naismith A, Watson IM, Clarisse L, Burton MR (2019) Initial constraints on
1970 triggering mechanisms of the eruption of Fuego volcano (Guatemala) from 3 June 2018 using
1971 IASI satellite data. *J Volcanol Geotherm Res* 376:59-61
1972 <https://doi.org/10.1016/j.jvolgeores.2014.12.005>

- 1973 Patanè D, Barberi G, De Gori P, Cocina O, Zuccarello L, Garcia-Yeguas A, Castellano M,
1974 D'Alessandro A, Sgroi T (2017) The shallow magma chamber of Stromboli Volcano (Italy),
1975 Geophys Res Lett 44 : 6589–6596. <https://doi.org/10.1002/2017GL073008>
- 1976 Patrick M, Anderson K, Poland M, Orr T, Swanson D (2015) Lava lake level as a gauge of magma
1977 reservoir pressure and eruptive hazard. *Geology* 43(9):831–834
- 1978 Patrick M, Johanson I, Shea T, Waite T (2020) The historic events at Kīlauea Volcano in 2018:
1979 summit collapse, rift zone eruption, and Mw 6.9 earthquake: preface to the special issue. *Bull*
1980 *Volcanol* 82:46. <https://doi.org/10.1007/s00445-020-01377-5>.
- 1981 Patrick M, Orta T, Anderson K, Swanson D (2019). Eruptions in sync: Improved constraints on
1982 Kīlauea Volcano's hydraulic connection. *Earth Planet Sci Lett* 507:50–61
1983 <https://doi.org/10.1016/j.epsl.2018.11.030>
- 1984 Patrick MR, Harris AJL, Ripepe M, Dehn J, Rothery DA, Calvari S (2007) Strombolian explosive
1985 styles and source conditions: insights from thermal (FLIR) video. *Bull Volcanol* 69:769-784
- 1986 Peck DL, Hamilton MS, Shaw HR (1977) Numerical analysis of lava lake cooling models: part II,
1987 application to Alae lava lake, Hawaii. *Am J Sci* 277:415-437
- 1988 Pering TD, Ilanko T, Wilkes TC, England RA, Silcock SR, Stanger LR, Willmott JR, Bryant RG,
1989 McGonigle AJS (2019) A Rapidly Convecting Lava Lake at Masaya Volcano, Nicaragua. *Front*
1990 *Earth Sci* 6:241. <https://doi.org/10.3389/feart.2018.00241>
- 1991 Perring TD, Ilanko T, EJ Liu (2019) Periodicity in Volcanic Gas Plumes: A Review and Analysis.
1992 *Geosciences* 9:394. <https://doi.org/10.3390/geosciences9090394>
- 1993 Pering TD, Liu EJ, Wood K, Wilkes TC, Aiuppa A, Tamburello G, Bitetto M, Richardson T,
1994 McGonigle, AJS (2020) Combined ground and aerial measurements resolve vent-specific gas
1995 fluxes from a multi-vent volcano. *Nature Communications* 11, 3039
- 1996 Peters N, Oppenheimer C, Killingsworth DR, Frechette J, Kyle P (2014a) Correlation of cycles in
1997 Lava Lake motion and degassing at Erebus Volcano, Antarctica. *Geochem Geophys Geosyst*, 15,
1998 <https://doi.org/10.1002/2014GC005399>.
- 1999 Peters N, Oppenheimer C, Kyle P, Kingsbury N (2014b) Decadal persistence of cycles in lava lake
2000 motion at Erebus volcano, Antarctica. *Earth Planet. Sci.* 395, 1-12
- 2001 Peters NJ, Oppenheimer, C, Brennan P, Lok LB, Ash M, Kyle P (2018) Radar altimetry as a robust
2002 tool for monitoring the active lava lake at Erebus volcano, Antarctica. *Geophys Res Lett*
2003 45:8897-8904. <https://doi.org/10.1029/2018GL079177>
- 2004 Pichavant M, MacDonald R (2007) Crystallization of primitive basaltic magma at crustal pressures
2005 and genesis of the calc-alkaline igneous suite: experimental evidence from Saint Vincent, Lesser
2006 Antilles arc. *Contr Mineral Petrol* 154:535-558. <https://doi.org/10.1029/2018GL079177>

- 2007 Pichavant M, Di Carlo I, Pompilio M, Le Gall N (2022) Timescales and mechanisms of paroxysm
 2008 initiation at Stromboli volcano, Aeolian. *Bull Volc* 83:36. [https://doi.org/10.1007/s00445-022-](https://doi.org/10.1007/s00445-022-01545-9)
 2009 01545-9 this issue
- 2010 Pioli L, Bonadonna C, Azzopardi BJ, Phillips JC, Ripepe M (2012) Experimental constraints on the
 2011 outgassing dynamics of basaltic magmas. *J Geophys Res* 117(B03204):1-17.
 2012 <https://doi.org/10.1029/2011JB008392>
- 2013 Poland MP, Carbone D (2018) Continuous gravity and tilt reveal anomalous pressure and density
 2014 changes associated with gas pistoning within the summit lava lake of Kilauea volcano, Hawai'i.
 2015 *Geophys Res Lett* 45:2319–2327. <https://doi.org/10.1002/2017GL076936>
- 2016 Pouclet A, Bram K (2021) Nyiragongo and Nyamuragira: a review of volcanic activity in the Kivu
 2017 rift, western branch of the East African Rift System. *Bull Volcanol* 83:10
- 2018 Radebaugh J, Lopes RM, Howell RD, Lorenz RD, Turtle EP (2016) Eruptive behavior of the
 2019 Marum/Mbwelesu lava lake, Vanuatu and comparisons with lava lakes on Earth and Io. *J*
 2020 *Volcanol Geotherm Res*, Special issue on Understanding volcanoes in the Vanuatu arc 322:105-
 2021 118
- 2022 Ramsey MS, Harris AJL (2013) Volcanology 2020: How will thermal remote sensing of volcanic
 2023 surface activity evolve over the next decade? *J Volcanol Geotherm Res* 249: 217–233
- 2024 Rasmussen DJ, Plank TA, Roman DC, Power JA, Bodnar RJ, Hauri EH (2018) When does eruption
 2025 run-up begin? Multidisciplinary insight from the 1999 eruption of Shishaldin volcano. *Earth*
 2026 *Planet Sci Lett* 486:1-14
- 2027 Richardson JP, Waite GP, Palma JL (2014) Varying seismic-acoustic properties of the fluctuating
 2028 lava lake at Villarrica volcano, Chile. *J Geophys Res Solid Earth* 119:5560–5573.
 2029 <https://doi.org/10.1002/2014JB011002>
- 2030 Ripepe M, Rossi M, Saccorotti G (1993) Image processing of the explosive activity at Stromboli
 2031 Volcano. *J Volcanol Geotherm Res* 54:335-351
- 2032 Ripepe M, Ciliberto S, Schiava MD (2001) Time constraints for modeling source dynamics of
 2033 volcanic eruptions at Stromboli. *J Geophys Res* 106:8713-8727
- 2034 Ripepe M, Marchetti E, Ulivieri G, Harris A, Dehn J, Burton M, Caltabiano T, Salerno G (2005)
 2035 Effusive to explosive transition during the 2003 eruption of Stromboli volcano. *Geol* 33(5):341-
 2036 344
- 2037 Ripepe M, Del Donne D, Harris A, Marchetti E, Ulivieri G (2008) Dynamics of Strombolian
 2038 Activity in The Stromboli Volcano: An Integrated Study of the 2002-2003 Eruption. *Geophys*
 2039 *Monogr Ser*, 182:39-48, edited by Calvari et al. AGU, Washington DC

2040 Ripepe M, Marchetti E (2002) Array tracking of infrasonic sources at Stromboli volcano. *Geophys*
2041 *Res Lett* 29: 22, 2076, <https://doi.org/10.1029/2002GL015452>

2042 Roberge J, Delgado Granados H, Wallace P (2009) Mafic magma recharge supplies high CO₂ and
2043 SO₂ gas fluxes from Popocatepetl volcano, México. *Geol Soc Am* 37:107-110.
2044 <https://doi.org/10.1130/G25242A.1>

2045 Rodríguez L, Watson IM, Rose WI, Branán YK, Bluth GJS, Chigna G, Mattías O, Escobar D, Carn
2046 S, Fischer TP (2004) SO₂ emissions to the atmosphere from active volcanoes in Guatemala and
2047 El Salvador, 1999-2002. *J Volcanol Geotherm Res* 138:325–344.
2048 <https://doi.org/10.1016/j.jvolgeores.2004.07.008>

2049 Roggensack K (2001) Unraveling the 1974 eruption of Fuego volcano (Guatemala) with small
2050 crystals and their young melt inclusions. *Geol* 29(10):911–914. <https://doi.org/10.1130/0091>

2051 Rose WI (1972) Pattern and mechanism of volcanic activity at the Santiaguito volcanic dome,
2052 Guatemala. *Bull Volcanol* 36:73-94

2053 Rose Jr, WI (1972) Notes on the 1902 eruption of Santa Maria volcano, Guatemala. *Bull Volcanol*
2054 36:29-45

2055 Rose Jr WI, Anderson Jr AT, Woodruff LG, Bonis SB (1978) The October 1974 basaltic tephra
2056 from Fuego volcano: description and history of the magma body. *J Volcanol Geotherm Res* 4(1-
2057 2):3–53. [https://doi.org/10.1016/0377-0273\(78\)90027-6](https://doi.org/10.1016/0377-0273(78)90027-6)

2058 Rose WI (1987) Santa Maria, Guatemala: Bimodal soda-rich calc-alkalic stratovolcano. *J Volcanol*
2059 *Geotherm Res* 33: 109-129

2060 Rose WI (1987) Volcanic activity at Santiaguito Volcano 1976-1984. *Geol Soc Am Spec Pap*
2061 212:17-27

2062 Rose Jr WI, Self S, Murrow PJ, Bonadonna C, Durant AJ, Ernst GGJ (2008) Nature and
2063 significance of small volume fall deposits at composite volcanoes: Insights from the October 14,
2064 1974 Fuego eruption, Guatemala. *Bull Volcanol* 70(9):1043–1067.
2065 <https://doi.org/10.1007/s00445-007-0187-5>

2066 Rose IW, Palma JL, Delgado Granados H, Varley N (2013a) Open-vent volcanisms and related
2067 hazards: Overview. In Rose WI, Palma JL, Delgado Granados H, Varley N (Eds) *Understanding*
2068 *open-vent volcanism and related hazards: Spec Paper* 498:vi-xiii.
2069 [https://doi.org/10.1130/2013.2498\(00\)](https://doi.org/10.1130/2013.2498(00))

2070 Rose WI, Palma JL, Escobar Wolf R, Matías-Gomez, RO (2013b) A 50 yr eruption of a basaltic
2071 composite cone: Pacaya, Guatemala. In Rose WI, Palma JL, Delgado Granados H, Varley N
2072 (Eds) *Understanding open-vent volcanism and related hazards: Spec Paper* 498: 1–21 *Geol Soc*
2073 *Amer.* [https://doi.org/10.1130/2013.2498\(01\)](https://doi.org/10.1130/2013.2498(01))

- 2074 Rosi M, Pistolesi M, Bertagnini A, Landi P, Pompillio M, Di Roberto A (2013) Stromboli volcano,
 2075 Aeolian Islands (Italy): present eruptive activity and hazards. *Geol Soc London, Mem* 37:473-
 2076 490. <https://doi.org/10.1144/M37.14>
- 2077 Rout SS, Wörmer G (2020) Constraints on the pre-eruptive magmatic history of the Quaternary
 2078 Laacher See volcano (Germany). *Contrib Mineral Petrol* 175:74. [https://doi.org/10.1007/s00410-
 2079 020-01710-3](https://doi.org/10.1007/s00410-020-01710-3)
- 2080 Ryder CH, Gill JB, Tepley F III, Ramos F, Reagan M (2006) Closed to open-system differentiation
 2081 at Arenal volcano (1968–2003). *J Volcanol Geoth Res* 157:75–93
- 2082 Sahetapy-Engel S, Harris AJL, Marchetti E (2008) Thermal, seismic and infrasound observations of
 2083 persistent explosive activity and conduit dynamics at Santiaguito lava dome, Guatemala. *J*
 2084 *Volcanol Geotherm Res* 173:1-14. <https://doi.org/10.1016/j.jvolgeores.2007.11.026>
- 2085 Sahetapy-Engel ST, Harris AJL (2009a) Thermal structure and heat loss at the summit crater of an
 2086 active lava dome. *Bull Volcanol* 71:15–28. [http:// dx.doi.org/10.1007/s00445-008-0204-3](http://dx.doi.org/10.1007/s00445-008-0204-3)
- 2087 Sahetapy-Engel ST, Harris AJL (2009b) Thermal-image-derived dynamics of vertical ash plumes at
 2088 Santiaguito volcano, Guatemala. *Bull Volcanol* 71:827–830. [http://dx.doi.org/10.1007/s00445-
 2089 009-0284-8](http://dx.doi.org/10.1007/s00445-009-0284-8)
- 2090 Sánchez C, Álvarez B, Melo F, Vidal V (2014) Experimental modeling of infrasound emission from
 2091 slug bursting on volcanoes. *Geophys Res Lett* 41:6705–6711.
 2092 <https://doi.org/10.1002/2014GL061068>
- 2093 Schaaf P, Stimac J, Siebe C, Macías JL (2005) Geochemical evidence for mantle origin and crustal
 2094 processes in volcanic rocks from Popocatepetl and surrounding monogenetic volcanoes, Central
 2095 Mexico. *J Petrol* 46:1243–1282. <https://doi.org/10.1093/petrology/egi015>
- 2096 Scharff L, Hort M, Harris AJ, Ripepe M, Lees J, Seyfried R (2008), Eruption dynamics of the SW
 2097 crater of Stromboli volcano, Italy. *J Volcanol Geotherm Res* 176:565–570.
 2098 <https://doi.org/10.1016/j.jvolgeores.2008.05.008>
- 2099 Scharff L, Ziemer F, Hort M, Gerst A, Johnson JB (2012) A detailed view into the eruption clouds
 2100 of Santiaguito volcano, Guatemala, using Doppler radar. *J Geophys. Res* 117:B04201.
 2101 <https://doi.org/10.1029/2011JB008542>
- 2102 Sawyer GM, Oppenheimer C, Tsanev VI, Yirgu G (2008). Magmatic degassing at Erta 'Ale
 2103 volcano, Ethiopia. *J Volcanol Geotherm Res* 178:837–846
- 2104 Sawyer GM, Salerno G, Le Blond JS, Martin RS, Spampinato L, Roberts TJ, Mather TA, Witt MLI,
 2105 Tsanev VI, Oppenheimer C (2011) Gas and aerosol emissions from Villarrica volcano, Chile. *J*
 2106 *Volcanol Geotherm Res* 203:62–75. <http://dx.doi.org/10.1016/j.jvolgeores.2011.04.003>

- 2107 Scott JAJ, Mather TA, Pyle DM, Rose WI, Chigna G (2012) The magmatic plumbing system
2108 beneath Santiaguito volcano, Guatemala. *J Volcanol Geotherm Res* 237-238:54–68.
2109 <http://dx.doi.org/10.1016/j.jvolgeores.2012.05.014>
- 2110 Scott JAJ, Pyle DM, Mather TA, Rose WI (2013) Geochemistry and evolution of the Santiaguito
2111 volcanic dome complex, Guatemala. *J Volcanol Geotherm Res* 252:92-107.
2112 <http://dx.doi.org/10.1016/j.jvolgeores.2012.11.011>
- 2113 Shinohara H (2008) Excess degassing from volcanoes and its role on eruptive and intrusive activity.
2114 *Rev Geophys* 46:RG4005. <http://dx.doi.org/10.1029/2007RG000244>
- 2115 Shinohara H (2013) Volatile flux from subduction zone volcanoes: insights from a detailed
2116 evaluation of the fluxes from volcanoes in Japan. *J Volcanol Geotherm Res* 268:46–63.
2117 <https://doi.org/10.1016/j.jvolgeores.2013.10.007>
- 2118 Shreve T, Grandin R, Boichu M, Garaebiti E, Moussallam E, Ballu V., Delgado F, Leclerc F,
2119 Vallée M, Henriot M, Cevuard S, Tari D, Lebellegard P, Pelletier B (2019) From prodigious
2120 volcanic degassing to caldera subsidence and quiescence at Ambrym (Vanuatu): the influence of
2121 regional tectonics. *Sci Rep* 9:18868. <https://doi.org/10.1038/s41598-019-55141-7>
- 2122 Sims KWW, Aster RC, Gaetani G, Blichert-Toft J, Phillips EH, Wallace PJ, Mattioli GS,
2123 Rasmussen D, Boyd ES, Mount Erebus (2021) Eds Smellie JL, Panter KS, Geyer, A *Volcanism*
2124 in Antarctica: 200 millions years of subduction, Rifting and Continental break-up Geological
2125 Society, London, *Memoirs*, 55, <https://doi.org/10.1144/M55-2019-8>
- 2126 Singer BS, Smith KE, Jicha BR, Beard BL, Johnson CM., Rogers NW (2011) Tracking open-
2127 system differentiation during growth of Santa Maria Volcano, Guatemala. *J Petrol* 52:2335–2363
- 2128 Spampinato L, Ganci G, Hernandez PA, Calvo D, Tedesco D, Pérez NM, Calvari S, Del Negro C,
2129 Yalire MM (2013) Thermal insights into the dynamics of Nyiragongo lava lake from ground and
2130 satellite measurements. *J Geophys Res Solid Earth* 118:5771-5784.
2131 <https://doi.org/10.1002/2013JB010520>
- 2132 Spampinato L, Oppenheimer C, Cannata A, Montalto P, Salerno GG, Calvari S (2012) On the time-
2133 scale of thermal cycles associated with open-vent degassing. *Bull Volcanol* 74:1281-1292
- 2134 Spampinato L, Oppenheimer C, Calvari S, Cannata A, Montalto P (2008) Lava lake surface
2135 characterization by thermal imaging: Erta 'Ale volcano (Ethiopia). *Geochem Geophys Geosyst*
2136 9(12):Q12008. doi:10.1029/2008GC00216
- 2137 Spina L, Taddeucci J, Cannata A, Gresta S, Lodato L, Privitera E, Scarlato P, Gaeta M, Gaudin D,
2138 Palladino DM (2016) Explosive volcanic activity at Mt. Yasur: A characterization of the acoustic
2139 events (9-12th July 2011). *J Volcanol Geotherm Res*, Special issue on Understanding volcanoes
2140 in the Vanuatu arc 322:175-183

2141 Stevenson DS, Blake S (1998) Modelling the dynamics and thermodynamics of volcanic degassing.
2142 Bull Volcanol 60:307-317

2143 Stix J (2007) Stability and instability of quiescently active volcanoes: The case of Masaya,
2144 Nicaragua. Geol 35(6):535–538. <https://doi.org/10.1130/G23198A>

2145 Streck MJ, Dungan MA, Malavassi E, Reagan M, Bussy F (2002) The role of basalt replenishment
2146 in the generation of basaltic andesites of the ongoing activity at Arenal volcano, Costa Rica:
2147 evidence from clinopyroxene and spinel. Bull Volcanol 64:316–327

2148 Suckale J, Qin, Z, Picchi D, Keller T, Battiato I (2018) Bistability of buoyancy-driven exchange
2149 flows in vertical tubes. J Fluid Mec. 850:525-550

2150 Taddeucci J, Scarlato P, Capponi A, Del Bello E, Cimarelli C, D. Palladino M, Kueppers U (2012a)
2151 High-speed imaging of Strombolian explosions: The ejection velocity of pyroclasts. Geophys
2152 Res Lett 39:L02301. <https://doi.org/10.1029/2011GL050404>

2153 Taddeucci, J, Alatorre-Ibargengoitia MA, Moroni M, Tornetta L, Capponi A, Scarlato P, Dingwell
2154 DB, De Rita D (2012b) Physical parameterization of Strombolian eruptions via experimentally-
2155 validated modeling of high-speed observations. Geophys Res Lett 39:L16306.
2156 <https://doi.org/10.1029/2012GL052772>

2157 Taddeucci J, Sesterhenn J, Scarlato P, Stampka K, Del Bello E, Pena Fernandez JJ, Gaudin D
2158 (2014) Highspeed imaging, acoustic features, and aeroacoustic computations of jet noise from
2159 Strombolian (and Vulcanian) explosions. Geophys Res Lett 41:3096–3102.
2160 <https://doi.org/10.1002/2014GL059925>

2161 Taddeucci, J, Pena Fernandez JJ, Cigala V, Kueppers U, Scarlato P, Del Bello E, Ricci T,
2162 Sesterhenn J, Panunzi S (2021) Volcanic vortex rings: Axial dynamics, acoustic features, and
2163 their link to vent diameter and supersonic jet flow. Geophys Res Lett, 48:e2021GL092899.
2164 <https://doi.org/10.1029/2021GL092899>

2165 Taddeucci J, Edmonds M, Houghton BH, James MR, Vergnolle S (2015) Hawaiian and
2166 Strombolian Eruptions - including Fire Fountaining. "Encyclopedia of Volcanoes", 2nd edition,
2167 ed. Sigurdsson H, Houghton B, Rymer H, Stix J, McNutt S, Academic press, 27:485-503

2168 Tamburello G, Aiuppa A, Kanzas EP, McGonigle AJS, Ripepe M (2012) Passive vs. active
2169 degassing modes at an open-vent volcano (Stromboli, Italy). Earth Planet Sci Lett 249-360:106–
2170 116

2171 Taquet N, Stremme W, Grutter M, Baylón J, Bezanilla A, Schiavo B, Rivera C, Champion R,
2172 Boulesteix T, Nieto-Torres A, Espinasa-Pereña R, Blumenstock T, Hase F (2019) Variability in
2173 the gas composition of the Popocatepetl volcanic plume. Front Earth Sci 7:114. [https://doi.org/](https://doi.org/10.3389/feart.2019.00114)
2174 [10.3389/feart.2019.00114](https://doi.org/10.3389/feart.2019.00114)

- 2175 Thivet S, Harris AJL, Gurioli L, Bani P, Bernie T, Bombrun M, Marchetti A (2021) Multi-
 2176 parametric field experiments links explosive activity and persistent degassing at Stromboli.
 2177 *Frontiers Earth Sci* 9:669661. <https://doi.org/10.3389/feart.2021.669661>
- 2178 Turcotte DL, Ockendon H, Ockendon JR, Cowley SJ (1990) A mathematical model of vulcanian
 2179 eruptions. *Geophys J Int* 103:211–217
- 2180 Valade S, Ripepe M, Giuffrida G, Karume K, Tedesco D (2018) Dynamics of Mount Nyiragongo
 2181 lava lake inferred from thermal imaging and infrasound array. *Earth Planet Sci Lett* 500:192–
 2182 204.
- 2183 Vergnolle S, Jaupart C (1986) Separated two-phase flow and basaltic eruptions. *J Geophys Res*
 2184 91(B12):12842-12860
- 2185 Vergnolle S, Brandeis G (1994) Origin of the sound generated by Strombolian explosion. *Geophys*
 2186 *Res Lett* 21:1959-1962
- 2187 Vergnolle S, Brandeis G (1996) Strombolian explosion: 1. A large bubble breaking at the surface
 2188 of a lava column as a source of sound. *J Geophys Res* 101:20,433-20,447
- 2189 Vergnolle S, Caplan-Auerbach J (2004) Acoustic measurements of the 1999 eruption of Shishaldin
 2190 volcano, Alaska: 2) Precursor to the Subplinian activity. *J Volcanol Geothermal Res* 137:135-
 2191 151
- 2192 Vergnolle S, Caplan-Auerbach J (2006) Basaltic thermals and Subplinian plumes: Constraints from
 2193 acoustic measurements at Shishaldin volcano, Alaska. *Bull Volcanol* 68(7-8):611-630
- 2194 Vergnolle S, Gaudemer Y (2015) From reservoirs and conduits to the surface: a review on the role
 2195 of bubbles in driving basaltic eruptions, Carey RJ, Cayol V, Poland MP, Weis D (eds.), *Am*
 2196 *Geophysical Union Monograph: "Hawaiian Volcanism: From Source to Surface"* 208(14): 289-
 2197 322. <https://doi.org/10.1002/9781118872079.ch14>, 2015.
- 2198 Vergnolle S, Bouche E (2016) Gas-driven lava lake fluctuations at Erta'Ale volcano (Ethiopia)
 2199 revealed by MODIS measurements. *Bull Volcanol* 78:60 [https://doi.org/10.1007/s00445-016-](https://doi.org/10.1007/s00445-016-1047-y)
 2200 1047-y
- 2201 Wade JA, Plank T, Melson WG, Soto GJ, Hauri EH (2006) The volatile content of magmas from
 2202 Arenal volcano. *J Volcanol Geotherm Res* 157:94–120.
 2203 <https://doi.org/10.1016/j.jvolgeores.2006.03.045>
- 2204 Wallace PJ, Edmonds M (2011) The sulphur budget in magmas. Evidence from melt inclusions,
 2205 submarine glasses and volcanic gas emissions. *Rev Mineral Geochem* 73:215-246.
 2206 <https://doi.org/10.2138/rmg.2011.73.8>
- 2207 Wallace PA, Lamb OD, DeAngelis S, Kendrick JE, Hornby AJ, Díaz-Moreno A, González PJ,
 2208 vonAulock FW, Lamur A, Utley JEP, Rietbrock A, Chigna G, Lavallée Y (2020) Integrated

2209 constraints on explosive eruption intensification at Santiaguito dome complex, Guatemala. *Earth*
2210 *Planet Sci Lett* 536:116139. <https://doi.org/10.1016/j.epsl.2020.116139>

2211 Williams-Jones G, Rymer H (2015) Hazards of volcanic gases. In Sigurdsson H, Houghton B,
2212 Rymer H, Stix J, McNutt S (eds). *The Encyclopedia of Volcanoes* pp 985-992.

2213 Witsil AJC, Johnson JB (2018) Infrasound explosion and coda signal investigated with joint
2214 analysis of video at Mount Erebus, Antarctica. *J Volcanol Geotherm Res* 357:306-320

2215 Witt MI, Mather TA, Pyle DM, Aiuppa A, Bagnato E, Tsanev VI (2008) Mercury and halogen
2216 emissions from Masaya and Telica volcanoes, Nicaragua. *J Geophys Res* 113(B6).
2217 <https://doi.org/10.1029/2007JB005401>

2218 Witter JB, Kress VC, Delmelle P, Stix J (2004) Volatile degassing, petrology, and magma dynamics
2219 of the Villarrica Lava Lake, Southern Chile. *J Volcanol Geotherm Res* 134:303-337.
2220 <https://doi.org/10.1016/j.jvolgeores.2004.03.002>

2221 Witter JB, Kress VC, Newhall CG (2005) Volcan Popocatepetl, Mexico. Petrology, magma mixing,
2222 and immediate sources of volatiles for the 1994 present eruption. *J Petrol* 46:2337–2366.
2223 <https://doi.org/10.1093/petrology/egi058>

2224 Woitischek J, Woods AW, Edmonds M, Oppenheimer C, Aiuppa A, Pering TD, Ilanko T, D'Aleo
2225 R, Garaebiti E (2020) Strombolian eruptions and dynamics of magma degassing at Yasur
2226 Volcano (Vanuatu). *J Volcanol Geotherm Res* 398:106869.
2227 <https://doi.org/10.1016/j.jvolgeores.2020.106869>

2228 Woods AW (1995) A model of vulcanian explosions. *Nuclear Engineering and Design*, 155:345–
2229 357

2230 Worster MG, Huppert HE, Sparks RSJ (1993) The crystallization of lava lakes. *J Geophys Res*
2231 98(B9):15891-15901

2232 Woulff G and McGetchin TR (1976) Acoustic noise from volcanoes: Theory and experiments.
2233 *Geophys J Roy Astron Soc* 45:601-616

2234 Wright, R (2016) MODVOLC: 14 years of autonomous observations of effusive volcanism from
2235 space. In Harris AJL, De Groot T, Garel F, Carn SA (eds) 2016. *Detecting, Modelling and*
2236 *Responding to Effusive Eruptions*. Geological Society, London, Special Publications, 426:23–53

2237 Yamamoto H, Watson IM, Phillips JC, Bluth GJ (2008) Rise dynamics and relative ash distribution
2238 in vulcanian eruption plumes at Santiaguito Volcano, Guatemala, revealed using an ultraviolet
2239 imaging camera. *Geophys Res Lett*, 35:8

2240 Zurek J, Moune S, Williams-Jones G, Vigouroux N, Gauthier P-J (2019) Melt inclusion evidence
2241 for long term steady-state volcanism at Las Sierras-Masaya volcano, Nicaragua. *J Volcanol*
2242 *Geotherm Res* 378:16-28.<https://doi.org/10.1016/j.jvolgeores.2019.04.007>

2243

2244 **Figure captions**

2245 **Fig. 1** SiO₂ distribution in magmas of Ert'a Ale (Field et al. 2012); Masaya (Zureck et al. 2019);
2246 Fuego (Berlo et al. 2012); Nyiragongo (Minissale et al. 2019; Demant and Lubala, 1994);
2247 Nyamuragira (Head et al. 2011); Stromboli (Landi et al. 2006, 2009; Bertagnini et al. 2008;
2248 Pompilio et al. 2011; Métrich et al. 2010, 2021); Ambrym (Allard et al. 2016a, b) ; Pacaya
2249 (Cameron et al. 2002) ; Yasur (Métrich et al. 2011); Erebus (Kelly et al. 2008); Arenal (Bolge et
2250 al. 2006); Santiaguito (Scott et al. 2013); Popocatepetl (Schaaf et al. 2005).

2251

2252 **Fig. 2** Plumbing systems and associated mechanisms at: a) Kilauea (slightly adapted from Ferguson
2253 et al. 2016); b) Nyiragongo (Pouclet and Bram, 2020); c) Stromboli during the small-scale
2254 paroxysms (slightly adapted from Métrich et al. 2021); d) from seismic tomographic inversion
2255 from combining artificial and natural seismic sources, showing the magma pathway (red arrows)
2256 and the high velocity zone associated to the crystallised magma body (slightly adapted from
2257 Patanè et al. 2017). SdF, Stcc and iso, HVB stand for Sciara del Fuoco, Strombolicchio,
2258 isosurface of constant seismic velocity propagation (iso6 is for 6 km/s) and high-velocity body.

2259

2260 **Fig. 3** Potential bubble geometries for rising bubbles (a) and stationary bubbles (b): left: small;
2261 middle: relatively large and defined as spherical cap bubble; right: very large and called Taylor
2262 bubble; b) flat bubble, i.e. thin and very long, resulting from a local coalescence within a foam
2263 accumulated below the crust at the top of a lava lake and defined in Bouche et al. 2010.

2264

2265 **Fig. 4** Lava lake of Kilauea at: a) Puu O'o on March 1988, showing a broken bubble of a few meters
2266 in diameter (photo by S. Vergniolle); b) summit on 29 July 2016 (courtesy of M. Patrick); c)
2267 summit on 6 May 2018, as the lake drained away during the 2018 lower East Rift Zone eruption,
2268 with a crater of diameter of 150 m (courtesy of M. Patrick). Note the difference in the lava lake
2269 level between 2b and 2c, analysed by Patrick et al, 2015.

2270

2271 **Fig. 5** Lava lake of Nyiragongo with a diameter of 250-260 m along the east-west axis and 200 m
2272 along the north-south axis (courtesy of B. Smets): a) Panoramic view of the lava lake on 12
2273 September 2011 displaying a hot central zone and a partly solidified annulus. b) Many
2274 incandescent cracks can be seen in central area on 12 September 2011; c) overflows of the lava

2275 lake with the former lava lake appearing as an annular incandescent ring, on 12 September 2011;
2276 d) bubble bursting at the surface of the lava lake, in 2016.
2277

2278 **Fig. 6** Top of exposed magma column of Erebus (courtesy of C. Oppenheimer): a) with a diameter
2279 of 60 m, 7 December 2003 at 11h15 UTC; b) low-level lava lake, 30-40 m in diameter, 3
2280 December 2012 at 9h54 UTC; c) fresh bombs can be seen on the side of the crater, 60 m in
2281 diameter, 15 December 2004 at 23h57 UTC; d) weak degassing (blue cloud), 17 December 2010
2282 at 10:44:05.

2283
2284 **Fig. 7** Lava lake of Erta 'Ale: a) 29-30 January 2003 (courtesy of J-M Bardintzeff), the diameter is
2285 nearly 90 m; b) 22 March, 2003 (photo taken by T. Staudacher and slightly adapted from
2286 Vergnolle and Bouche, 2016); the diameter is 30 m; c) December 2004, the lava lake is entirely
2287 encrusted (diameter > 100 m; courtesy of J-M Bardintzeff); d) thermal image on 26 March 2003
2288 (taken by T. Staudacher) with a lava lake of diameter equal 30 m, and with insert of visible
2289 image of a spherical cap bubble in March 2001 (adapted from Bouche et al. 2010 photo 4d).
2290

2291 **Fig. 8** Lava lakes of Ambrym: a) Benbow crater (courtesy of J-M Bardintzeff), with diameters of 2
2292 km for the caldera, 800 m for the largest crater in front, 200-300 m for the two small craters; b)
2293 Marum crater, 80 m in diameter, 13 August 2013 at 14h01 (courtesy of T. Boyer); c) Marum,
2294 bubble diameter of 8-10 m, photo taken at 80 m distance, October 2007 (courtesy of P. Allard);
2295 d) Marum, bubble bursting on 22 June 2015 at 12h34 (courtesy of T. Boyer); e) Marum,
2296 diameter of 90 m, depth of 350m, 14 November 2016 at 11h20, the lava lake had a partial thin
2297 crust cover, with incandescent cracks (courtesy T. Boyer); f) lava flow on 9 March 2015, the
2298 cone in the back is Niri Maben Mbwelesu (courtesy T. Boyer).

2299
2300 **Fig. 9** Lava lake at Masaya, a) 16 January 2009, degassing from hidden thermally radiating lava
2301 lake (courtesy of P. Delmelle); b) in 2016 dimensions of 40x30 m, depth: 250 m (courtesy of J-
2302 M Bardintzeff); c) 18 February 2017 (courtesy of P. Delmelle) approximately 15 m of
2303 diameter.
2304

2305 **Fig. 10** Sketch for the variations of the lava lake level at Erta 'Ale, explained to result from the
2306 variations in the thickness of a foam accumulated at the top of the magma reservoir (slightly
2307 adapted from Vergnolle and Bouche, 2016): a) lava lake is at a high level when the foam is
2308 growing in the reservoir due to a non-zero underlying gas flux, as in 9-13 Dec 2002; b) low level

2309 lava lake, when the underlying gas flux in the reservoir had stopped leading to the foam thinning
 2310 due to its spreading in the conduit, as for the period December 2002-May 2003; c) changes of the
 2311 lava lake volume, as deduced from MODIS records (diamonds) and compared with a model of
 2312 foam thickness, used independently with two different boundary conditions, a non-zero
 2313 underlying gas flux (rise of lava lake) and a zero underlying gas flux (descent of the lava lake).
 2314 The best fit between the MODIS records and the numerical solving gives two constrains, on the
 2315 underlying gas flux and the area of the magma reservoir (Vergniolle and Bouche, 2016). Note
 2316 that μ_l , ρ_l , Q_{in} and Q_{out} stand for magma viscosity, magma density, underlying gas flux below the
 2317 foam and the gas flux at the surface. The foam with a gas volume fraction, ϵ , moves towards
 2318 the conduit at a velocity U_b and has a thickness $h(r,t)$, which varies with the radial
 2319 coordinate, r , within the radius of the magma reservoir, R_c , and the time t . t_{rise} and t_{fall} are the
 2320 times at which the level of the lava lake rises and ΔV_{NTI} is the relative volume of the lava lake in
 2321 respect to that of March 2003 (see details in Vergniolle and Bouche, 2016).

2322
 2323 **Fig. 11** Models of degassing in the conduit, initially proposed for Erta 'Ale (Bouche et al. 2010) and
 2324 applied to: a) Erta 'Ale with an updated value of the magma viscosity; b-c) Ambrym at two
 2325 different periods marked by different bubble diameters at the surface. The degassing at Erta Ale
 2326 is driven by the rise of large bubbles able to produce a bubbly wake, as deep as 1 km and up to
 2327 the surface, while this type of degassing only exist from 500-1000m to the surface at Nyiragongo
 2328 and at shallow depths at Villarica. The degassing at Ambrym is relatively similar to that of Erta
 2329 Ale, when the bubbles are large, >8.5 m (see text for details). The drastic change in magma
 2330 viscosity with the loss of dissolved water and the calculation of the gas volume fraction by
 2331 assuming stagnant small bubbles and a fully degassing magma from gas exsolution had led us to
 2332 use the viscosity of the undegassed magma below 500 m and that of the fully degassed magma
 2333 above (see text and table 3 for details). Note that U_b and U_w are the vertical velocities of the
 2334 driving large bubble and its detached bubbly wake (of length L_w), respectively, while α_l and α_w
 2335 are the gas volume fractions within the lava lake and the wake, respectively.

2336
 2337 **Fig. 12** Stromboli, a) a typical strombolian explosion in 1979, approximately of 150 m in height
 2338 (courtesy of J-M Bardintzeff); b) gas-rich explosion October 2005, height of ejecta between 3
 2339 and 5 m (photo taken by N. Métrich), 20 m in height (T Ricci); c) start of an ash-rich explosion
 2340 at vent N1, 29 September 2019 at 10h55 local time, approximately 30 m in height, (courtesy of
 2341 T. Ricci); d) southwestern vent in 1970, showing the top of the nearby magma column, an
 2342 exceptional photo due to danger, as well as on its information on Stromboli's eruptive pattern 40

2343 years ago (courtesy of G. Sartoris), with an opening potentially of 1 m (order of magnitude) ; e)
2344 lava pond due to bubble rise at vent N2, 16 November 2008 at 15hr46, length of major axis of
2345 the red ellipse between 3 and 4 m, (courtesy of T. Ricci); f) a few seconds later at vent N2, 16
2346 November 2008, 15hr46 (scale identical to e) (courtesy of T. Ricci).

2347
2348 **Fig. 13** a) an ash-rich explosion at Yasur, reaching a maximum height of 100m with ejecta falling
2349 back in crater in a radius of 150m from the emission point, on 1 August 2008 at 17h18 (local
2350 hour) (courtesy of A. Finizola); b-d) Arenal's edifice (courtesy of O. Aragon) with b) a typical
2351 vulcanian explosion, leading to a small eruptive column of 400 m in height, in 1990, c) a typical
2352 strombolian explosion with lava flows, in 1995 at 20h20, the red part with ballistic blocks is
2353 approximately 500-600 m; d) close-up of a typical strombolian explosion with lava flows, in
2354 1989 at 20h15, between 100 and 200 m, showing the two different vents existing in the C crater.

2355
2356 **Fig. 14** a-b) Popocatépetl with a crater of 300 m in diameter (courtesy of R. Campion) with a) lava
2357 dome at a high level, showing the passive degassing on an annular ring at the origin of the large
2358 SO₂ flux, on 28 February 2019 and b) lava dome at a low level, on 18 February 2020, the rise of
2359 the lava dome remaining puzzling for this dacitic magma composition, leading to vulcanian
2360 explosions, hence initiated below a sealed vent; c) small ash-and-gas explosion at Santiaguito,
2361 reaching a height of 500-1000 m, in 1978 (courtesy of J-M Bardintzeff).

2362
2363 **Fig. 15** Bi-directional flow models for open-vent volcanoes, such as Stromboli, Yasur, Erebus and
2364 lava lakes, (see text for details), a) developed for explaining the excess degassing (slightly
2365 adapted from Stevenson and Blake, 1998); b) assuming that the velocity of the degassing
2366 magma, v_s , is maximum and adding the degassing and ignore the crystallisation path at
2367 Stromboli (slightly adapted from Burton et al. 2007b). Note that v_d is the velocity of the
2368 descending fluid of viscosity η and density ρ , while ϕ is gas volume fraction in the ascending
2369 fluid and r_s the radius of the ascending fluid; c) core-annular flow including lateral gradients in
2370 magma viscosity and density and solving for inclined and vertical conduit and combined with
2371 petrologic data on magmatic volatile content at Villarica (slightly adapted from Palma et al.
2372 2011). Note that ρ and μ stand for magma density and viscosity for the ascending fluid (subscript
2373 c) and the descending fluid (subscript a). R is the conduit radius and r the radial coordinate; d) 3
2374 regimes are possibly as a function of the viscosity ratio, although the core-annular flow is the
2375 most frequent (slightly adapted from Beckett et al. 2014). Note that the ascending fluid is marked
2376 in grey; e) convective velocity and height of the convective cells, estimated from the re-

2377 dissolution of the tiny bubbles within the downwards motion of the degassed magma (slightly
2378 adapted from Carey et al. 2013).

2379

2380

2381

2382 **Table captions:**

2383 Table 1 Main features of open-vent volcanoes (geodynamic context, activity period, magma
2384 composition, temperature, crystal volume fraction, magma supply rate) and associated references
2385 for : a) persistent lava lakes (Nyiragongo, Erta Ale, Masaya, Villarica, Kilauea, Ambrym) ; b)
2386 our selection of open-vent volcanoes without a lava lake (Stromboli, Yasur, Erebus,
2387 Popocatépetl, Arenal, Pacaya, Fuego, Santiaguito).

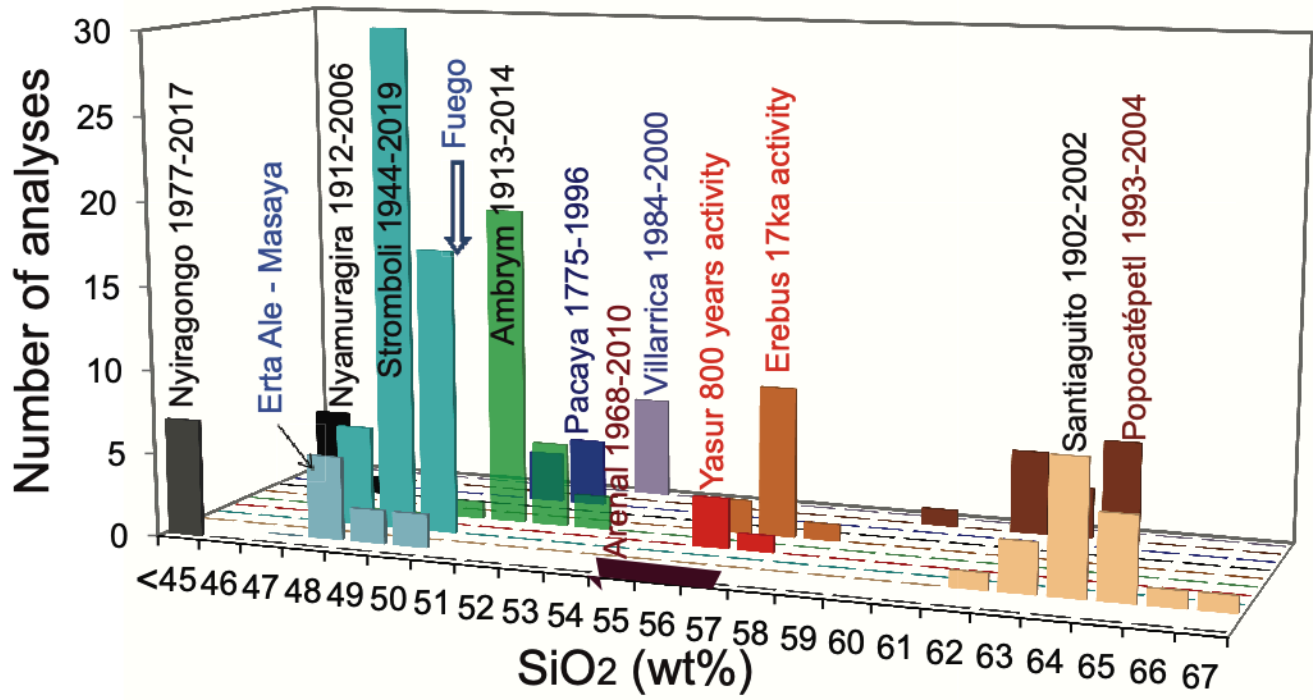
2388

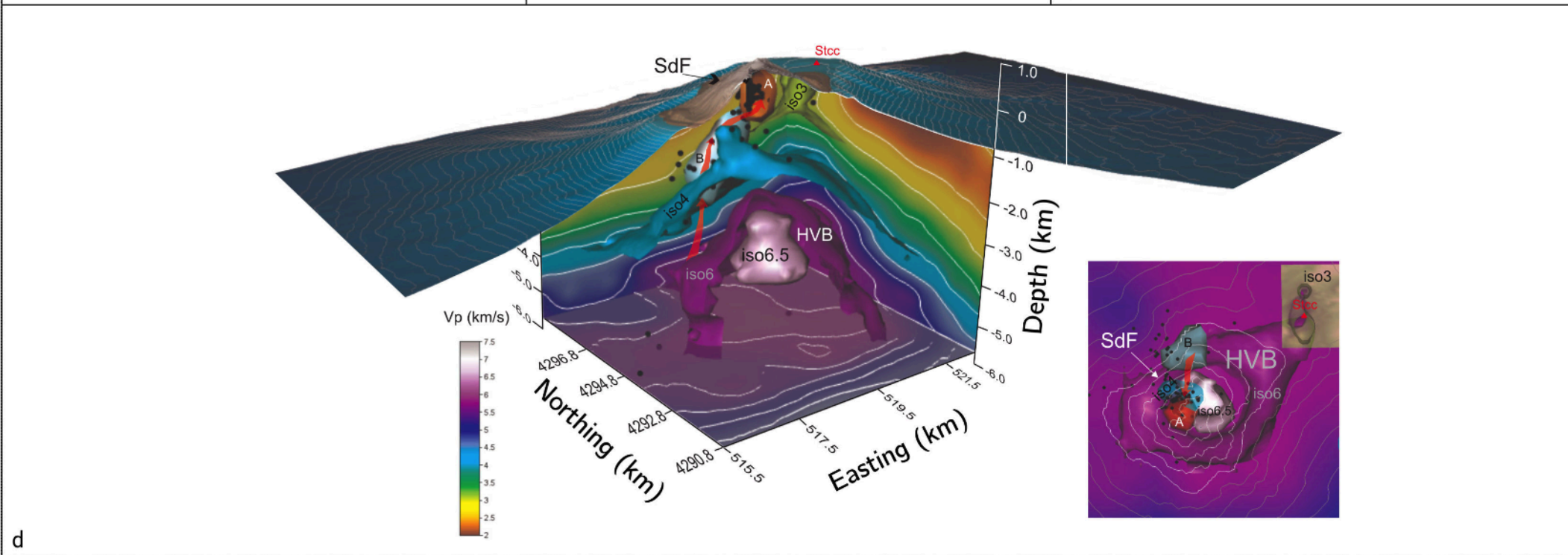
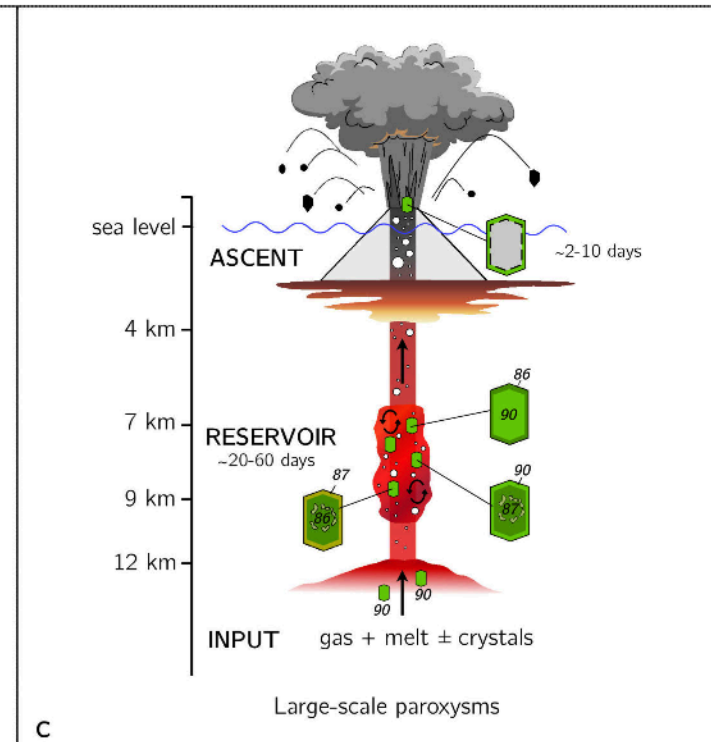
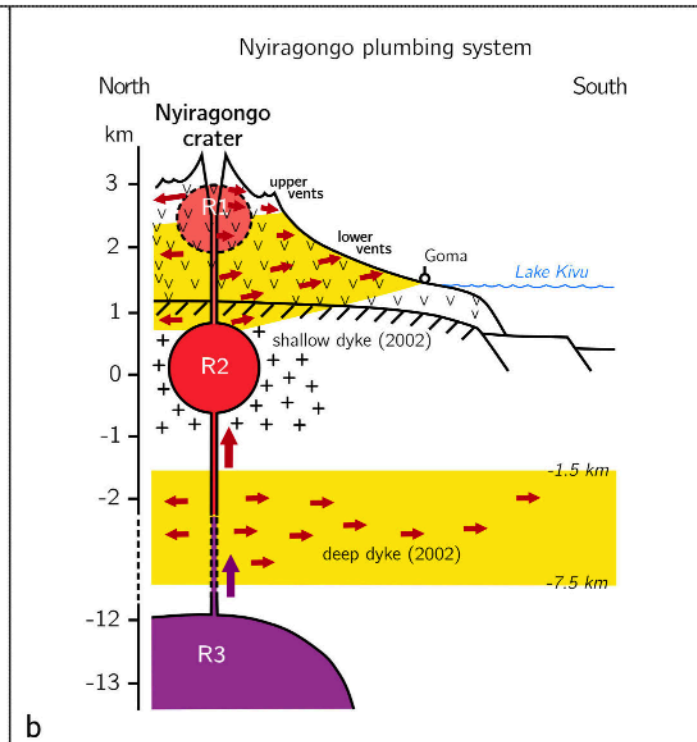
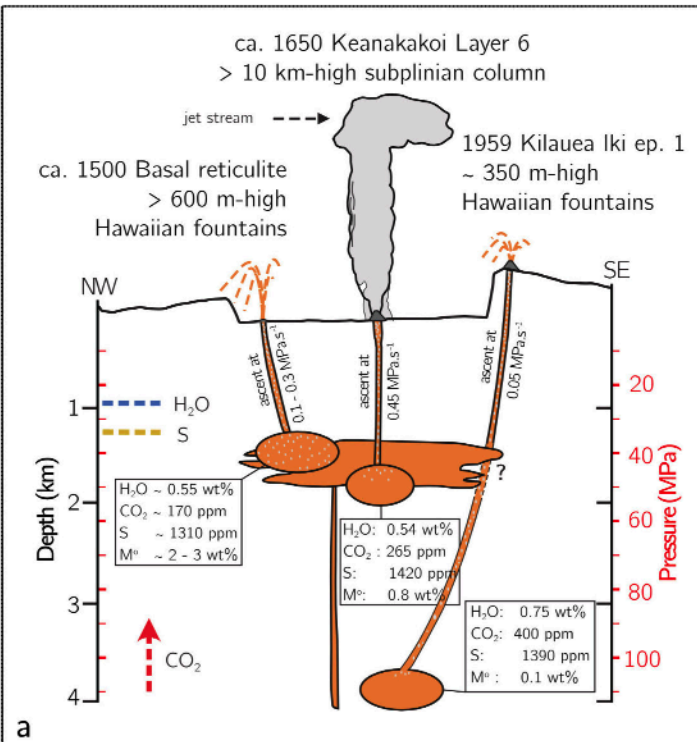
2389 Table 2 Dissolved sulphur amounts in magmas (wt%) and SO₂ fluxes for open-vent volcanic
2390 systems a) hosting a lava-lake (Nyiragongo, Erta Ale, Masaya, Villarica, Kilauea, Ambrym); b)
2391 without a lava lake (Stromboli, Yasur, Erebus, Popocatépetl, Arenal, Pacaya, Fuego, Santiaguito).

2392

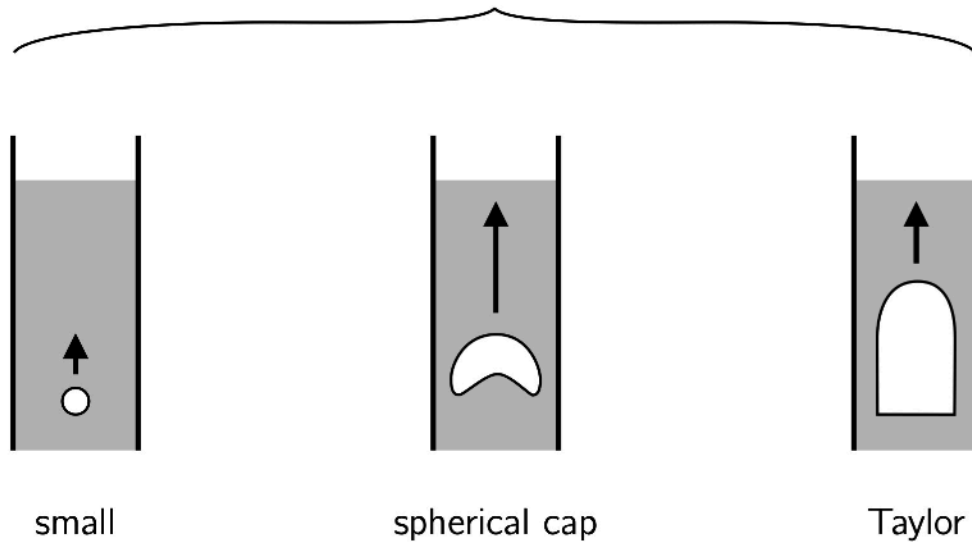
2393 Table 3 Parameters (silica content, temperature, dissolved water content, viscosity, bubble volume
2394 observed at the surface, Reynolds numbers) used for the calculation of the Reynolds number at lava
2395 lakes and at different depths (500 m, 100m, 0m), assuming undegassed magma below 500 m and
2396 fully degassed magma above (see text for details).

2397

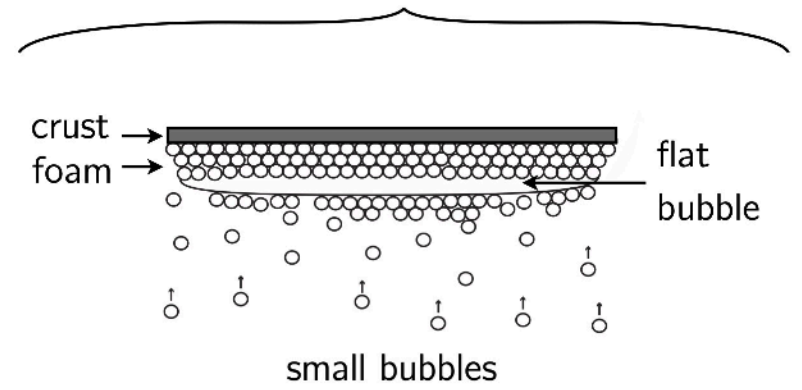




(a) Rising bubble

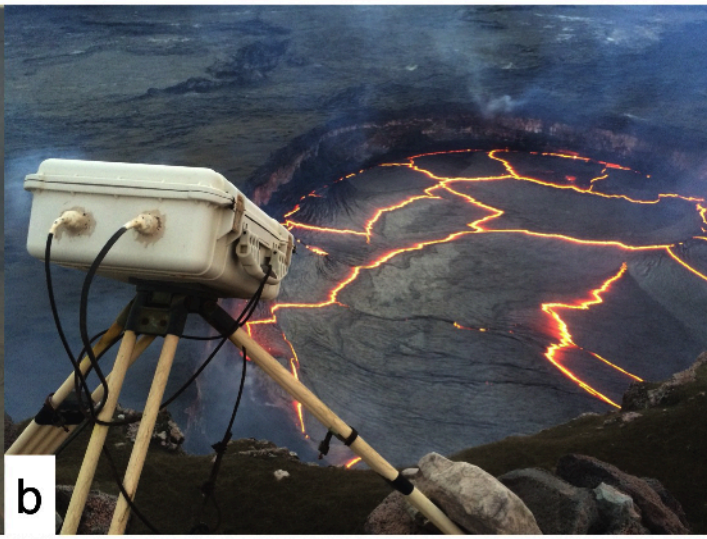


(b) Stationary bubble





a



b



c



a



b

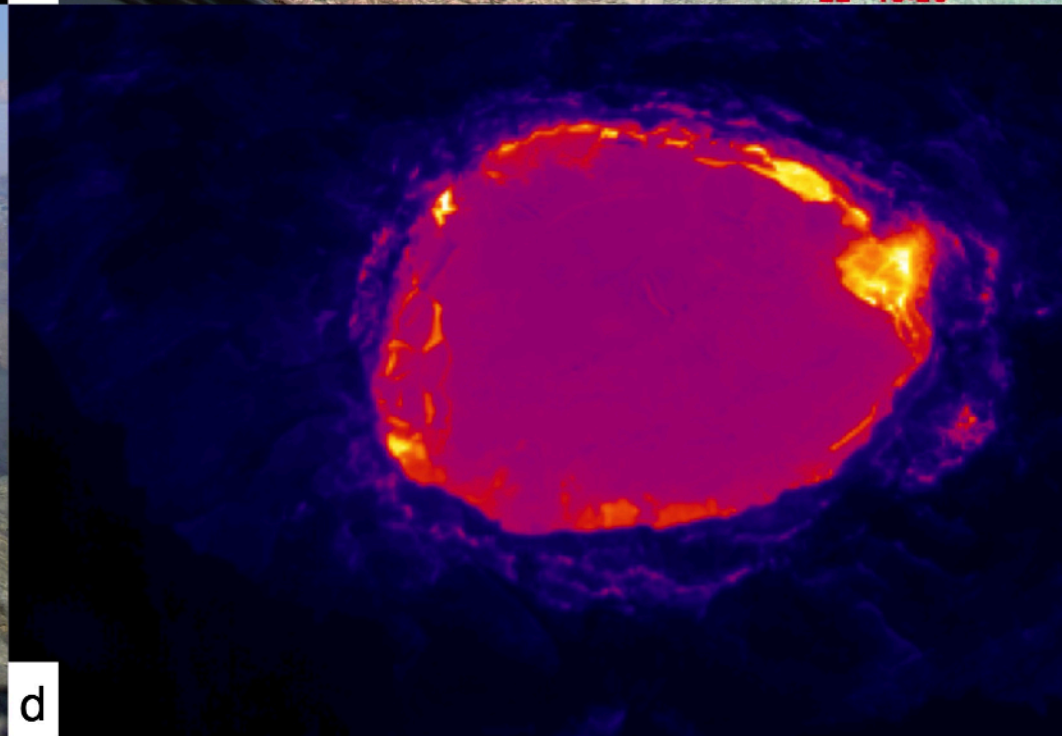


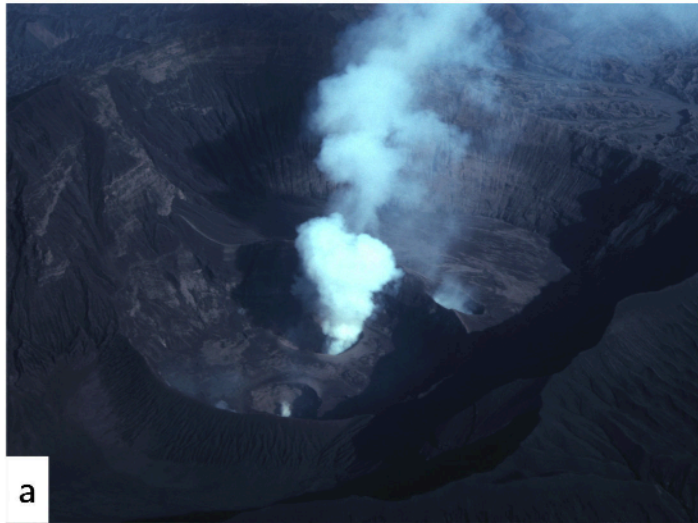
c



d









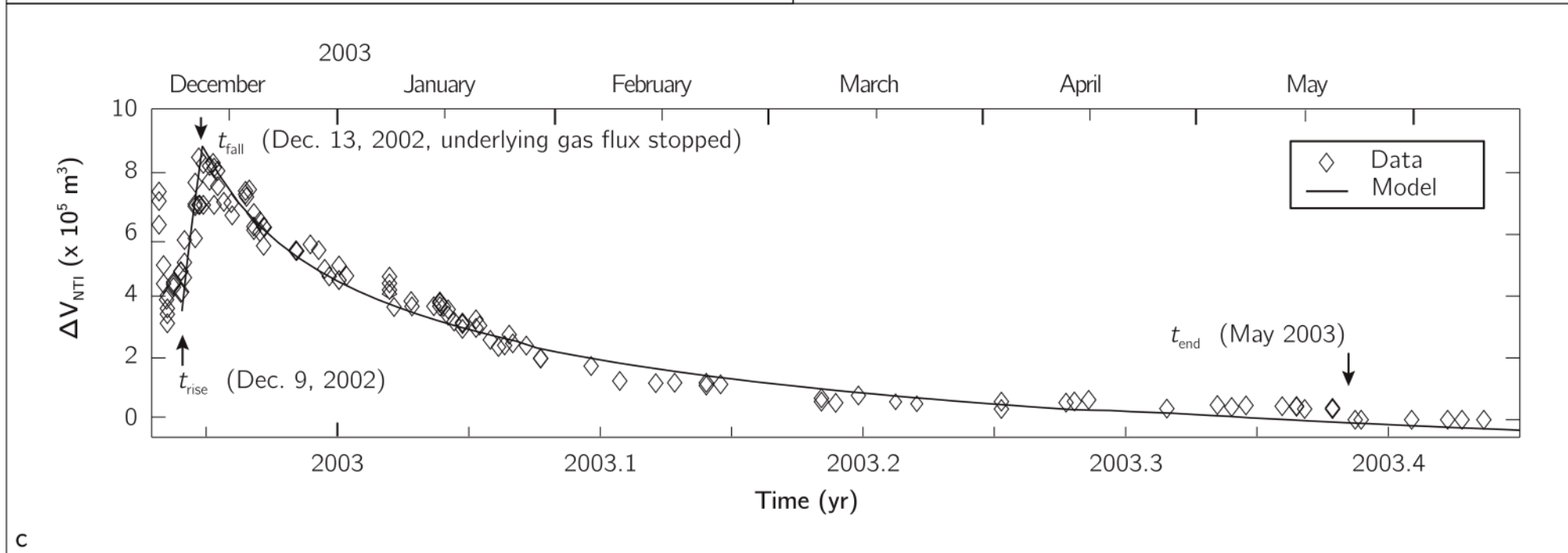
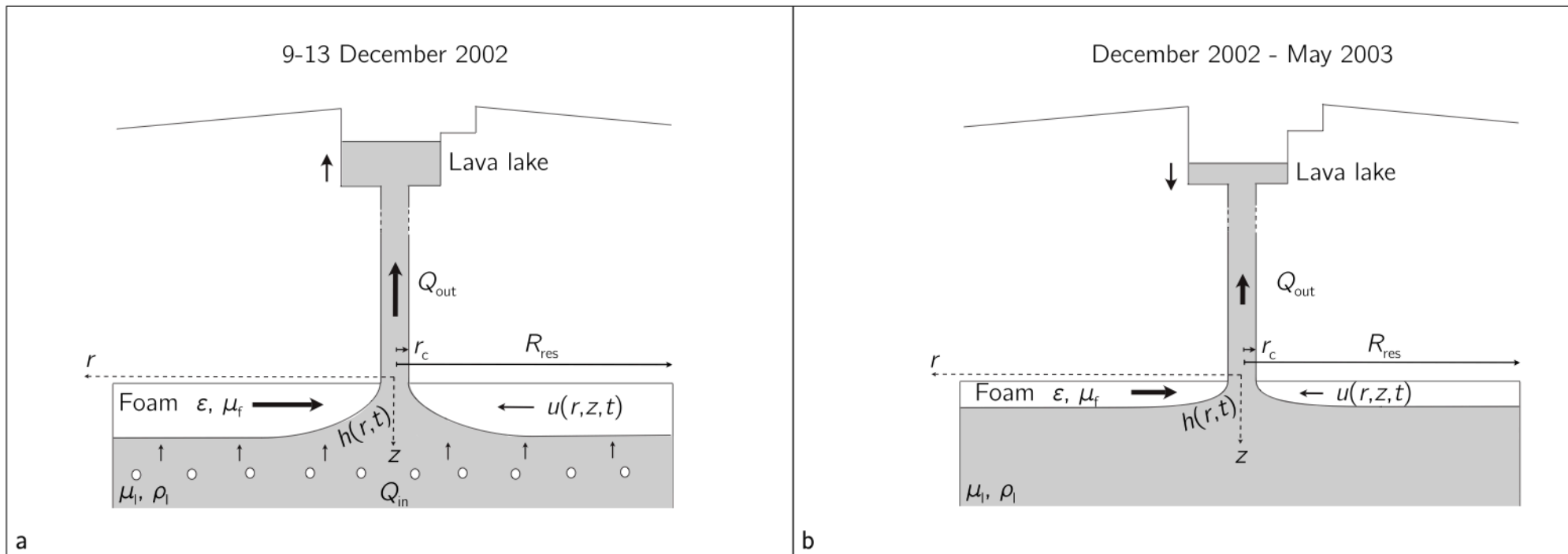
a



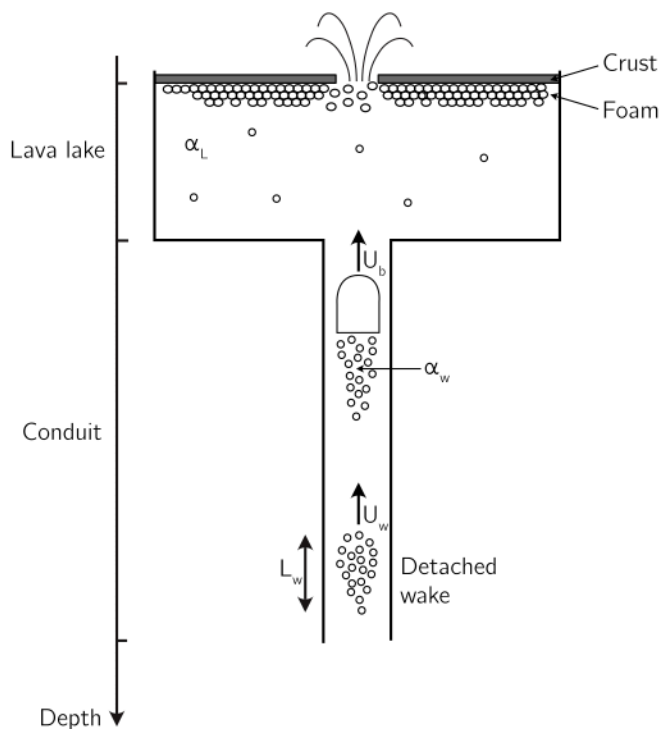
b



c

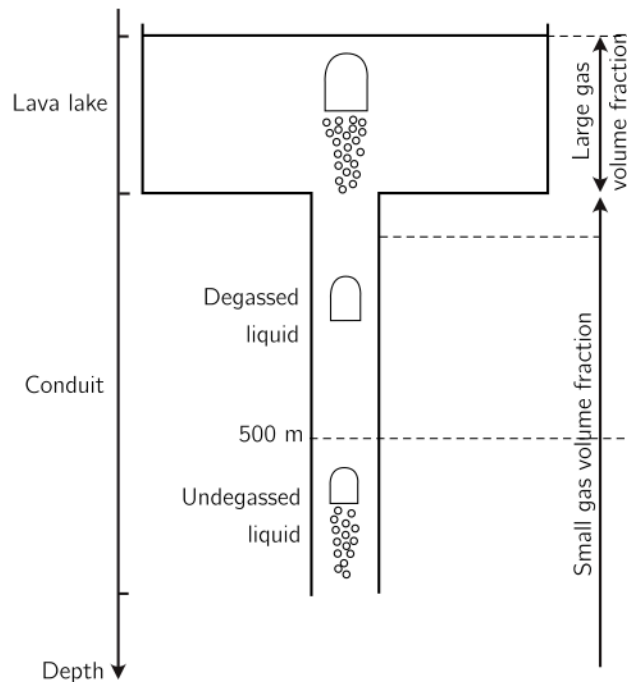


Open wake
Lava fountains



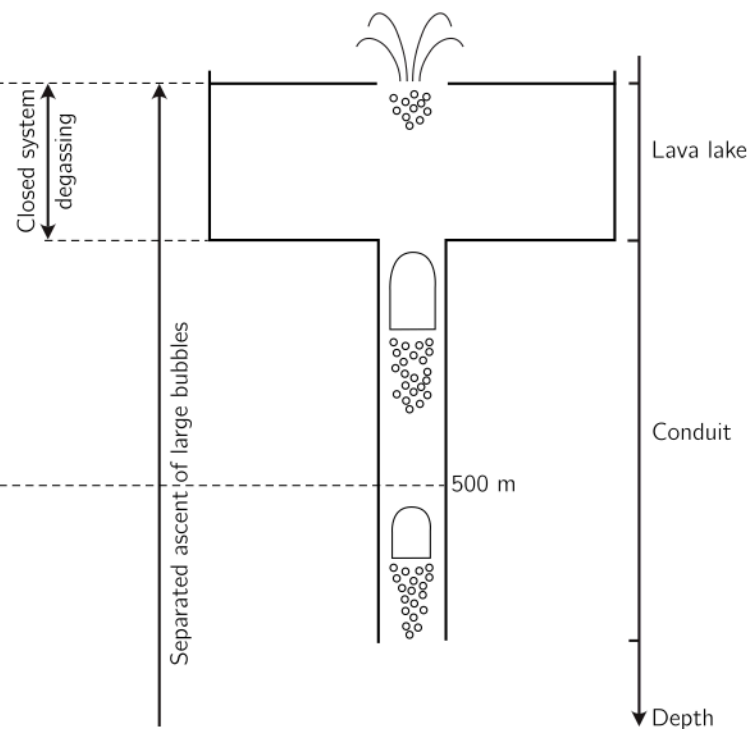
Erta Ale (up to 1 km depth)
Nyiragongo (up to 500 m)
Villarica (shallow depths)

No open wake in conduit



Ambrym
october 5, 2008, 5 - 8.5 m bubbles

Open wake in conduit
Lava fountains



Ambrym
october 5, 2008, 8.5 - 10 m bubbles
mid-may, 2014, 12 - 16 m bubbles



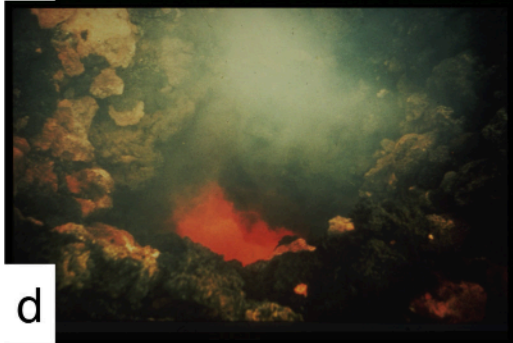
a



b



c



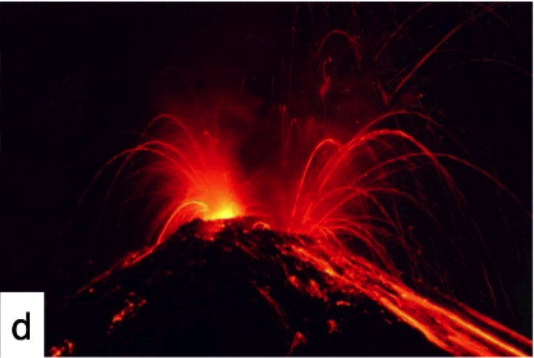
d



e



f





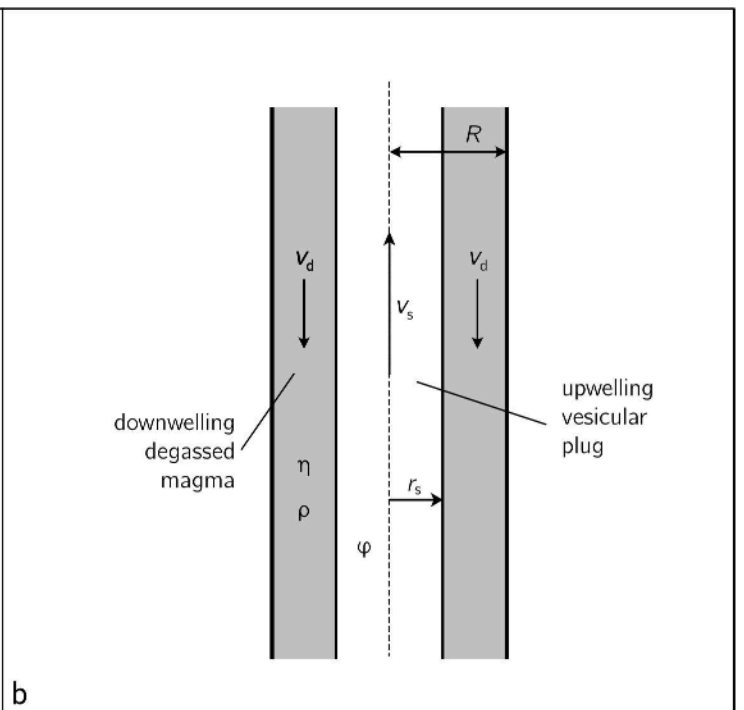
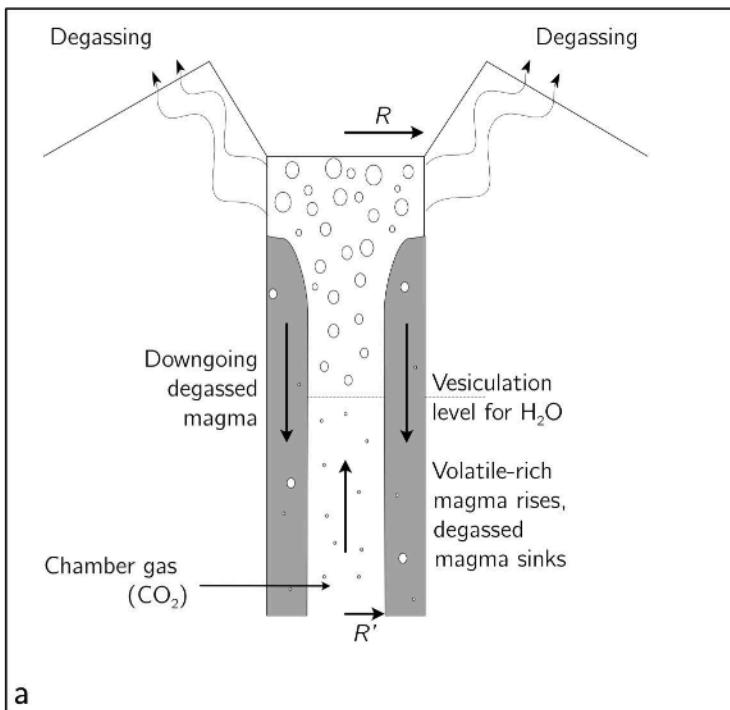
a



b

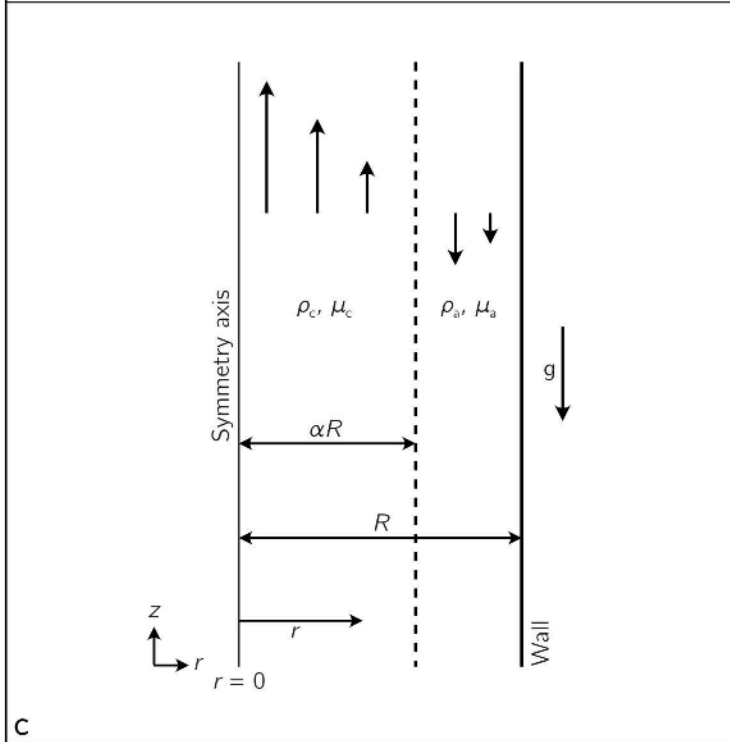


c

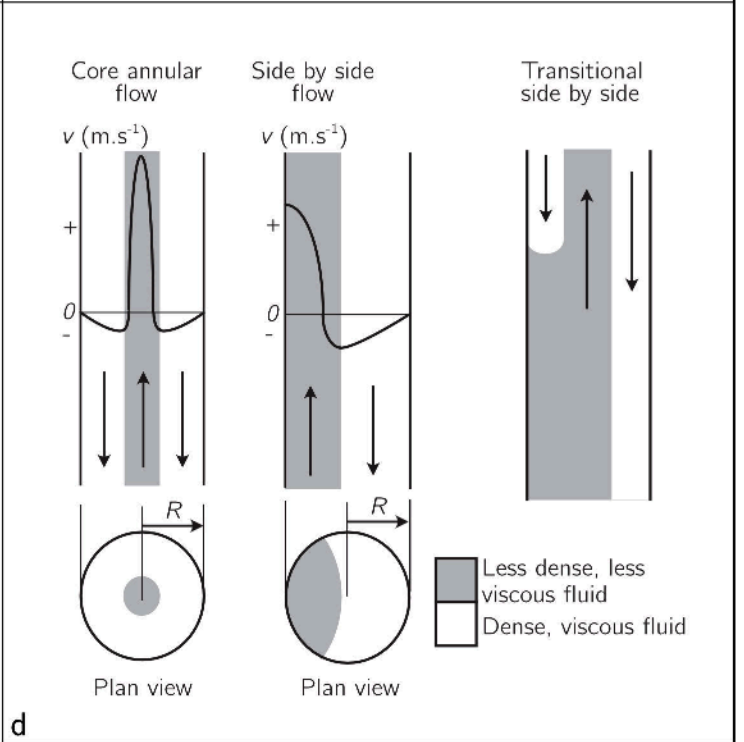


a

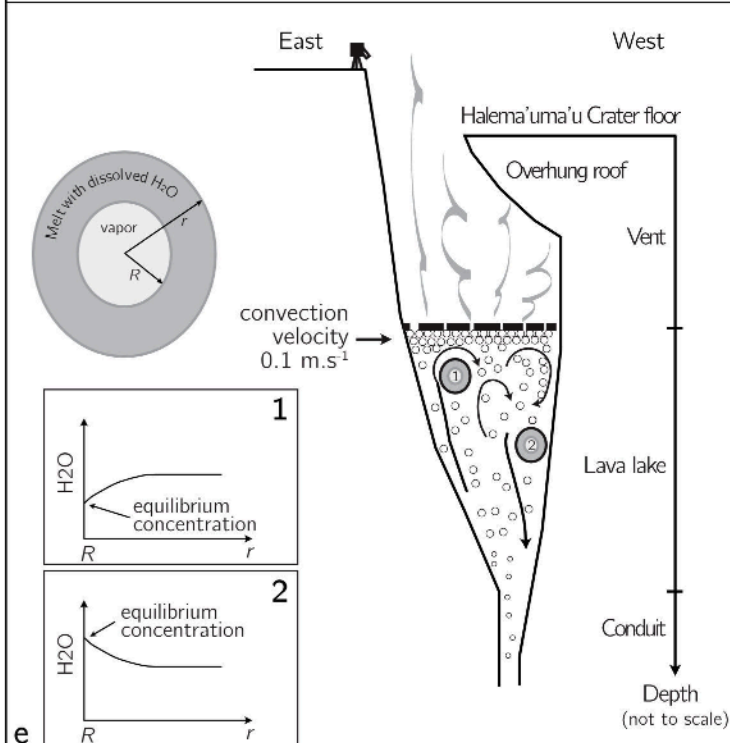
b



c



d



e

Supplementary material by Vergnolle and Metrich

“An interpretative view of open-vent volcanoes”

Figure caption:

Figure S1: **Fig S1 (a)** Viscosity (log Pa.s) as a function of inverse temperature (K^{-1}) for anhydrous and crystal- and bubble-free phonolite melts of Erebus (Le Losq et al., 2015); for phonolite from Vesuvius (GP79) the experimental data are from Giordano et al., (2009), for rhyolite and andesite melts from Neuville et al. (1993), and for a basalt melt from Villeneuve et al. (2008). Figure redrawn from Le Losq et al., (2015). **(b)** Viscosity (log Pa.s) as a function the temperature and the H_2O content of trachyandesitic melt of Yasur varying from 0 to 2.5 wt%, after Giordano et al., (2008). 52 wt% SiO_2 refers to Yasur present-day bulk rock and 56 wt% to the glassy matrix (Métrich et al., 2011). **(c)** Relative increase in magma viscosity as a function of the solid volume fraction, see text for details (slightly adapted from Mader et al., 2013). **(d)** Relative increase in magma viscosity as a function of the bubble shape, here quantified by the capillary number, see text for details, (slightly adapted from Mader et al., 2013).

